Addis Ababa Science and Technology University

College of Electrical and Mechanical Engineering

Department of Electro-Mechanical Engineering

Design and Control of an Autonomous Forklift for EPHARM Pharmaceuticals

A thesis submitted in partial fulfillment of the requirements for the degree of Bachelor of Science in Electro-Mechanical Engineering

Authors

Abenezer Girma Taye (**Group Leader**)
Abel Chernet
Abinet H/Mariam
Abebaw Shiferaw

Thesis Advisor

Dr. Solomon Genene Gudeta

Academic Year 2016–2017

Declaration of Authorship

We, the undersigned students, declare that this thesis titled *"Design and Control of an Automated Guided Vehicle for EPHARM Pharmaceutical Industry"* and the work presented in it are our own. No part of this thesis has been submitted elsewhere for any other degree or qualification, and all work is our own unless referenced to the contrary in the text. Where we have consulted the published work of others, it is always clearly attributed.

No.	**Student Name**	**Signature**	**Date**
1	Abenezer G. Taye	_____	_____
2	Abel Chernet	_____	_____
3	Abinet H/Mariam	_____	_____
4	Abebaw Shiferaw	_____	_____

We, the undersigned, further declare that the attached thesis is wholly our own work, and that no part of it has been:

- copied by manual or electronic means from any work produced by any other person, present or past;
- produced by automatic tools or aids;
- modified to contain falsified output; or
- copied from any other source, including websites.

We understand that submitting work that is not wholly our own may result in academic penalties.

No.	Student Name	Signature	Date
1	Abenezer G. Taye	_____	_____
2	Abel Chernet	_____	_____
3	Abinet H/Mariam	_____	_____
4	Abebaw Shiferaw	_____	_____

Bonafide Certificate

Certified that this thesis entitled *"Design and Control of an Autonomous Forklift EPHARM Pharmaceuticals"* is a bonafide work carried out under my supervision. To the best of my knowledge, the work reported herein does not form part of any other thesis or dissertation on the basis of which a degree or award was conferred on an earlier occasion.

Name of Head of Department: _____

Signature of HOD: _____

Name of Thesis Advisor: _____

Signature of Advisor: _____

Date: _____

Abstract

Manual material handling in a pharmaceutical industry is an activity with a great risk and economically ineffective. The chemicals which are exposed to the atmosphere of the industry makes the working condition extremely hazardous for the workers and the exposure of the manufactured drugs to a human contact increases the probability of the drugs to be failed to satisfy the rigid requirements of the standards of a pharmaceutical industry. On top of this using manual material handling to transport packed items in the industry is an activity which is tedious and consumes unnecessary cost and time of the production. Therefore The task intended to do in this project is to replace currently used material handling system, which is manual material handling, with an automated guided vehicle (AGV), which is expected to transport packed items from end of production point to warehouse, for EPHARM pharmaceutical industry. As a result the company can save a high amount of cost outflowed for material handling and make its warehouse fully computerized and secure the safety of its employees.

Acknowledgements

First and foremost we would like to thank the Almighty GOD. Next to that this project owes its existence and development by the help, support and inspiration of several people. We would like to express our sincere gratitude to our advisor Mr. Solomon Genene for his guidance, support and comments have been very helpful in the development of the project. Mr. Melaku who is EPHARM worker, helped us in obtaining the right data about the factory's material handling problems, their limitations and updates.

We would also like to thank the college of electrical and mechanical engineering for providing proper learning methods and techniques that helped us in our entire project.

Dedication

For those who are suffering from any engineering problem.

Contents

Declaration of Authorship . . . . . **i**

Bonafide Certificate . . . . . **iii**

Abstract . . . . . **iv**

Acknowledgements . . . . . **v**

Dedication . . . . . **vi**

List of Abbreviations . . . . . **xii**

1 Introduction **1**

1.1 Background 1

1.2 Statement of the Problem 2

1.3 Scope of the Thesis 2

1.4 General Objective 2

1.5 Specific Objectives 2

2 Literature Review **3**

2.1 History of AGV 3

2.2 Guidance Systems of AGVS 5

2.3 Locomotion of Mobile Robots 6

2.4 Drive Types of Wheeled Mobile Robots 8

2.5 Wheel Geometry 9

3 Conceptual Design **11**

4 Design and Analysis of the Mechanical System **21**

4.1 Selection of Lifting Mechanism for the Forklift 21

4.2 Determining Forklift Truck Capacity Requirement 22

4.3 Physical Modeling of the System 24

4.4 Design of Some Basic Mechanical Machine Elements 28

5 Design and Analysis of the Electrical System **45**

5.1 Selection of Battery 45

5.2 Battery Charging Circuit Design 46

5.3 Selection of Controller 48

5.4 Drive System 52

5.5 Selection of Actuator 54
6 Design and Analysis of the Control System 56
6.1 Wheel and Drive Type Selection 56
6.2 Kinematic and Dynamic Modelling of the Robot 56
6.3 Modeling of the Actuator 70
6.4 Trajectory Generation 72
6.5 Control System Design for the Drive System 73
6.6 Lyapunov Stability of the Controller 74
6.7 Control System Design for the Lifting Mechanism 76
7 Simulation and Results 78
7.1 Simulation of the Mechanical Design 78
7.2 Simulation of the Control System 81
8 Economic Analysis 85
8.1 Future Value 86
8.2 Payback Period 90
9 Conclusion and Future Works 91
9.1 Conclusion 91
9.2 Limitations 92
9.3 Future Works 92
A MATLAB Functions for Drive Mechanism Simulation 95

List of Figures

2.1 Components of a forklift 4
2.2 Conventional wheel types: (A) fixed wheel, (B) castor wheel, (C) powered steering wheel without offset, (D) powered steering wheel with longitudinal offset. 7
2.3 Three designs of universal wheel. 7
2.4 Mecanum wheel variants: (A) $\alpha = +45°$ (left wheel), (B) $\alpha = -45°$ (right wheel), (C) photograph of an actual Mecanum wheel. 7
2.5 Omnidirectional WMR drive 9

3.1 Operational area of the AGV 12

4.1 Free body diagram of the forklift 23
4.2 Free body diagram of the forklift (side view) 23
4.3 Free body diagram of the whole vehicle. 24
4.4 Physical model of the whole system 26
4.5 Lifting mechanism overview: schematic and free body 26
4.6 Schematic diagram of the lifting mechanism. 26
4.7 Free body diagram of the fork. 26
4.8 Free body diagram of the screw. 27
4.9 Free body diagram of the screw. 27
4.10 Bending stress analysis of the fork 28
4.11 Drive system of the lifting mechanism. 38
4.12 Drive system schematic. 38
4.13 Motion profile of the lifting mechanism motor 40
4.14 Drive motor and gear arrangement 42
4.15 Gear inertia diagram 42

5.1 Schematic diagram of the battery charging circuit 46
5.2 Circuit diagram of battery charger 47
5.3 Olimex development board for PIC16F877A microcontroller.[1] 50
5.4 Arduino Uno board with ATmega 328 chip.[2] 51
5.5 XBee communication module.[3] 52
5.6 PWM waveforms showing 10%, 50%, and 90% duty cycles.[4] 53

5.7 L293D Bridge IC 54

6.1 Inertial and Robot coordinate systems of a mobile robot 57
6.2 The differential drive mobile robot model 58
6.3 The velocities of the robot center 63
6.4 The robots free body diagram 66
6.5 Modeling diagram of DC motor 70
6.6 Block diagram of kinematic back stepper controller 74
6.7 Block diagram of the control loop of the lifting mechanism 76

7.1 Stress analysis of the AGV frame 79
7.2 Stress analysis of the lift structure 79
7.3 Strain analysis of the lift structure 80
7.4 Strain analysis of fork 80
7.5 Stress analysis of the fork 81
7.6 Simulink simulation diagram of the low level controller 82
7.7 Simulation diagram of the control system 82
7.8 Kinematic back stepping controller simulation 82
7.9 The simulation result of low level controllers of the left and right motors 83
7.10 Control system simulation output — angular speed response 83
7.11 Simulink simulation diagram of the lift control system 84
7.12 Simulation result of the lift control system 84

8.1 Comparison of cash flow of the two material handling systems 89
8.2 Net present value over project lifetime 89

List of Tables

3.1 Relative importance of customer requirements 14
3.2 Evaluation of competing AGV products against customer requirements 15
3.3 Physical and technical engineering specification priorities 16
3.4 Relationship between customer requirements and physical specifications (House of Quality) 17
3.5 Relationship between customer requirements and technical specifications (House of Quality) 18
3.6 Maximum and minimum values of physical specifications 19
3.7 Maximum and minimum values of technical specifications 19
3.8 Engineering targets of physical specifications 20

4.1 Comparison of ferrous metals for structural frame selection 30

6.1 Comparison of different drive systems for AGV 56
6.2 Representative parameters of the drive DC motor (PM71-110 PG56) . . 72
6.3 Representative parameters of the lift DC motor (PM60-105 PG28) . . . 72

8.1 Operational cost of the project 86
8.1 Operational cost of the project 87
8.2 Detailed cost breakdown of AGV components 87
8.3 Operational cost comparison: manual handling vs. AGV system 88
8.4 Eight-year cash flow comparison: manual handling vs. AGV system . . 88

List of Abbreviations

AGV	Automated Guided Vehicle
EPHARM	Ethiopian Pharmaceutical Manufacturing Share Company
GMP	Good Manufacturing Practice
API	Active Pharmaceutical Ingredient
WMR	Wheeled Mobile Robot
PID	Proportional-Integral-Derivative (Controller)
ADC	Analog-to-Digital Converter
DAC	Digital-to-Analog Converter
AS/RS	Automated Storage and Retrieval System
FMS	Flexible Manufacturing System
DOF	Degree of Freedom
NiCad	Nickel Cadmium (battery)
NiMH	Nickel Metal Hydride (battery)
PLC	Programmable Logic Controller
RAM	Random Access Memory
PWM	Pulse-Width Modulation
PBP	Payback Period
TD	Total Depreciation
FV	Future Value
OI	Original Investment
AT	Availability Time
WL	Work Load
K_T	Motor Torque Constant
K_b	Back-EMF Constant
KVL	Kirchhoff's Voltage Law
QFD	Quality Function Deployment
EMF	Electromotive Force
DC	Direct Current
IC	Integrated Circuit
ORS	Oral Rehydration Salts

Chapter 1

Introduction

1.1 Background

Materials handling is a system or combination of methods, facilities, labor, and equipment for moving, packing, and storing materials to meet specific objectives [1]. Effective material handling is central to manufacturing and distribution: it can account for 30–75% of an item's total production cost and for 25% of the workforce, 55% of factory space, and 87% of production time in a typical plant. Designing an optimum system therefore has a direct and significant impact on overall productivity.

This project addresses the design of a material handling system for EPHARM pharmaceutical industry – specifically, an automated guided vehicle (AGV) that transports packed items from the end of the production line to the warehouse and places them on shelves according to warehouse management rules.

Safety and GMP Considerations

Pharmaceutical manufacturing is subject to Good Manufacturing Practice (GMP) standards that impose strict controls on human contact with products at every stage [2]. Epidemiological studies of pharmaceutical plant workers document elevated rates of hypertension, respiratory disease, and occupational cancer linked to chemical exposure [3]. GMP guidelines require personnel to avoid direct contact with active pharmaceutical ingredients (APIs), maintain clean body coverings, and refrain from handling materials when ill [4]. Automating material transport with an AGV eliminates the main source of contamination risk and satisfies these requirements directly.

Computerization and Mechanization

Modern warehouse management in the pharmaceutical sector demands full traceability: products must be segregated, tracked, and delivered in strict conformance with regulatory rules [1]. A computer-controlled AGV integrates naturally with flexible manufacturing systems, automated storage and retrieval systems, shop-floor control systems, and process control equipment. This integration removes human error from the handling loop and makes the entire material flow fully mechanized and auditable.

1.2 Statement of the Problem

EPHARM currently uses manual material handling to transport packed items within the facility. This introduces four interconnected problems. First, GMP compliance requires costly controls to limit human contact with sensitive products; any lapse creates contamination risk. Second, long-term exposure to pharmaceutical compounds is hazardous to workers, with documented links to respiratory illness and other chronic conditions. Third, manual execution of complex warehouse management rules is error-prone and difficult to audit. Fourth, round-the-clock manual handling is expensive and limits throughput scalability. This project proposes replacing the manual system with a non-wire, non-floor-path guidance AGV to address all four problems simultaneously.

1.3 Scope of the Thesis

This thesis covers the full design cycle of a forklift AGV intended for EPHARM: mechanical design (lifting mechanism selection, machine element sizing, motor sizing), electrical design (battery, charging circuit, controller hardware, communication network, actuator selection), control system design (kinematic and dynamic modelling, actuator modelling, drive and lift controllers), simulation, and economic analysis.

1.4 General Objective

The objective of this project is to design an automatically guided vehicle that transports packed items from the production line to the warehouse, reduces material handling cost, eliminates worker exposure hazards, and enables fully computerized warehouse management.

1.5 Specific Objectives

To accomplish this, the project covers the following tasks: lifting mechanism selection; machine element design and stress analysis; drive and lift motor sizing; battery selection and charging circuit design; controller hardware selection; drive system design; actuator selection; wheel and drive type selection; kinematic and dynamic modelling of the drive mechanism; actuator modelling; drive controller design; lift controller design; mechanical and control system simulation; and economic viability analysis.

Chapter 2

Literature Review

2.1 History of AGV

Automatic Guided Vehicles have played a role in moving material and product for more than 40 years. The first AGV system was built and introduced in 1953. It was a modified towing tractor that was used to pull a trailer and follow an overhead wire in a grocery warehouse. By the late 50's and early 60's towing AGVs were in operation in many types of factories and warehouses. In 1973, Volvo in Kalmar, Sweden set out to develop non-synchronous assembly equipment as an alternative to the conventional conveyor assembly line. The result was 280 computer-controlled assembly AGVs.

The first big development for the AGV industry was the introduction of a unit load vehicle in the mid-1970s. These unit load AGVs gained widespread acceptance in the material handling marketplace because of their ability to serve several functions; a work platform, a transportation device and a link in the control and information system for the factory. Today there are several hundred systems using unit load vehicles in operation which were produced by a number of manufacturers. These systems transport material in warehouses, factories, mills, hospitals, and other industrial and commercial settings.

In the 1970's the principal guidance technology was to induce an electronic frequency through a wire that was buried in the floor. A device called a 'floor controller' turned the frequency on the wires on and off and directed the AGV through its intended route. The AGV was considered 'dumb' since the vehicle was just following signals in the floor. The intelligence for the routing of the vehicles was in the floor controllers. So, the systems of this day were considered "smart floors" and "dumb vehicles".

In the late 1980s, non-wire guidance was introduced for AGV systems. Laser and inertia guidance are two examples of non-wire guidance which allow for increased system flexibility and accuracy. When changes to the original guide path are needed, there is no need for floor alterations or production interruption.

The market demand for AGVs can be measured by the increased number of AGV

manufacturers. During the late 1970s there were fewer than 6 AGV vendors in the United States and only 3 different types of vehicles. By 1990 there were more than 40 worldwide vendors and more than 15 vehicle types, with an increasing emphasis on standard design. The future will be marked by still more change which will be driven partly by even more technological advances. But it will also be driven by increases in the use of AGVS, which in turn will foster more investment in research and development.

A forklift is a powered truck that is used for lifting and transportation of materials. The latter developed since 1920s has become an indispensable piece of equipment in all manufacturing and warehousing companies. Forklifts are rated for specific weights and center of gravity. One of the main advantages of forklifts is their increase maneuverability in making tight corners, which is due to rear wheel steering [5].

A typical counterbalanced forklift contains several components that include truck frame, counterweight, cab, overhead guard, power source, tilt cylinders, mast, carriage, load back rest, and different attachments depending on varies applications, see figure below [6].

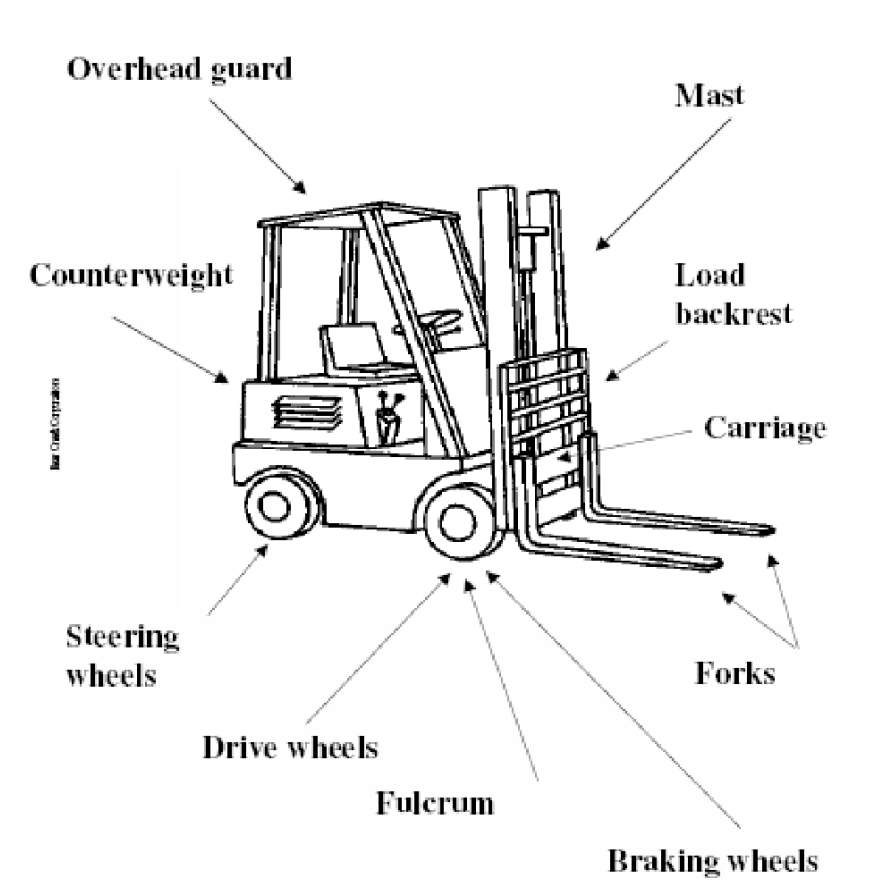

Figure 2.1. *Components of a forklift*

An Automated Guided Vehicle system (AGVs) is a material handling system that is independently operated, steerable, wheeled vehicle, driven by electric motors using storage batteries; and it follows a predefined path along an aisle [7].

An automated guided vehicle system mainly consists of the following four components: The vehicle that is mainly used to transport materials within the system, the guide path that guides the vehicle to move along a particular path, the control unit that monitors and directs the system operations. And the computer interface that interfaces with other systems and computers such as mainframe host computer, the automated storage and retrieval system (AS/RS) and flexible manufacturing system [8].

2.2 Guidance Systems of AGVS

Wire guidance. In a wire guided guidance system, an energized wire is embedded in the floor along the AGV guide path. In embedded guide wire method, electrical wires are placed in a small channel cut into the surface of the floor. After the guide wire is installed, the channel is filled with cement to eliminate the discontinuity in the floor surface. The guide wire is connected to a frequency generator, which emits a low-voltage, low current signal. This induces a magnetic field along the pathway that can be followed by sensors on-board in each vehicle.

Non-wire guidance. There are two general types of non-wire guidance method; non-wire floor-path guidance and non-wire non floor path guidance. Non-wire floor-path guidance this may take the form of optical guidance, painted or chemical stripe. In an optical guidance system, colorless fluorescent particles are painted or taped on the concrete floor. Photo sensors on the vehicle read the path and follow the laid path. In Painted or Chemical Stripe system, the floor is painted with a fluorescent color or chemical stripe that forms a guide-path for the AGV. The vehicles are equipped with sensors underneath to follow the guide-path. The sensor on the AGV follows the path and reads various information codes along the guide-path. The information codes instruct the AGV to perform various operations and to identify stop locations.

Non-wire non-floor-path guidance may take the form of laser guidance, inertial guidance, Dead Reckoning. In laser guidance system, a laser beam is used to scan wall-mounted bar-coded reflectors. Accurate location and maneuvering of an AGV is achieved with the help of these signals. In inertial guidance system, the inertial guidance system uses a gyroscope to determine the direction the AGV is moving. The vehicle can be programmed to take a variety of courses without additional costs due to moving wire or setting up new “targets”. In dead reckoning system, it uses odometer, where the relative position of the vehicle is tracked by using an optical encoder to measure the precise rotation of the drive wheel and steer angle. This guidance system is used in

short distance material handling [9].

2.3 Locomotion of Mobile Robots

A mobile robot needs locomotion mechanisms that enable it to move unbounded throughout its environment. Because there are a large variety of possible ways to move, the selection of an appropriate locomotion strategy is a critical design decision [10]. Locomotion mechanisms are broadly classified into legged and wheeled types. Since the forklift AGV operates on a flat warehouse floor, wheeled locomotion is adopted; legged locomotion is not considered further (a detailed treatment is given in [11]).

Wheeled locomotion. The maneuverability of a WMR depends on the wheels and drives used. The WMRs that have three DOF are characterized by maximal maneuverability which is needed for planar motions, such as operating on a warehouse floor, a road, a hospital, a museum, etc. Non-holonomic WMRs have less than three DOF in the plane, but they are simpler in construction and cheaper because less than three motors are used. A holonomic vehicle can travel in every direction and function in tight areas. This capability is called Omni-directionality. Balance is inherently assured in WMRs with three or more wheels. But in the case of m-wheel WMRs (m>= 3) a suspension system must be used to assure that all wheels can have ground contact in rough terrains. The main problems in WMR design are the traction, maneuverability, stability, and control that depend on the wheel types and configurations (drives) [12].

WMR wheels fall into two families: *conventional wheels* and *special wheels*. Conventional wheels are distinguished in powered fixed wheels, castor wheels, and powered steering wheels. Powered fixed wheels (Figure 2.2A) are driven by motors mounted on fixed positions of the vehicle. Their axis of rotation has a fixed direction with respect to the platform's coordinate frame. Castor wheels (Figure 2.2B) are not powered but they can also rotate freely about an axis perpendicular to their axis of rotation.

Powered steering wheels have a driving motor for their rotation and can be steered about an axis perpendicular to their axis of rotation. They can be without offset (Figure 2.2C) or with offset (Figure 2.2D) in which case the axes of rotation and steering do not intersect. To achieve Omni directionality with conventional castor and powered steering wheels some kind of motion redundancy should be used, for example, n-wheel drives (n>2) with all wheels driven and steered. Conventional wheels have higher load capacities and higher tolerance for ground irregularities compared to special wheel configurations. But due to their non-holonomic constraints are not truly omnidirectional wheels [13].

Figure 2.2. *Conventional wheel types: (A) fixed wheel, (B) castor wheel, (C) powered steering wheel without offset, (D) powered steering wheel with longitudinal offset.*

Special wheels are designed to provide active traction in one direction and passive motion in another, enabling greater maneuverability in congested environments. The three main types are the universal wheel, the Mecanum wheel, and the ball wheel. The universal wheel provides a combination of constrained and unconstrained motion during turning. It contains small rollers around its outer diameter which are mounted perpendicular to the wheel's rotation axis. This way the wheel can roll in the direction parallel to the wheel axis in addition to the normal wheel rotation.

Figure 2.3. *Three designs of universal wheel.*

The Mecanum wheel is similar to the universal wheel except that the rollers are mounted at an angle α other than 90 (usually ± 45).

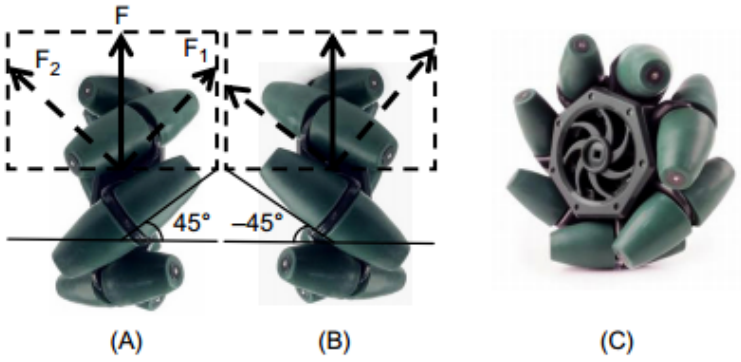

Figure 2.4. *Mecanum wheel variants: (A) $\alpha = +45°$ (left wheel), (B) $\alpha = -45°$ (right wheel), (C) photograph of an actual Mecanum wheel.*

The ball (or spherical) wheel places no direct constraints on the motion, that is, it is omnidirectional like castor or special universal and Mecanum wheels. In other words, the rotational axis of the wheel can have any arbitrary direction. One way to achieve this is by using an active ring driven by a motor and gearbox to transmit power to the ball via rollers and friction, which is free to rotate in any direction instantaneously. Because of its difficult construction the ball wheel is very rarely used in practice.

2.4 Drive Types of Wheeled Mobile Robots

WMR drives are distinguished into six configurations: differential drive, tricycle, omnidirectional, synchro drive, Ackerman steering, and skid steering. Each is described below.

Differential drive. This drive consists of two fixed powered wheels mounted on the left and right side of the robot platform. The two wheels are independently driven. One or two passive castor wheels are used for balance and stability. Differential drive is the simplest mechanical drive since it does not need rotation of a driven axis. If the wheels rotate at the same speed, the robot moves straight forward or backward. If one wheel is running faster than the other, the robot follows a curved path along the arc of an instantaneous circle. If both wheels are rotating at the same velocity in opposite directions, the robot turns about the midpoint of the two driving wheels. The above locomotion modes are illustrated in Figure 2.6

Tricycle. This drive has a single wheel which is both driven (powered) and steered. For stability, two free-running (unpowered) fixed wheels in the back are used, in order to have always the three point contact required. The linear and angular velocities of the wheel are fully decoupled. For driving straight, the wheel is positioned in the middle position and driven at the desired speed. When the front wheel is at an angle the vehicle follows a curved path. If the front wheel is positioned at 90, the robot will rotate following a circular path the center of which is in the middle point of the rear wheels and not in the robot's geometric center.

Omnidirectional. This drive can be obtained using three, four, or more omnidirectional wheels as shown in Figure 2.8. WMRs with three wheels use universal wheels that have a 90 roller angle as shown in Figure 2.8A. Omnidirectional WMRs with four wheels use Mecanum wheels in the configuration shown in Figure 2.8B.

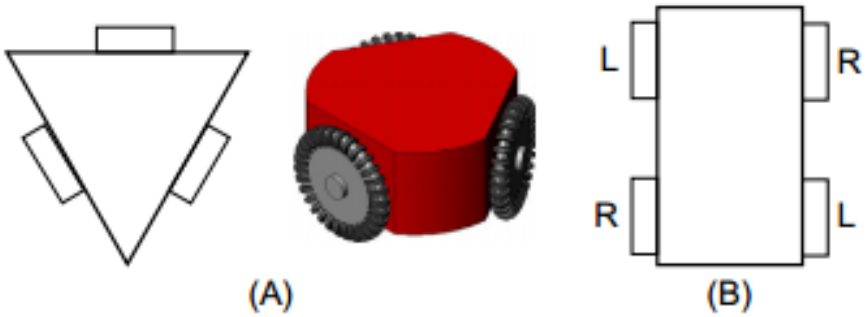

Figure 2.5. *Omnidirectional WMR drive*

Synchro drive. This drive has three or more wheels that are mechanically coupled such that all of them rotate in the same direction at the same speed and rotate together about their own steering axes when perform a turn. This mechanical steering synchronization can be realized in several ways, for example, using a chain, a belt or gear drive. Actually, synchro drive is an extension of a single driven and steered wheel and so it still has only two DOF. But a synchro drive WMR is nearly a holonomous vehicle because it can move in any desired direction. However, it cannot drive and rotate at the same time. To change its driving from forward to sideways this WMR must stop and realign its wheels. Figure 2.9 shows pictorially how a three-wheel WMR with synchro drive is moving and rotated.

Ackerman steering. This is the standard steering used in automobiles. It consists of two combined driven rear wheels and two combined steered front wheels. An Ackerman-steered vehicle can move straight (because the rear wheels are driven by a common axis), but cannot turn on the spot (it requires a certain minimum radius). The rear driving wheels experience slippage (when moving in curves). Ackerman steering is designed so as to ensure that at turns the wheels of all axes have a common cross point (instantaneous center of rotation (ICR)), in order to avoid geometrically caused wheel slippage.

Skid steering. This is a special implementation of differential drive and realized in track form on bulldozer vehicles. Its difference from a differential drive vehicle is the increased maneuverability in uneven terrains, and the higher friction which is due to its tracks and the multiple contact points with the terrain (rough or even).

2.5 Wheel Geometry

The choice of wheel types for a mobile robot is strongly linked to the choice of wheel arrangement, or wheel geometry. As a mobile robot designer, one must consider these two issues simultaneously when designing the locomotion mechanism of a wheeled robot.

Wheel type and wheel geometry is a very crucial matter because the three fundamental characteristics of a robot are governed by these choices: maneuverability, controllability, and stability [10].

Stability

Surprisingly, the minimum number of wheels required for static stability is two. A two-wheel differential-drive robot can achieve static stability if the center of mass is below the wheel axle. However, under ordinary circumstances such a solution requires wheel diameters that are impractically large. Dynamics can also cause a two-wheeled robot to strike the floor with a third point of contact, for instance, with sufficiently high motor torques from standstill. Conventionally, static stability requires a minimum of three wheels, with the additional caveat that the center of gravity must be contained within the triangle formed by the ground contact points of the wheels. Stability can be further improved by adding more wheels, although once the number of contact points exceeds three, the hyper static nature of the geometry will require some form of flexible suspension on uneven terrain [14].

Maneuverability

Some robots are omnidirectional, meaning that they can move at any time in any direction along the ground plane regardless of the orientation of the robot around its vertical axis. This level of maneuverability requires wheels that can move in more than just one direction.

Controllability

There is generally an inverse correlation between controllability and maneuverability. For example, the omnidirectional designs such as the four-castor wheel configuration require significant processing to convert desired rotational and translational velocities to individual wheel commands. Therefore controlling an omnidirectional robot for a specific direction of travel is also more difficult and often less accurate when compared to less maneuverable designs. In a differential-drive vehicle, the two motors attached to the two wheels must be driven along exactly the same velocity profile, which can be challenging considering variations between wheels, motors, and environmental differences.

In summary, there is no “ideal” drive configuration that simultaneously maximizes stability, maneuverability, and controllability. Each mobile robot application places unique constraints on the robot design problem, and the designer’s task is to choose the most appropriate drive configuration possible from among this space of compromises.

Chapter 3

Conceptual Design

Quality Function Deployment (QFD) of the project

QFD is a tool to understand the problem and develop the engineering specification. It drives model and prototype development and evaluation. It is a method for developing a design quality to satisfy the consumer and then translating the consumer's demand into design targets. It is a structured procedure used to translate the expressed or perceived needs of customers first into specific product or service design characteristics and features, and then into process and operational characteristics.

In this section QFD is developed for designing a mobile robot AGV.

Step1: CUSTOMER IDENTIFICATION

The customer that is involved in the product of this project is EPHARM pharmaceutical industry. EPHARM is a very relevant factory in Ethiopia creating healthy environment throughout the country by providing qualified medicines for the past 50 years. The factory has eight production lines, and each has its own code.

1. Code -1- Capsule
2. Code -2- Vials
3. Code -3- Tablets
4. Code -4- IV
5. Code -5- Syrup
6. Code -6- Ampoules
7. Code-7- Ointment
8. Code -8- ORS

Six of the products are manufactured at the main branch located at Bisrate Gebriel Addis Ababa. And the rest is manufactured at Sarbet Addis Ababa. The firm employs about 570 employees.

Building information

There are two stores in the company, raw material and finished product store. The raw

material coming from the raw material store undergoes to the process after getting the approval from some chemical analysis. And will be released to market from the finished product store as a finished product after getting the approval from quality control department. The store at which the AGV material handling system will implemented on is the finished product store.

The detailed building information in which the AGV is expected to work is shown in the figure below:

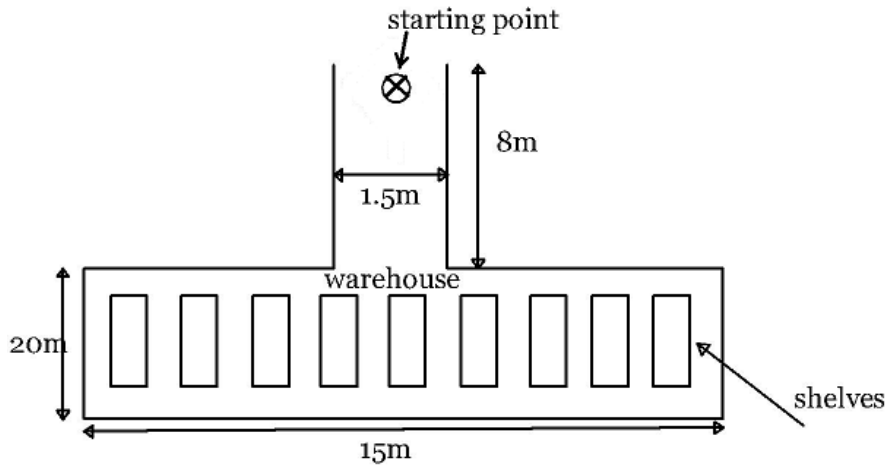

Figure 3.1. *Operational area of the AGV*

STEP2: CUSTOMER REQUIREMENTS

Basically there are two properties of requirements

Orthogonal: each requirement must uniquely identify a characteristic of the product. Eliminate requirements that are dependent..

1. Maneuverability: the ability of the system to move in narrow space and change direction.
2. Stability: stable with respect to external disturbances and must be safe for the user-interface device.
3. Controllability: the ability of the robot to move in the required direction with desired speed
4. Lifting capacity: it is required that the robot must lift maximum weight of 100 kg
5. Dynamic performance: it is expected that our robot to move at average speed of 60m/min
6. Compactness: describes the amount of space taken by the robot
7. Autonomous: collision avoidance, path detection and independent battery source.
8. Cost: the cost outflowed to implement this robot must be minimized.

STEP 3: RELATIVE IMPORTANCES OF REQUIREMENTS

The goal of this step is the definition of the importance of each requirement of each requirement by giving a weight. The best way to define the weight is the definition of a relative scale. If the requirements have the same relative importance, verify that they are orthogonal. Rate 1 if it is more important, or 0 if it is less important or equally important.

Table 3.1. *Relative importance of customer requirements*

	Maneuverable	Stability	Controllability	Lift capacity	Dynamics	Compactness	Autonomy	Cost	Score
Maneuverability	-	1	1	1	1	1	1	1	7
Stability	0	-	0	1	1	1	1	1	5
Controllability	0	0	-	0	1	1	1	0	3
Lifting capacity	0	0	1	-	1	0	0	0	2
Dynamic performance	0	0	0	0	-	0	1	0	1
Compactness	0	0	0	1	1	-	0	0	2
Autonomous	0	0	0	1	1	1	-	0	3
Cost	1	0	1	0	0	1	1	-	4

STEP 4:- IDENTIFY AND EVALUATE COMPETITORS

The goal of this step is to understand the consumer perception of the ability of competitors to meet the requirements (Competition benchmarking). And create awareness of what is already available in the market now and also highlights the chance to improve what is already available.

Each selected product is going to be evaluated against the requirements according to the following scale:

The product does not satisfy the requirement: (1); the product slightly satisfies the requirement: (2); the product somehow satisfies the requirement: (3); the product quite satisfies the requirement: (4); the product fully satisfies the requirement: (5).

In our case the product for benchmark evaluation is an AGV more specifically an autonomous forklift which is expected to work in a pharmaceutical industry. There are different competitors such as Toyota Toyota Material Handling Europe,[1] Egemin Automation, JBT forklift AGVs are used.

Table 3.2. *Evaluation of competing AGV products against customer requirements*

	Toyota	Egemin Automation	JBT	Our design
Maneuverability	3	4	4	4
Stability	5	4	4	4
Controllability	4	5	3	5
Lifting capacity	3	3	4	3
Dynamic performance	5	2	5	4
Compactness	4	4	2	4
Autonomous	4	4	4	3
Cost	2	2	3	5

STEP 5: IDENTIFY ENGINEERING SPECIFICATIONS

The goal of this step is to transform the customer requirements into objective, measurable quantities (engineering specifications). Each specification must be expressed in physical or technical units so that it can be verified by measurement or test.

[1] http://www.bt-forklifts.com

Table 3.3. *Physical and technical engineering specification priorities*

Physical specification	Unit	Priority
Overall length	m	70
Overall width	m	70
Overall collapsed height	m	70
Max lifting height	m	90
Fork dimension	mm	50
Wheel radius	mm	100
Under clearance	m	80
Weight of the AGV	Kg	60
Technical specification	Unit	Priority
Battery life	Hours	80
Travel speed	m/min	100
Wheel motor power	W	70
Lift speed	m/min	90
Lowering speed	m/min	90
Load capacity	Kg	100

STEP 6: RELATIONS AMONG REQUIREMENT AND SPECIFICATION

The goal of this step is to understand the relationship between the engineering specifications and the customer requirements. This check ensures that every customer requirement is covered by at least one engineering specification. The relationship strength is encoded using the standard HOQ symbols: **9** = strong relationship, **3** = moderate relationship, **1** = weak relationship, and **0** = no relationship. The priority score for each specification is computed as the sum of (relationship value $\times$ customer-requirement score) across all requirements.

Table 3.4. *Relationship between customer requirements and physical specifications (House of Quality)*

	Score	Dimension	Lift height	Fork dimension	Wheel radius	clearance	Weight
Maneuverability	7	3	0	0	9	1	3
Stability	5	9	3	0	9	3	9
Controllability	3	1	1	0	9	1	3
Lifting capacity	2	9	9	9	1	1	9
Dynamic performance	1	3	3	0	9	9	3
Compactness	3	9	3	3	1	1	3
Autonomous	1	0	0	0	1	0	1
Cost	4	3	3	3	1	1	3
Physical priority		129	60	39	154	43	118
Physical difficulty		2	3	2	2	1	3

Table 3.5. *Relationship between customer requirements and technical specifications (House of Quality)*

	Score	Battery life	Travel speed	Wheel Power	Lift speed	Load
Maneuverability	7	0	9	1	0	3
Stability	5	0	9	1	3	9
Controllability	3	0	9	1	0	3
Lifting capacity	2	9	0	0	9	9
Dynamic performance	1	9	9	9	3	9
Compactness	2	1	1	1	1	9
Autonomous	3	9	3	1	1	3
Cost	4	3	9	3	3	9
Technical priority		68	191	41	53	165
Technical difficulty		2	3	3	2	1

STEP 7: ENGINEERING TARGETS

The goal of this step is the identification of a target value for each specifications and the possible maximum and minimum value. It is an overall evaluation of the specification with respect to requirements. The final priority of the specification is the sum of the single priorities with respect to requirements.

Table 3.6. *Maximum and minimum values of physical specifications*

Physical specification	Unit	Max value	Min value
Overall length	M	3.52	1.89
Overall width	M	1.118	0.6
Overall collapsed height	M	2.34	1.26
Max lifting height	M	3.43	1.84
Fork dimension	mm	49.4×131.3	26.6×70.7
Wheel radius	mm	169	91
Under clearance	M	0.065	0.035
Weight of the AGV	Kg	390	210

Table 3.7. *Maximum and minimum values of technical specifications*

Technical Specification	Unit	Max value	Min value
Battery life	Hours	7.8	4.2
Travel speed	m/min	78	42
Wheel motor power	W	650	350
Lift speed	m/min	16.9	9.1
Lowering speed	m/min	19.5	10.5
Load capacity	Kg	130	70

Table 3.8. *Engineering targets of physical specifications*

Physical specification	Unit	Desired value
Overall length	M	2.71
Overall width	M	0.86
Overall collapsed height	M	1.8
Max lifting height	M	2.64
Fork dimension	mm	38×101
Wheel radius	mm	130
Under clearance	M	0.05
Weight of the AGV	Kg	300
Technical specification	Unit	Priority
Battery life	Hours	6
Travel speed	m/min	80
Maximum acceleration	m/sec	0.26
Wheel motor power	W	500
Lift speed	m/min	13
Lowering speed	m/min	13
Load capacity	Kg	100

Chapter 4

Design and Analysis of the Mechanical System

This section discusses the design and selection of different mechanical parts of the robot. Locomotion mechanisms can be classified the mechanical system in to two major subsystems. The chassis which is the system that carries the load of the components and act as a frame for attaching other components. And the steering system which is used to create the desired motion of the robot. As it's discussed in the second chapter, the selected steering system of our robot is of a differential type. The chassis of our robot consists the structure that supports the components of the steering system, the counterbalance weight, the structure that supports the components of the lifting mechanism and the lifting mechanism itself.

4.1 Selection of Lifting Mechanism for the Forklift

There are a number of mechanisms and material handling equipment that can be used to create the required motion of the fork of the vehicle. Among them hydraulic system is the commonly used type of lifting mechanism in conventional manually operated forklifts. The advantages of hydraulic systems that makes them preferable in conventional forklift types are they doesn't require larger space to implement, less wear, high efficiency, consistence delivery of power etc... but hydraulic systems have also the following disadvantages that makes them inappropriate for our specific application there is always leaking of the oil which is totally undesired situation in the pharmaceutical environment, High power requirement, increases the structural weight and size of the system, high capital cost [15]. Due to the stated disadvantages of using hydraulic systems as a lifting mechanism we can't use it for our application. And the design has to select an appropriate lifting mechanism for our vehicle that can operate in the environment effectively.

Among material handling mechanisms the most common types of equipment are pneumatic systems, power screws and wire ropes. What we will do in this section is to compare the advantages and disadvantages of each alternatives one by one based on our application requirements.

Pneumatic systems are systems that uses pressurized gases (mostly air) in order to perform the desired task of the actuator. These systems have a number of advantages such as the working fluid (Air) is abundantly available, return line for the fluid is not necessary, high speed of actuation and explosion and fire safety. But pneumatic systems have also many draw backs that makes them inappropriate for our specific task. Among these drawbacks the major ones are they are less controllable, have high initial cost, increases the structural weight and size of the system and requires high amount of power.

Power screw is a mechanical device that is used to convert the rotational motion into translational motion by using the action of screw and nut [15]. This device have the following advantages that makes it suitable for our application among them the followings are the major ones it can provide large mechanical advantage, highly accurate and precisely controlled linear motion, smooth and noiseless service without maintenance, can be designed with self-locking property and they are compact in their construction. The major disadvantage of power screws is high friction in threads cause rapid wear of the screw or the nut therefore it requires proper and timely maintenance.

4.2 Determining Forklift Truck Capacity Requirement

Generally forklift trucks work on the principle of a load counterbalanced over a fulcrum; the same principle as a seesaw. The weight of the forklift truck counterbalances the load on the forks. The fulcrum or pivot point of the "seesaw" is the centerline of the front wheels of the truck.

The capacity rating of a forklift truck defines the maximum load that the truck can safely handle. The capacity rating of a forklift truck has two components: Weight and Load Center. The weight is simply the weight of the load. The load center of the load is also known as the horizontal center of gravity of the load, see figure below [1]. For uniform loads which have uniform weight distribution from one end to the other, the load center is in the middle or center of the load; i.e. at that point that is half of its length. The free body diagram of the system will be

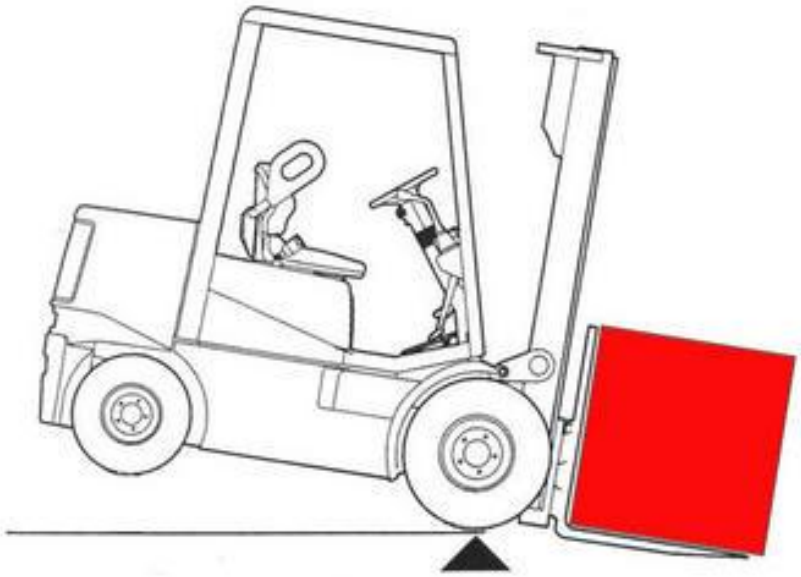

Figure 4.1. *Free body diagram of the forklift*

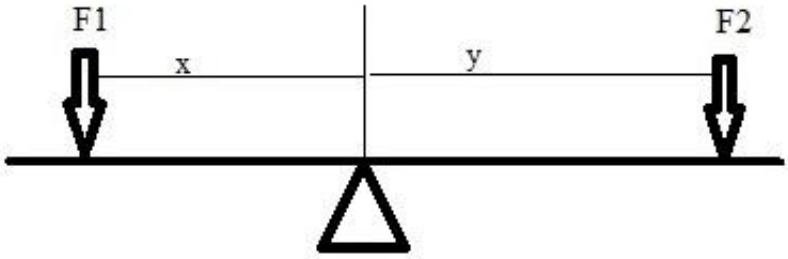

Figure 4.2. *Free body diagram of the forklift (side view)*

where F_1 is the generalized force acting to the left of the front wheels, F_2 is the generalized force acting to the right, X is the distance from the centroid of the left-side mass to the front wheels, and Y is the corresponding distance for the right-side mass. Applying the moment equation at the front wheels

$$M_o = F_1 X - F_2 Y = 0 \tag{4.1}$$

F2= (weight of the frame supporting the lifting mechanism) + (weight of the screw, bearings and the motor) + (weight of the fork) + (maximum weight of the load)

$F2 = (40 + 11.8 + 7 + 7 + 100)Kg = 165.8\,\text{kg}$

F1= (weight of the frame that supports the counterbalance) + (weight of the back wheels, battery, motors and other electrical components) + (weight of the counterbalance)

$F1 = 16.36 + 5 + 0.54 + 15 + 3 + CB = 40 + CB$

From Equation (4.1)

$$F1 = \frac{F2 \times Y}{X} = \frac{165.8 \times 37}{27.5} = 223\,\text{kg} \tag{4.2}$$

$CB = F1 - 40 = 183\,\text{kg}$

4.3 Physical Modeling of the System

The following assumptions are taken into account while modelling the system

The model uses the following assumptions: spring elements resist deflection linearly ($F = K(X_1 - X_2)$ translational; $\tau = K(\theta_1 - \theta_2)$ rotational); damper elements resist motion linearly ($F = B(\dot{X}_1 - \dot{X}_2)$ translational; $\tau = B(\dot{\theta}_1 - \dot{\theta}_2)$ rotational); wheels do not slip on the surface; and permanently joined mechanical parts are treated as a single mass.

The physical modeling of the system is done by isolating the independent motions of the system and applying the newton's equations of motion for each free body diagram of the independent motion. Considering the system carefully, we can have two independent motions on the vehicle. The first one is the horizontal motion of the vehicle which is caused by the rotational motions of the two front wheels. The other is the vertical motion of the fork that is caused by the mutual action of the screw and the motor that actuates the screw. Therefore in the following session we will start to study each motions independently.

Horizontal motion of the vehicle. Consider the free body diagram of the whole vehicle to find the equivalent single mass of the system.

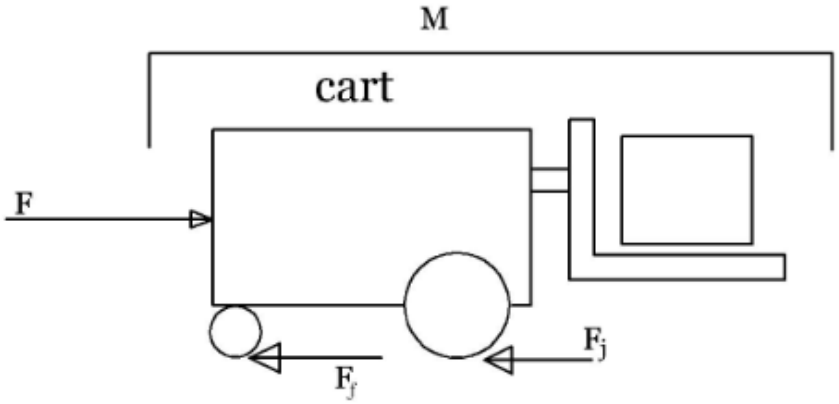

Figure 4.3. *Free body diagram of the whole vehicle.*

where M is the mass of the whole system, m_f is the mass of one front wheel, and m_b is the mass of one back wheel. Note that F_J is not a friction force: although it arises from the wheel–surface contact, it is the reaction force required to accelerate the rotational inertia of the wheel. F_f is the sliding friction force between the back wheels and the surface. Applying Newton's second law to the vehicle

$$(M + 2m_f + 2m_b)\ddot{x} = F - 2F_J - 2F_f$$

Applying the newton's second law of motion on one wheel

$$\tau = J\dot{\omega} = F_J r \tag{4.3}$$

Assuming no slip condition

$$v = \dot{x} = \omega r, \quad \omega = \frac{\dot{x}}{r}, \quad \dot{\omega} = \frac{\ddot{x}}{r} \tag{4.4}$$

Substituting $\dot{\omega} = \frac{\ddot{x}}{r}$ into the wheel equation

$$F_J = \frac{J}{r^2}\ddot{x} \tag{4.5}$$

Back substituting the expression for F_J into the vehicle equation

$$(M + 2m_f + 2m_b)\ddot{x} = F - 2\frac{J}{r^2}\ddot{x} - 2F_f$$

$$(M + 2m_f + 2m_b + 2\frac{J}{r^2})\ddot{x} = F - 2F_f$$

$$M_{\text{equ}} = \left(M + 2m_f + 2m_b + \frac{2J}{r^2}\right) \tag{4.6}$$

$$F_f = \mu \times g \times M_{\text{equ}} \tag{4.7}$$

$$F = M_{\text{equ}}\ddot{x} + (2 \times \mu \times g \times M_{\text{equ}}) \tag{4.8}$$

From the quality function deployment (QFD) analysis the design has maximum expected acceleration of the robot to be 0.26 m/s. Now let us model the system with horizontal motion using physical elements (mass, spring and damper)

$$M_{\text{equ}}\ddot{X} = F - 2(K_1 + K_2)X - 2(C_1 + C_2)\dot{X} \tag{4.9}$$

where K_1 and K_2 the spring constants of the front and back wheels respectively and C_1 and C_2 are the damping constants of the front and back wheels.

$$F = 2(K_1 + K_2)X + 2(C_1 + C_2)\dot{X} + M_{\text{equ}}\ddot{X} \tag{4.10}$$

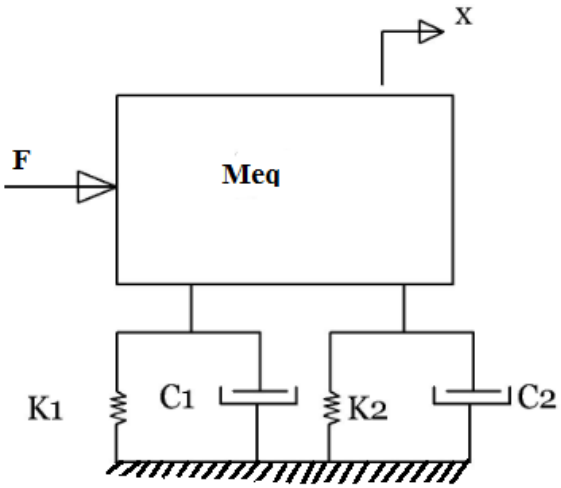

Figure 4.4. *Physical model of the whole system*

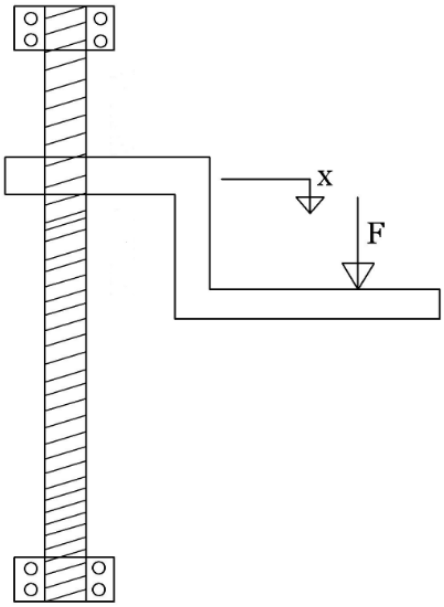

Figure 4.5. *Lifting mechanism overview: schematic and free body*

$$\frac{F(s)}{X(s)} = M_{\text{equ}}s^2 + 2(C_1 + C_2)s + 2(K_1 + K_2) \tag{4.11}$$

Modelling of the lifting mechanism: The free body diagram of the fork is shown below.

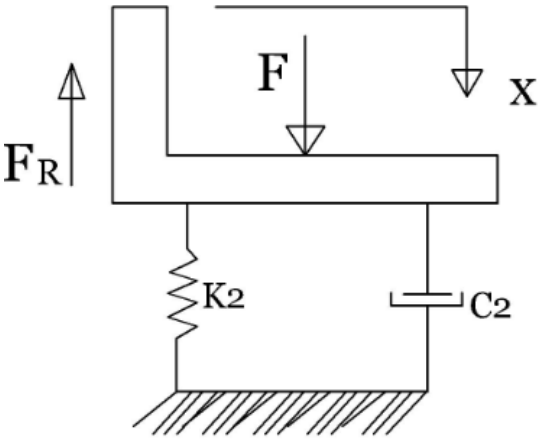

Figure 4.6. *Schematic diagram of the lifting mechanism.*

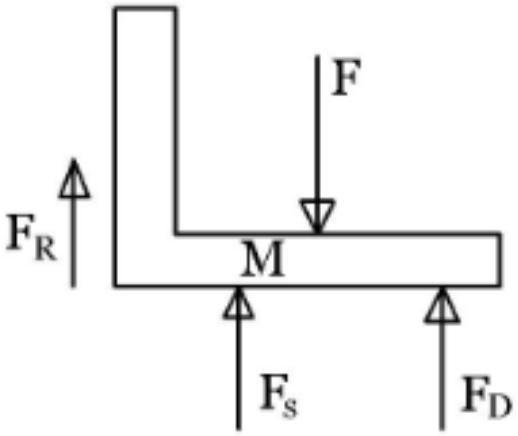

Figure 4.7. *Free body diagram of the fork.*

Applying newton's second law

$$\overrightarrow{F} = M\overrightarrow{a} = F - F_R - F_S - F_D = M\ddot{X} \tag{4.12}$$

$$F - F_1 - C_2\dot{X} - K_2X = M\ddot{X} \tag{4.13}$$

where F_R is the reaction force exerted by the screw on the fork, $F_S = K_2X$ is the spring

(stiffness) force, $F_D = C_2\dot{X}$ is the damping force, and F is the weight of the load to be lifted. The free body diagram of the screw is shown below.

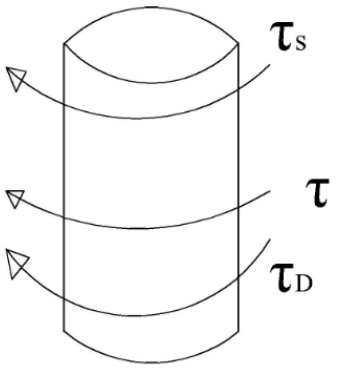

Figure 4.8. *Free body diagram of the screw.*

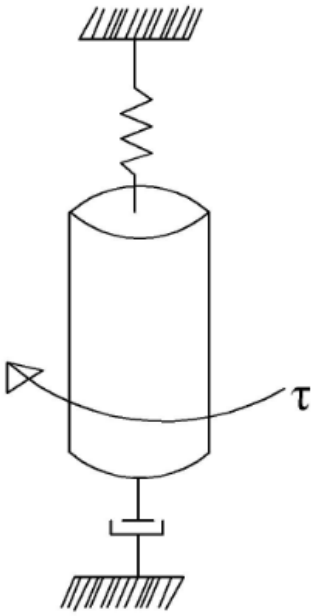

Figure 4.9. *Free body diagram of the screw.*

$$\tau = J\alpha = \tau - \tau_s - \tau_D = J\ddot{\theta} \tag{4.14}$$

$$J\ddot{\theta} = \tau - C_1\dot{\theta} - K_1\theta \tag{4.15}$$

noting the relationship between x and θ $X = \frac{P}{2\pi}\theta$, where P is pitch $X = N\theta$ and $N = \frac{P}{2\pi}$. Assuming the lead screw to be ideal (no friction present) there is 100% efficiency in power conversion from linear to the rotational motion domain. Therefore:

$$F_R X = \tau\theta \tag{4.16}$$

Taking the Laplace transform of the fork equation and the screw equation

$$F(s) - F_R(s) = (Ms^2 + C_2 s + K_2)X(s) \tag{4.17}$$

$$\tau(s) = (Js^2 + C_1 s + K_1)\theta(s) \tag{4.18}$$

$$F(s) - (Js^2 + C_1 s + K_1)\frac{X(s)}{N^2} = (Ms^2 + C_2 s + K_2)X(s) \tag{4.19}$$

$$\frac{X(s)}{F(s)} = \frac{1}{\left(M + \frac{J}{N^2}\right)s^2 + \left(C_2 + \frac{C_1}{N^2}\right)s + \left(K_2 + \frac{K_1}{N^2}\right)} \tag{4.20}$$

4.4 Design of Some Basic Mechanical Machine Elements

Under this section we will discuss the mechanical design of some components of the robot in order to check whether the components will fail or not. And also to calculate the maximum torque required to be exerted by the motor to actuate the system. Here the design of the power screw, the fork, the gear set at the screw and at the wheels are discussed.

Bending stress analysis of the fork

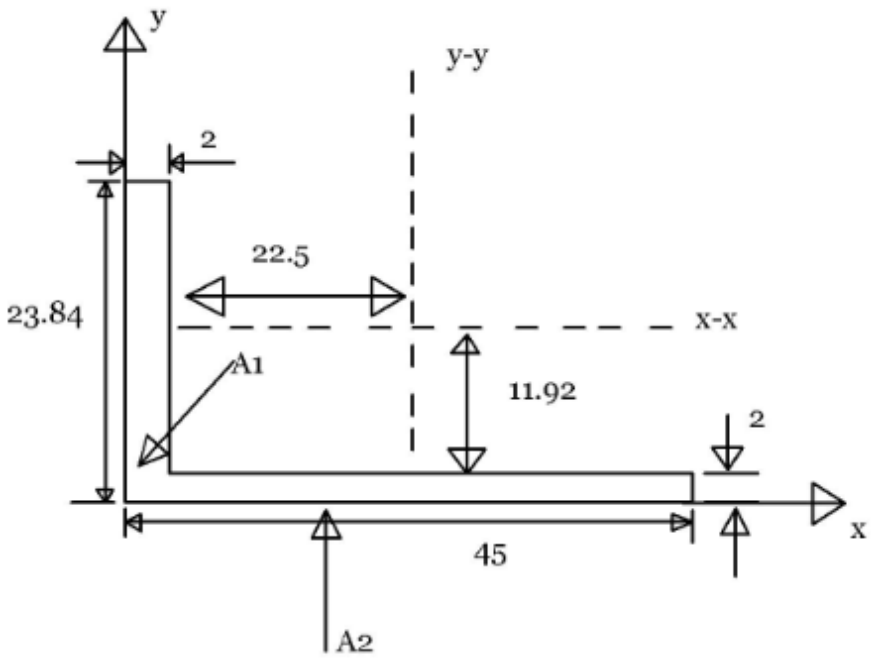

Figure 4.10. *Bending stress analysis of the fork*

Note the dimensions of the fork are taken from the dimensions of standard pallets

First let us find the moment of inertia (I)

$A_1 = (23.84 - 2) \times 2 = 43.68\,\text{cm}^2$

$A_2 = 45 \times 2 = 90\,\text{cm}^2$

Moment of inertia along X-X axis

Y_1= 11.92cm Y_2=1cm

$$Y' = \frac{(A_1 \times Y_1) + (A_2 \times Y_2)}{(A_1 + Y_1)} \tag{4.21}$$

$$Y' = \frac{43.68 \times 11.92 + 90 \times 1}{(43.68 + 90)} = 4.5cm \tag{4.22}$$

$$I_{xx1} = \frac{b_1 h_1^3}{12} + A_1(Y')^2 = \frac{2 \times (11.92)^3}{12} + 43.68 \times (4.5)^2 = 1166.8\,\text{cm}^4 \tag{4.23}$$

Moment of inertia along Y-Y axis X_1= 1cm X_2=22.5

$$X' = \frac{(A_1 \times X_1) + (A_2 \times X_2)}{(A_1 + A_2)} \tag{4.24}$$

$$X' = \frac{(43.68 \times 1) + (90 \times 22.5)}{(43.68 + 90)} = 15.47cm \tag{4.25}$$

$$I_{yy1} = \frac{b_1 \times h_1^3}{12} + A_1 \times (d_1)^2 \tag{4.26}$$

where $d_1 = (X_1 - X'_1)$

$$I_{yy} = \frac{43 \times 2^3}{12} + 43.68 \times (1 - 15.47)^2 = 9174.4 \text{ cm}^4 \tag{4.27}$$

$$I_{yy} = \frac{b_2 \times h_2^3}{12} + A_2 \times (d_2)^2 \tag{4.28}$$

where $d_2 = (X_2 - X')$

$$I_{yy} = \frac{2 \times 45^3}{12} + 90 \times (7.03)^2 = 19635.4\text{cm}^4 \tag{4.29}$$

$$I_{\text{yy}} = I_{yy1} + I_{yy2} = 9174.4 + 19635.4 = 28809.7\text{cm}^4 \tag{4.30}$$

The fork is loaded vertically (gravity acts downward on a horizontal fork arm), so bending occurs about the horizontal X–X axis only. Therefore only I_{xx} is the relevant second moment of area; I_{yy} applies to lateral bending and is not used here.

$$I = I_{xx} = 1166.8\,\text{cm}^4 \tag{4.31}$$

$$\sigma = \frac{M \cdot Y}{I} \tag{4.32}$$

where σ is the bending stress, M is the bending moment, and Y is the distance from the neutral axis to the outermost fibre in the bending plane. Bending moment (M) = force × perpendicular distance = $(120 \times 9.81)\,\text{N} \times 0.225\,\text{m}$, $M = 264.87\,\text{N m}$. Maximum distance from neutral axis: $Y = h_1 - Y' = 11.92 - 4.5 = 7.42\,\text{cm} = 0.0742\,\text{m}$

$$\sigma = \frac{M \cdot Y}{I_{xx}} = \frac{264.87 \times 0.0742}{1166.8 \times 10^{-8}} = 1.68\,\text{MPa} \tag{4.33}$$

Therefore by taking the factor of safety to be 2 in order to make the design safe, a material having a yield strength of more than $2 \times 1.68 = 3.36\,\text{MPa}$ should be selected.

Material selection

While selecting an appropriate material type for a given mechanical part the design has

to consider some important factors. Among those factors the major ones are:

Mechanical properties of the material: these are properties of the material that determines the ability of the material to resist the stress and loads applied to it. Therefore, the material which is going to be selected must have properties that qualifies the expected level of performance. Here the design has to select a material with a yielding stress of more than 3.36 MPa.

Material cost and material's availability: when considering the cost of a certain material, the design has to carefully study both material's purchasing and processing (manufacturing) costs. Since the cost of the material have a huge effect on the affordability of the robot, the design has to select a material with an appropriate amount of cost that doesn't make the cost of the robot more than the customer affording capacity.

The manufacturing process in which the material is going to pass is also another important factor while selecting a material for our design. The manufacturing process of the fork is mostly undertaken by welding. Hence the material which is going to be selected have to be easy to weld.

Environment: before deciding to select the material based on the above criteria the design has to make sure the suitability of the material in that specific condition of service.

By considering the above factors the design has decided to choose our material from the family of ferrous metals. Because this metals are known by their high strength to weight ratio, high availability, versatility, easy repair and durability. Within the family of ferrous metals there are three major material types, namely cast iron, wrought iron and steel. Cast iron is well known for its low cost, good casting characteristics, high compressive strength and wear resistance [kurmi p20]. Wrought iron have good malleability and ductility. And steel is well known for its high strength and durability that makes it popular for the application of making structures exposed to high amount of stress.

Table 4.1. *Comparison of ferrous metals for structural frame selection*

	Mechanical property	Cost & Availability	Manufacturing process	Environment
Cast Iron	Good	Best	Good	Good
Wrought Iron	Good	Bad	Bad	Good
Steel	Best	Good	Good	Good

As we can clearly see form the comparison table the best material type for the application of the fork is steel. Among the other steel types, based on its mechanical properties, steel type with AISI number of 1006 is selected from Table 20 of Richard_G._Budynas,_J._Keith_Nis_shigley. Eighth edition (2008). Mechanical Engineering Design., page1020

Design of the power screw. The design data are as follows: major diameter $d = 32\,\text{mm}$ (length $= 2\,\text{m}$) [15]; pitch $P = 4\,\text{mm}$; number of starts $n = 1$ (single-start thread); load to be lifted $F = 120 \times 9.81 = 1.2\,\text{kN}$; coefficient of friction $f = 0.08$.

Self-locking check. For a power screw to be self-locking the lead must satisfy $l \leq \pi f d_m$ [15]. The mean diameter is

$$d_m = d - \frac{P}{2} = 32 - \frac{4}{2} = 30\,\text{mm} \tag{4.34}$$

With $n = 1$ start: $l = n \times P = 1 \times 4 = 4\,\text{mm}$.

Maximum self-locking lead: $\pi f d_m = \pi \times 0.08 \times 30 = 7.54\,\text{mm}$.

Since $l = 4\,\text{mm} < 7.54\,\text{mm}$, the self-locking condition is satisfied. (The original two-start design with $l = 8\,\text{mm}$ was *not* self-locking because $8 > 7.54\,\text{mm}$, which would allow the load to back-drive the screw under gravity; the single-start design eliminates this safety hazard.)

Torque required to raise the load:

$$\tau_R = \frac{F\,d_m}{2}\left(\frac{l + \pi f d_m}{\pi d_m - f l}\right) \tag{4.35}$$

where l is the lead, d_m is the mean diameter, and f is the coefficient of friction.

$$\tau_R = \frac{1.2 \times 10^3 \times 30 \times 10^{-3}}{2}\left(\frac{4 \times 10^{-3} + \pi \times 0.08 \times 30 \times 10^{-3}}{\pi \times 30 \times 10^{-3} - 0.08 \times 4 \times 10^{-3}}\right) = 2.21\,\text{Nm} \tag{4.36}$$

Torque required to lower the load:

$$\tau_L = \frac{F\,d_m}{2}\left(\frac{\pi f d_m - l}{\pi d_m + f l}\right) \tag{4.37}$$

$$\tau_L = \frac{1.2 \times 10^3 \times 30 \times 10^{-3}}{2}\left(\frac{\pi \times 0.08 \times 30 \times 10^{-3} - 4 \times 10^{-3}}{\pi \times 30 \times 10^{-3} + 0.08 \times 4 \times 10^{-3}}\right) = +0.674\,\text{Nm} \quad (4.38)$$

The positive value of τ_L confirms that the screw is self-locking: an external torque must be applied to lower the load, and the screw will hold the fork stationary when the motor is de-energised.

Overall efficiency in raising the load:

$$e = \frac{F\,l}{2\pi\tau_R}, \quad e = \frac{1.20 \times 10^3 \times 4 \times 10^{-3}}{2 \times \pi \times 2.21} = 0.346 \quad (4.39)$$

The body shear stress τ due to torsional moment T_R at the outside of the screw body is:

$$\tau = \frac{16\,T_R}{\pi d^3} = \frac{16 \times 2.21}{\pi \times (28 \times 10^{-3})^3} = 514.3\,\text{kPa} \quad (4.40)$$

The axial nominal normal stress is:

$$\sigma = \frac{-4F}{\pi d_r^2} = \frac{-4 \times 1.2 \times 10^3}{\pi(28 \times 10^{-3})^2} = -1.95\,\text{MPa} \quad (4.41)$$

The thread bearing (crushing) stress with one thread in contact is:

$$\sigma_B = \frac{-2(0.38\,F)}{\pi d_m(1)P} = \frac{-2 \times 0.38 \times 1.2 \times 10^3}{\pi \times 30 \times 10^{-3} \times 1 \times 4} = -2.42\,\text{MPa} \quad (4.42)$$

The thread root bending stress with one thread is:

$$\sigma_b = \frac{6 \times 0.38 \times F}{\pi d_r(1)P} = \frac{6 \times 0.38 \times 1.2 \times 10^3}{\pi \times 28 \times 10^{-3} \times 4} = 7.77\,\text{MPa} \quad (4.43)$$

Therefore the two principal stress will be given by [15]

$$\sigma_{1,2} = \frac{\sigma_z + \sigma_y}{2} \pm \sqrt{\left(\frac{\sigma_z - \sigma_y}{2}\right)^2 + \tau^2} = -1.21 \pm 6.19 \quad (4.44)$$

Therefore $\sigma_1 = -7.4\,\text{MPa}$ and $\sigma_2 = 4.98\,\text{MPa}$

Since there is no shear stress on the X face, σ_x is also a principal stress, Ordering the principal stress gives σ_1,σ_2, σ_3 = 7.77 MPa, 4.98 MPa, -7.4 MPa.

Substituting this values in the equation for the Von Mises stress [15]

$$\sigma' = \left[\frac{(\sigma_1 - \sigma_2)^2 + (\sigma_2 - \sigma_3)^2 + (\sigma_3 - \sigma_1)^2}{2}\right]^{1/2} \tag{4.45}$$

$$\sigma' = [\frac{(7.77 - 4.98)^2 + (4.98 + 7.4)^2 + (-7.4 - 7.77)^2}{2}]^{1/2} = 13.98\,\text{MPa} \tag{4.46}$$

The maximum shear stress (τ_{max}) is given by

$$\tau_{\max} = \frac{\sigma_1 - \sigma_3}{2} = \frac{7.77 - (-7.4)}{2} = 7.58\,\text{MPa} \tag{4.47}$$

$$\sigma_1 - \sigma_3 = \frac{S_y}{n} \tag{4.48}$$

or equivalently

$$\tau_{\max} = \frac{S_y}{2n} \tag{4.49}$$

Where S_y the yield strength of the material and n is the factor of safety [15]

Considering the factor of safety (n) to be 2 the allowable yielding strength of the material of the power screw should be S_y =30.34 MPa or 30.32 MPa.

Design of gear set at the wheels The maximum power expected to be transmitted $(P)_{\max}$:

$$(P)_{\max} = \tau_{\max}\omega_{\max} \tag{4.50}$$

$$\tau_{\max} = \frac{F}{2} \times r \tag{4.51}$$

$$F = M_{\text{eq}}\ddot{x} + (2\text{ţ}gM_{\text{eq}}) \tag{4.52}$$

$$M_{\text{eq}} = M + 2m_f + 2m_b + \frac{2J}{r^2} \tag{4.53}$$

$$M_{\text{eq}} = 388.8 + 2 \times 3.88 + 2 \times 0.897 + \frac{2 \times 0.025}{12 \times 10^{-2}} = 398.77\text{kg} \tag{4.54}$$

$$F = 398.77 \times 0.26 + 2 \times 0.5 \times 9.81 \times 398.77 = 4015.6\,\text{N} = 4.01\,\text{kN} \tag{4.55}$$

Maximum torque is required to be transmitted by the motor when driving the vehicle with full loading:

$$\tau_{\max} = \frac{F}{2} \times r = \frac{4015.6}{2} \times 12 \times 10^{-2} = 241\text{Nm} \tag{4.56}$$

$$\omega_{\max} = \frac{V_{\text{lift}}}{r} = \frac{1.33}{12{\times}10^{-2}} = \frac{11.08\,r}{\text{s}} = 106\,r \tag{4.57}$$

$$P_{\max} = \tau_{\max}\omega_{\max} = 241 \times 11.08 = 2670.28\,\mathrm{W} = 2.67\,\mathrm{kW} = 3.6\,\mathrm{hp} \tag{4.58}$$

Design decision

The reduction ratio of spur gear will be 3:1. Function: 3.6 hp, 318 r, R=0.95, N=10cycle, K_o=1. Design factor for unquantifiable exigencies: n_d= 2. Tooth system: ϕ=20°. Tooth count: N_p = 12teeth, N_G = 36teeth. Material selected for gear design is grade 1 material with quality number (Q_v) 6; it is Nitralloy 135M which is alloy of steel that composed of carbon, silicon, chromium, aluminium and nickel: Quality number: Q_v = 6, grade 1 material. $m_B \geq 1.2$, then K_B = 1. Pitch: select diametrical pitch of P = 4teeth/in. Thus

$$d_p = \frac{N_p}{P} = \frac{12}{4} = 3in \tag{4.59}$$

$$d_G = \frac{N_G}{P} = \frac{32}{4} = 8in \tag{4.60}$$

From table 14-2 (Shigley p-718) we can get the value of Lewis form factor based on the number of teeth on both pinion and gear. Y_p = 0.245 and Y_G = 0.3775(interpolated). From figure 14-6(shigley p-733) the value of bending strength geometry factor J(Y_s) will be: J_p = 0.21 and J_G = 0.38. Pitch velocity (V):

$$V = \frac{\pi d_p n_p}{12} = \frac{\pi \times 3 \times 318}{12} = 250ft/min \tag{4.61}$$

Tangential component force transmitted load (W^t):

$$W^t = \frac{33000H}{V} = \frac{33000 \times 3.6}{250} = 475.2\,\mathrm{lbf} \tag{4.62}$$

$$B = 0.25(12 - Q_v)^{2/3} = 0.25(12 - 6)^{2/3} = 0.825 \tag{4.63}$$

$$A = 50 + 56(1 - B) = 50 + 56(1 - 0.825) = 59.77 \tag{4.64}$$

$$K_v = \left(\frac{A + \sqrt{V}}{A}\right)^B = \left(\frac{59.77 + \sqrt{250}}{59.77}\right)^{0.825} = 1.213 \tag{4.65}$$

$$K_R = 0.659 - 0.0759ln\,(1 - R) = 0.659 - 0.059ln\,(1 - 0.95) = 0.8863 \tag{4.66}$$

For N = 10cycle, stress cycle factor (Y_N and Z_N) from figure 14-14&15(shigley p-743):

$$(Y_N)_p = 1.3557N^{-0.0178} = 1.3557(10^9)^{-0.0178} = 0.937 \tag{4.67}$$

$$(Y_N)_G = 1.3557(N/4)^{-0.0178} = 1.3557(10^9/4)^{-0.0178} = 0.96 \tag{4.68}$$

$$(Z_N)_p = 1.4488N^{-0.023} = 1.4488(N)^{-0.023} = 0.9 \tag{4.69}$$

$$(Z_N)_G = 1.4488(N/4)^{-0.023} = 1.4488(N^9/4)^{-0.023} = 0.928 \tag{4.70}$$

As general rule, spur gear should have face width (F) is between 3 to 5 times circular pitch (p). Thus, $F = 4p = \frac{4\pi}{P} = \frac{4\pi}{4} = 3.14in.$

$$K_s = 1.192(\frac{F}{P})^{0.0535} = 1.192(\frac{3.14}{4})^{0.0535} = 1.133 \tag{4.71}$$

$$K_m = 1 + C_{\text{mc}}(C_{\text{pf}}C_{\text{pm}} + C_{ma}C_e) \tag{4.72}$$

$C_{\text{mc}} = 1$(uncrowned teeth) and $C_{\text{pm}} = C_{\text{e}} = 1$.

$$C_{\text{pf}} = \frac{F}{10d} - 0.0375 + 0.0125F = \frac{3.14}{10 \times 3} - 0.0375 + 0.0125 \times 3.14 = 0.106 \tag{4.73}$$

$$C_{ma} = A + BF + CF^2 \tag{4.74}$$

The value of empirical constant (A, B& C) obtained from table 14-9 (shigley p-738) for commercial, enclosed units: A=0.127, B=0.0158 and C= -0.93×10^{-4}

$$C_{ma} = A + BF + CF^2 = 0.127 + (0.0158 \times 3.14) - 0.93 \times 10^{-4} \times 3.14^2 = 0.175 \tag{4.75}$$

$$K_m = 1 + C_{\text{mc}}(C_{\text{pf}}C_{\text{pm}} + C_{ma}C_e) = 1 + 1\left[(0.106 \times 1) + (0.175 \times 1)\right] = 1.28 \tag{4.76}$$

$$I = \frac{\cos\phi \sin\phi}{2m_N} \frac{m_G}{m_{G+1}} \tag{4.77}$$

where, m_N= 1 for spur gear.

$$m_G = \frac{N_G}{N_P} = \frac{d_G}{d_P} = \frac{36}{12} = 3 \tag{4.78}$$

$$I = \frac{\cos\phi \sin\phi}{2m_N} \frac{m_G}{m_G + 1} = \frac{\cos 20^\circ \sin 20^\circ}{2 \times 1} \times \frac{3}{3+1} = 0.120 \tag{4.79}$$

Pinion tooth bending

With the above estimates of K_s and K_m from diametrial pitch, we check to see if the mesh width (F) is controlled by bending or wear consideration.

$$(F)_{\text{bend}} = n_d W^t K_o K_v K_s \frac{K_m K_B}{J_p} \frac{K_m K_R}{S_t Y_N} \tag{4.80}$$

From table 14-5(shigley p-730), the hardness range of Nitralloy 135M is Rockwell C32-36(306-335 Brinell). Choosing a midrange hardness as attainable, using 320 Brinell. From figure 14-4(shigley p-728), allowable bending stress (S_t) for Nitralloy 135M: $S_t = 86.2 \times 320 + 12730 = 40{,}314\,\text{psi}$. *From table 14-6(shigley p-731)* allowable contact

stress (S_c) for Nitralloy 135M: $S_c = 170{,}000$ psi. And temperature factor $K_T = 1$

$$(F)_{\text{bend}} = \frac{1.28 \times 1}{0.21} \times \frac{1 \times 0.8863}{40{,}314 \times 0.937} = 0.74\,\text{in} \tag{4.81}$$

Elastic coefficient (C_p) from table 14-8 (shigley p-737): $C_p = 2300$. Surface condition factor (C_f) specified by AGMA is greater than unity, $C_f = 1$

$$(F)_{\text{wear}} = \left(\frac{2300 \times 0.9}{170{,}000 \times 1 \times 0.8863}\right)^2 = 0.87\,\text{in} \tag{4.82}$$

Decision: Face width (F) = 0.9in, then correct the value of K_s and K_m

$$K_s = 1.192(\frac{F}{P})^{0.0535} = 1.192(\frac{0.9}{4})^{0.0535} = 1.06 \tag{4.83}$$

$$C_{ma} = A + BF + CF^2 = 0.127 + (0.0158 \times 0.9) - 0.93 \times 10^{-4} \times 0.9^2 = 0.133 \tag{4.84}$$

$$K_m = 1 + C_{\text{mc}}(C_{\text{pf}}C_{\text{pm}} + C_{ma}C_e) = 1 + 1\,[(0.05 \times 1) + (0.143 \times 1)] = 1.186 \tag{4.85}$$

Bending stress induced by W^t in bending

$$(\sigma)_p = W^t K_o K_v K_s \frac{P}{F} \frac{K_m K_B}{J_p} \tag{4.86}$$

$$(\sigma)_p = 475.2 \times 1 \times 1.213 \times 1.06 \times \frac{4}{0.9} \times \frac{1.183 \times 1}{0.21} = 15297.69\,\text{psi} \tag{4.87}$$

The AGMA factor of safety in bending of the pinion

$$(S_F)_p = \frac{(S_t(Y_N)_p)/(K_T K_R)}{(\sigma)_p} = \frac{(40{,}314 \times 0.937)/(1 \times 0.8863)}{15297.69\,\text{psi}} = 2.78 \tag{4.88}$$

Gear tooth bending

We use cast gear blank because of 9in pitch diameter and we use the same material, heat treatment and Nitriding of pinion gear. The load induced bending stress is in the ratio of $\frac{J_p}{J_G}$, then

$$(\sigma)_G = (\sigma)_p \frac{J_p}{J_G} = 15297.69\,\text{psi} \times \frac{0.21}{0.38} = 8453.98\,\text{psi} \tag{4.89}$$

The factor of safety of gear bending:

$$(S_F)_G = \frac{S_t(Y_N)_G/(K_T K_R)}{(\sigma)_G} = \frac{(40{,}314 \times 0.937)/(1 \times 0.8863)}{8692.81} = 5.04 \tag{4.90}$$

Pinion tooth wear

Contact stress on the pinion gear:

$$(\sigma_c)_p = C_p(W^t K_o K_v K_s \frac{K_m C_f}{d_p F I})^{1/2} \tag{4.91}$$

$$= 2300(475.2 \times 1 \times 1.213 \times 1.06 \times \frac{1.183 \times 1}{3 \times 0.9 \times 0.120})^{1/2} = 108634.87\,\text{psi} \tag{4.92}$$

Factor of safety of pinion wear:

$$(S_H)_p = \frac{S_c(Z_N)_p/(K_T K_R)}{(\sigma_c)_p} = \frac{(170{,}000 \times 0.9)/(1 \times 0.8863)}{108{,}634.97} = 1.589 \tag{4.93}$$

By our definition of factor of safety, pinion bending is $(S_F)_p = 2.78$ and wear is $(S_H)_p{}^2 = 1.56^2 = 2.52$. *Gear tooth wear* The hardness of the gear and pinion are the same. Thus from figure 14-12 (Shigley p-742), $C_H = 1$, then the contact stress on the gear is the same as the pinion, $(\sigma_c)_G = 110{,}158.66\,\text{psi}$. The wear strength is also the same. $S_c = 170{,}000\,\text{psi}$. The factor of safety of the gear in wear is:

$$(S_H)_G = \frac{S_c(Z_N)_G/(K_T K_R)}{(\sigma_c)_G} = \frac{(170{,}000 \times 0.928)/(1 \times 0.8863)}{108{,}634.97} = 1.63 \tag{4.94}$$

So for the gear in bending, $(S_F)_G = 5.04$ and wear $(S_H)_G{}^2 = 1.62^2 = 2.68$

Rim: Keep $m_B \geq 1.2$. The whole depth is $h_t = addendum + dedendum = \frac{1}{P} + \frac{F}{P} = \frac{1}{4} + \frac{0.9}{4} = 0.475in$. The rim thickness t_R is $t_R \geq m_B h_t = 1.2 \times 0.475 = 0.575in$. Finally, the inside diameter of both pinion and gear is 0.8in and outside diameter of pinion $D_p = d_p + \frac{1}{P} = 3 + \frac{1}{4} = 3.25in$ and the outside of diameter of gear

$$D_G = d_G + \frac{1.25}{P} = 9 + \frac{1.25}{4} = 9.312in \tag{4.95}$$

Motor Sizing

Motor sizing is the process of selecting the best motor for a motion control application, following the procedure in [16]. The motion profile and system inertia determine the required motor speed, acceleration, and torques; cost, physical size, and drive power requirements are also considered. The four primary criteria are: inertia ratio (J_R), motor speed (ω_m), peak torque (T_{peak}), and RMS torque (T_{RMS}).

There are 3 motors in the robot which enables the machine to do its intended work (task). Two of them are connected to the wheels by using the chain-sprocket mechanism in order to make the robot able to move to the desired location, the other motor is connected with the power screw of the lifting mechanism.

Motor sizing for the lifting mechanism

The total inertia seen by the motor connected to the power screw is computed from the schematic drive arrangement shown below.

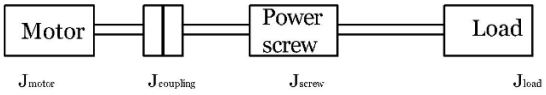

Figure 4.11. *Drive system of the lifting mechanism.*

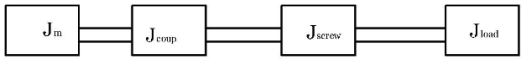

Figure 4.12. *Drive system schematic.*

The total inertia seen by the motor is

$$J_{\text{total}} = J_{\text{motor}} + J_{\text{coupling}} + J_r^{\text{trans}} \tag{4.96}$$

J_{motor} : − Referring to the motor catalog [23] at the maximum speed with a lowest motor inertia

$$J_{\text{motor}} = 1.3417 \times 10^{-4}\text{kg}m^2 \tag{4.97}$$

J_{coupling} : − The coupling connects the motor shaft to the screw in the linear track with a material of stainless steel ($\rho = 7800\ Kg/m^3$) from the catalog of the motor, the motor shaft diameter is 30 mm this is also the inner diameter of the coupler. Then, we can calculate the coupler inertial as a hollow cylinder as

$$J_{\text{coupling}} = \frac{\pi \times L \times \rho(r_o^4 - r_i^4)}{2} \tag{4.98}$$

$$J_{\text{coupling}} = \frac{\pi \times 40 \times 10^{-3} \times 7800 \times \left[(60 \times 10^3)^{-4} - (40 \times 10^{-3})^4\right]}{2} = 5.09 \times 10^{-3}\text{kg}m^2 \tag{4.99}$$

J_r^{trans} : − The inertia reflected by the screw transmission consists of the screw inertia and the load inertia reflected to the input shaft of the truck.

$$J_r^{\text{trans}} = J_{\text{screw}} + J_{L-in} \tag{4.100}$$

Approximating the screw as a solid round shaft with a mean diameter of 30 mm and length of 2m and selecting the material to be steel which have a density of 7800 kg/m^3

then, the inertia of the screw as a solid cylinder is

$$J_{\text{screw}} = \frac{\pi L \rho r^4}{2} \tag{4.101}$$

$$J_{\text{screw}} = \frac{\pi \times 2 \times 7800 \times (30 \times 10^{-3})^4}{2} = 0.0397\,\text{kg}/m^2 \tag{4.102}$$

$$J_{load-in} = \frac{1}{\eta N_s^2}(\frac{W_L + W_F}{g}) \tag{4.103}$$

where N_s is the transmission ratio of the screw, $\eta = 0.346$ is the screw efficiency, $W_L = 100 \times 9.81 = 981\,\text{N}$ is the load weight, $W_F = 7 \times 9.81 = 68.67\,\text{N}$ is the fork weight, and g is gravitational acceleration.

$$N_S = 2\pi P, \quad P = \frac{1}{\text{lead}} \tag{4.104}$$

$l = 4\,\text{mm/rev} = 0.004\,\text{m/rev}$ (single-start redesign)

$$P = \frac{1}{0.004\,\text{m/rev}} = 250\,r \tag{4.105}$$

$$N_s = 2\pi \times \frac{250\,r}{m} = \frac{1570.8\,r}{m} \tag{4.106}$$

$$J_{load-in} = \frac{1}{0.346 \times (1570.8)^2}\left(\frac{981 + 68.67}{9.81}\right) \tag{4.107}$$

$$J_{load-in} = 1.25 \times 10^{-4}\,\text{kg}\,m^2 \tag{4.108}$$

$$J_r^{\text{trans}} = 0.0397 + 1.25 \times 10^{-4} = 0.0399\,\text{kg}\,m^2 \tag{4.109}$$

$$J_{\text{total}} = J_{\text{motor}} + J_{\text{coupling}} + J_r^{\text{trans}} \tag{4.110}$$

$$J_{\text{total}} = 1.3417 \times 10^{-4}\,\text{kg}\,m^2 + 5.09 \times 10^{-3}\,\text{kg}\,m^2 + 0.0399\,\text{kg}\,m^2 \tag{4.111}$$

$$J_{\text{total}} = 0.0451\,\text{kg}\,m^2 \tag{4.112}$$

The load torque reflected by the screw to the motor side consists friction force, gravitational loading and process forces.

$$F_f = \mu(W_L + W_F)\cos(\beta) \tag{4.113}$$

Where: β is the angle between the direction of motion and the horizontal, which is 90º.Since $\cos(90) = 0, F_f = 0$.

$$F_g = (W_L + W_F)\sin(\beta) = (981 + 68.67)\sin(90) = 1049.67N \tag{4.114}$$

Since the system is not pushing against any external forces $F_P = 0$.

$$F_{\text{ext}} = F_f + F_g + F_P = 1049.67N \tag{4.115}$$

The load torque reflected to the motor by the screw is given by

$$T_{load-in} = \frac{F_{\text{ext}}}{\eta N_s} \tag{4.116}$$

$$T_{load-in} = \frac{1049.67\,\text{N}}{0.346 \times 1570.8} = 1.932\,\text{Nm} \tag{4.117}$$

The acceleration (peak) torque can be found from

$$\ddot{\theta}_{\text{motor}} = \frac{\omega_{\text{motor}}}{t_a} \tag{4.118}$$

We know maximum speed of the motor

$$\omega_{\text{motor}} = P \times V_{\text{lift}} \tag{4.119}$$

$$\omega_{\text{motor}} = \frac{1570.8\,r}{m} \times \frac{0.2166\,\text{m}}{\text{s}} = 340.2\,\frac{r}{\text{s}} = 3249\,r \tag{4.120}$$

Taking maximum allowable acceleration time of the screw to be 2 s

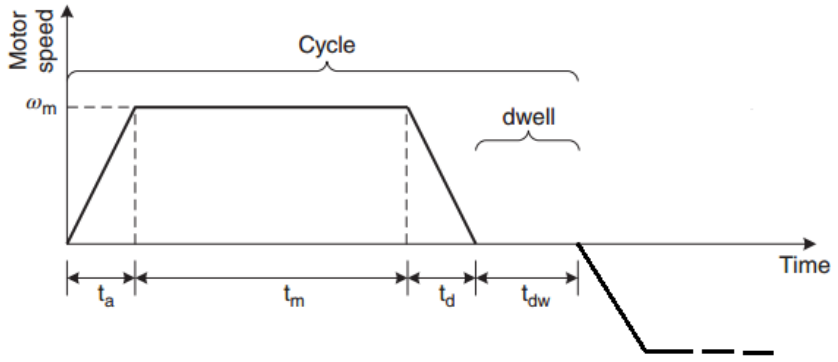

Figure 4.13. *Motion profile of the lifting mechanism motor*

$$\ddot{\theta}_{\text{motor}} = \frac{\omega_{\text{motor}}}{t_a} = \frac{340.2\,r}{2\,\text{s}} = 170.1\,\frac{r}{\text{s}^2} \tag{4.121}$$

$$T_{\text{acc}} = J_{\text{total}} \times \ddot{\theta}_{\text{motor}} + T_{load-in} \tag{4.122}$$

$$T_{\text{acc}} = 0.0451 \times 170.1 + 1.932 = 7.667 + 1.932 = 9.60\,\text{Nm} \tag{4.123}$$

Deceleration torque is

$$T_{\text{dec}} = T_{load-in} - J_{\text{total}} \times \ddot{\theta}_{\text{motor}} \tag{4.124}$$

$$T_{\text{dec}} = 1.932 - 0.0451 \times 170.1 = 1.932 - 7.667 = -5.74\,\text{Nm} \tag{4.125}$$

The running torque is simply equal to the load torque reflected to the motor:

$$T_r = T_{load-in} = 1.932\,\text{Nm} \tag{4.126}$$

The continuous torque (RMS) is calculated using

$$T_{\text{RMS}} = \sqrt{\frac{T_{\text{acc}}^2\, t_a + T_r^2\, t_m + T_{\text{dec}}^2\, t_d + T_{\text{dw}}^2\, t_{\text{dw}}}{t_a + t_m + t_d + t_{\text{dw}}}} \tag{4.127}$$

t_m (time at maximum speed) can be calculated as

$$t_m = \frac{L}{V_m} - t_a \tag{4.128}$$

where L is the total distance travelled by the fork axis, which is 2 m; $t_m = 2/0.2166 - 2 = 7.23\,\text{s}$; $T_{\text{dw}} = 0$, $t_{\text{dw}} = 10\,\text{s}$, and $t_d = t_a = 2\,\text{s}$:

$$T_{\text{RMS}} = \sqrt{\frac{184.3 + 27.0 + 65.9}{21.23}} = \sqrt{13.07} = 3.38\,\text{Nm} \tag{4.129}$$

Therefore the motor selection criteria are summarised below. The inertia ratio is:

$$J_R = \frac{J_{\text{coupling}} + J_r^{\text{trans}}}{J_m} = \frac{5.09 \times 10^{-3} + 0.0399}{1.3417 \times 10^{-4}} = 335 \tag{4.130}$$

Note: $J_R = 335$ far exceeds the servo-motor guideline of $J_R \leq 5$, primarily because the 2-m lead screw contributes $J_{\text{screw}} \approx 0.0397\,\text{kg m}^2$, which dominates the inertia budget. For a low-bandwidth lift application with PID control this ratio is operationally acceptable; a future refinement should consider a shorter or hollow-section screw or an additional gear stage to reduce J_R. Motor speed (ω_m) is 3249 rpm; peak torque (T_{peak}) is 9.60 Nm; RMS torque (T_{RMS}) is 3.38 Nm.

By considering the catalogs of DC motor suppliers the design selects a DC motor from planetary motors with model number PM60-105PG28 (representative values from manufacturer catalog). This model provides adequate peak torque at 3249 rpm. (Note: the original PM60-105PG56 was sized for the two-start screw at 1624 rpm; the single-start redesign doubles the required motor speed and therefore requires a model with the lower-ratio PG28 planetary gearbox).

Motor sizing for the drive mechanism

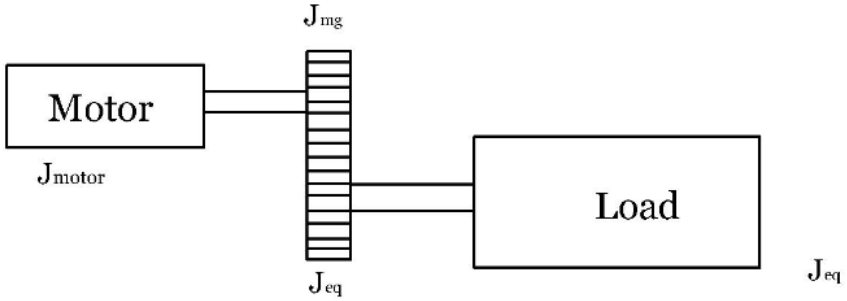

Figure 4.14. *Drive motor and gear arrangement*

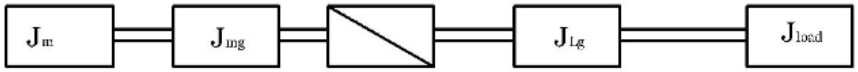

Figure 4.15. *Gear inertia diagram*

J_{lg} (Inertia of the gear at the load side) can be calculated by assuming the gear as a hollow cylinder

$$J_{\text{lg}} = \frac{\pi l \rho ({r_o}^4 - {r_i}^4)}{2} \tag{4.131}$$

Where ρ is the density of the material of the gear which is Nitralloy 135M and l is the face width of the gear which is $3 \times 10^{-2} m$

$$r_i = \frac{2.5 \times 10^{-2}}{2} = 1.25 \times 10^{-2} m \tag{4.132}$$

$$r_o = \frac{22 \times 10^{-2}}{2} = 0.11 m \tag{4.133}$$

$$J_{\text{lg}} = \frac{\pi \times 3 \times 10^{-2} \times 8220 \times ((0.11)^4 - (1.25 \times 10^{-2})^4)}{2} \tag{4.134}$$

$$J_{\text{lg}} = 0.0567\,\text{kg m}^2 \tag{4.135}$$

$$J_{\text{total}} = J_m + \ J_{\text{mg}} + [J_{\text{lg}} + J_{\text{wheel}}](1/(N_{\text{GB}}^2) \tag{4.136}$$

$$J_{\text{lg}} + J_{\text{wheel}} = (0.0567 + 0.025)\,\text{kg m}^2 = 0.0817\,\text{kg m}^2 \tag{4.137}$$

Taking the efficiency of the gear set from the datasheet of the gear set =0.95 and the design has $N_{\text{GB}} = \frac{r_l}{r_m} = 3.5$ from the design. Similarly we can calculate the inertia of the gear at the motor side J_{mg} as

$$J_{\text{mg}} = \frac{\pi l \rho ({r_o}^4 - {r_i}^4)}{2} \tag{4.138}$$

$$r_i = \frac{2 * 10^{-2}}{2} = 1 \times 10^{-2} m \tag{4.139}$$

$$r_o = \frac{7.6 \times 10^{-2}}{2} = 0.038 m \tag{4.140}$$

$$J_{\text{mg}} = \frac{\pi \times 3 \times 10^{-2} \times 8220 \times ((0.038)^4 - (0.01)^4)}{2} \tag{4.141}$$

$$J_{\text{mg}} = 8.038 \times 10^{-4} \text{kg} m^2 \tag{4.142}$$

J_m (Motor inertia) $= 5.2 \times 10^{-3} \text{kg} m^2$ from the catalog of the motor [*planetary motors*].

$$J_{\text{total}} = 5.2 \times 10^{-3} + 8.038 \times 10^{-4} + \frac{0.0817}{0.95 \times 3^2} = 0.01556 kgm^2 \tag{4.143}$$

The acceleration (peak) torque can be found from

$$T_{\text{acc}} = J_{\text{total}} \times \ddot{\theta}_{\text{motor}} + T_{load-in} \tag{4.144}$$

We know maximum speed of the motor ω_{motor}= 318.4 r and taking maximum allowable acceleration time to be 5 s we can calculate the angular acceleration of the motor to be

$$\ddot{\theta}_{\text{motor}} = \frac{\omega_{\text{motor}}}{t_a} = \frac{318.4\, r \times 2\pi/60}{5\,\text{s}} = \frac{33.35\, r}{5} = 6.67\, \frac{r}{\text{s}^2} \tag{4.145}$$

Drive motor load torque derivation. The maximum driving force derived in Section 4.4 (Equation for $\tau_{\max}$) gives the load torque at the wheel:

$$T_{\text{load}} = \tau_{\max} = \frac{F}{2} \times r = \frac{4015.6}{2} \times 0.12 = 241\,\text{Nm} \tag{4.146}$$

This is the torque at the output (wheel) side of the gearbox. The load torque reflected to the motor shaft through the gear set (ratio $N_{\text{GB}} = 3$, efficiency $\eta = 0.95$) is

$$T_{load-in} = \frac{T_{\text{load}}}{\eta N_{\text{GB}}} = \frac{241\,\text{Nm}}{0.95 \times 3} = 84.6\,\text{Nm} \tag{4.147}$$

$$T_{\text{acc}} = J_{\text{total}} \times \ddot{\theta}_{\text{motor}} + T_{load-in} = 0.01556 \times 6.67 + 84.6 = 0.104 + 84.6 = 84.7\,\text{Nm} \tag{4.148}$$

Deceleration torque is

$$T_{\text{dec}} = T_{load-in} - J_{\text{total}} \times \ddot{\theta}_{\text{motor}} = 84.6 - 0.01556 \times 6.67 = 84.5\,\text{Nm} \tag{4.149}$$

The running torque is simply equal to the load torque reflected to the motor:

$$T_r = T_{load-in} = 84.6\,\text{Nm} \tag{4.150}$$

The continuous torque (RMS) is calculated using

$$T_{\mathrm{RMS}} = \sqrt{\frac{T_{\mathrm{acc}}^2\, t_a + T_r^2\, t_m + T_{\mathrm{dec}}^2\, t_d + T_{\mathrm{dw}}^2\, t_{\mathrm{dw}}}{t_a + t_m + t_d + t_{\mathrm{dw}}}} \tag{4.151}$$

t_m (time at maximum speed) can be calculated as

$$t_m = \frac{L}{V_m} - t_a \tag{4.152}$$

where L is the total distance travelled, which is 40 m; $t_m = 40/1.33 - 5 = 25\,\mathrm{s}$; $T_{\mathrm{dw}} = 0$, $t_{\mathrm{dw}} = 10\,\mathrm{s}$, $t_d = t_a = 5\,\mathrm{s}$:

$$T_{\mathrm{RMS}} = \sqrt{\frac{35{,}851 + 178{,}929 + 35{,}702}{45}} = \sqrt{5565} = 84.6\,\mathrm{Nm} \tag{4.153}$$

Therefore the motor selection criteria are summarised below. The inertia ratio is:

$$J_R = \frac{J_{\mathrm{mg}} + \left[J_{\mathrm{lg}} + J_{\mathrm{wheel}}\right]/N_{\mathrm{GB}}^2}{J_m} \tag{4.154}$$

$$J_R = \frac{8.038 \times 10^{-4} + 0.0817/9}{5.2 \times 10^{-3}} = \frac{8.038 \times 10^{-4} + 9.078 \times 10^{-3}}{5.2 \times 10^{-3}} = 1.90 \tag{4.155}$$

$J_R \approx 1.9$, well within the recommended criterion of $J_R \leq 5$, confirming a good motor–load inertia match. Motor speed (ω_m) is 318 rpm; peak torque (T_{peak}) is 84.7 Nm; RMS torque (T_{RMS}) is 84.6 Nm. By considering the catalogs of DC motor suppliers the design selects a DC motor from planetary motors with model number PM71-110 PG56 (representative values from manufacturer catalog). The peak torque capacity of this motor (approximately 110 Nm) exceeds the required 84.7 Nm, confirming a valid selection.

Chapter 5

Design and Analysis of the Electrical System

This section deals with the design and selection of different components of the electrical system. Such as battery pack, battery charging circuit, the controller and the wireless communication.

5.1 Selection of Battery

To achieve required energy supply we decide to make our battery pack. Nowadays a popular voltage seems to be 12V, 24V and 36V. There is some specification to meet certain performance goal of battery. These goals are: quick discharge and recharge capability, long cycle life (the number of discharge before becoming unserviceable), low costs, recyclable, high specific energy (amount of usable energy in watt hour per kilogram), high energy density (amount of energy stored per unit volume in watt hour per litter), specific power and ability to work in wide temperature.

There are different type of rechargeable battery such as nickel cadmium (NiCd), nickel metal hydride (NiMH), lithium ion (Li-ion) and lead acid battery.

Nickel Cadmium (NiCd) batteries support fast and simple charging, deliver a high number of charge/discharge cycles, and perform well at low temperatures; they are economically priced and available in a wide range of sizes. Their main drawbacks are relatively low energy density compared to newer chemistries, high self-discharge, susceptibility to memory effect if not exercised regularly, and poor environmental profile due to cadmium content.

Nickel Metal Hydride (NiMH) batteries offer 30–40% higher energy density than NiCd, are less prone to memory effect, and are more environmentally friendly since their nickel content makes recycling economically viable. On the other hand, they have a limited service life, require a complex charging algorithm, generate significant heat during fast charge and high-load discharge, and are approximately 20% more expensive than NiCd.

Lead-acid batteries are inexpensive, reliable, and based on well-understood technology. They exhibit low self-discharge and can sustain high discharge rates. Their limitations

include inability to be stored in a discharged state, low energy density, a restricted number of full discharge cycles, and susceptibility to thermal runaway under improper charging conditions.

Lithium-ion (Li-ion) batteries provide the highest energy density of the options considered, combined with relatively low self-discharge, a long service life, and no priming requirement. They require a dedicated protection circuit, are subject to gradual capacity loss with age, produce only moderate discharge current, are sensitive to high temperatures, and carry a manufacturing cost approximately 40% above that of NiCd.

Therefore no battery currently available meet above performance goal. However nickel metal hydride (NiMH) batteries fulfil this condition. They have a high specific energy between 60-120Wh/kg. Only Lithium ion battery score better specific energy between 110-160Wh/kg. But Lithium ion batteries are very expensive. NiCd battery are very similar to NiMH battery. Both types of battery has high specific energy and higher energy density than advanced Lead acid batteries. So we choose NiMH battery to supply the required amount of voltage which is 24V. To get such amount of voltage total of 20 cell and cell with 1.2V needed.

5.2 Battery Charging Circuit Design

Batteries need to recharge once their charge is finished. This section presents the design of an automatic battery charger with automatic cutoff. The charger is built with easily available electronic components which are cheap and can be easily find [17].

Any automatic battery charging circuit has the following major components

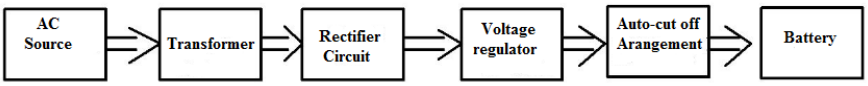

Figure 5.1. *Schematic diagram of the battery charging circuit*

The AC supply that we get from the national grid is 220V with 50Hz frequency. This voltage should be converted to a voltage level that is suitable for the charging of the battery. This voltage level conversion is taken place by an electrical machine called transformer. In order to have 12V at the battery ports, the design has to have 15-20V at the secondary side of the transformer. The rectifier circuit which is found next to the transformer is used to convert the AC signal to DC one. The output of rectifier is pulsating DC which must be smoothed before applied to regulator. A capacitor which is used to smoothen the voltage is connected at output of bridge rectifier. Pure DC is then given to the voltage regulator LM317. The output of rectifier is unregulated so a

voltage regulator is installed to get regulated voltage or to maintain a constant voltage level automatically. Now regulated voltage can be sent to the battery for charging, but supplying a constant voltage when battery is fully charged may harm the battery. In order to solve this, auto cutoff arrangement is needed which have a duty to detach the battery from charger once charging is complete.

The 12 V battery charger uses the following components: a 220/25 V transformer, 1N4007 diodes, a 470 µF smoothing capacitor, an LM317 voltage regulator, assorted resistors, a ZPD12RL Zener diode, a BD139 transistor, and a 12 V relay, powered from a 220 V / 50 Hz AC supply. These components form the automatic battery charging circuit shown below.

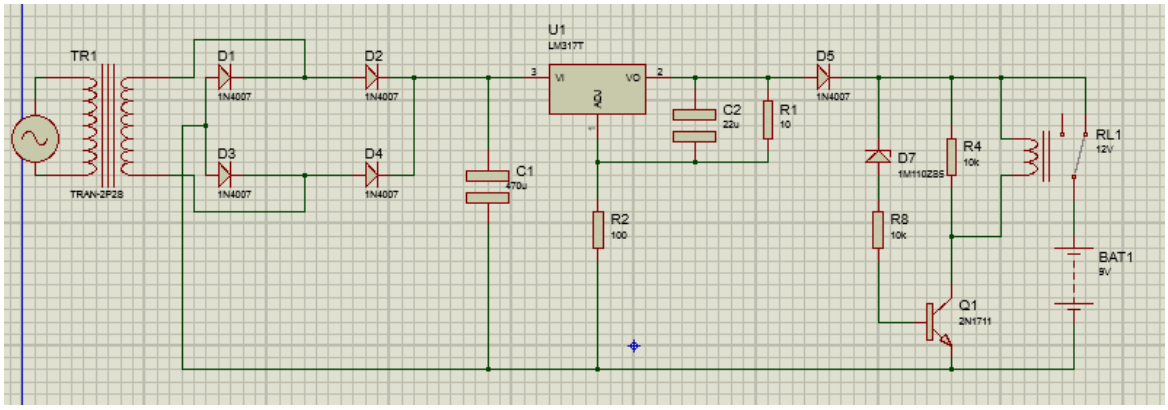

Figure 5.2. *Circuit diagram of battery charger*

The output of LM317 is given as:

$$V_o = V_{\text{Ref}}(1 + \frac{R1}{R2}) \tag{5.1}$$

In series with R2, a variable resistor RV4 is connected so that the output voltage of regulator can be adjusted. The reference voltage is the input voltage.

A capacitor is connected at the output of voltage regulator whose duty is to stabilize the output of the voltage regulator.

A diode D_5 is connected after the resistor at the output of regulator. Since it's a diode, it allows the flow of current only from the regulator towards the battery but not the reverse. In this manner it keeps the battery from being discharged through the regulator.

Zener diode together with transistor, a couple of resistors and 12V relay makes the automatic cutoff arrangement for the battery charging circuit. Zener diode will start conducting due to Zener breakdown as soon as the voltage exceeds form 13V. When

it starts conducting, current is supplied to the base of transistor and it makes the transistor on. This makes the collector of transistor which was previously at 12V (due to cutoff) become at ground level (or near to ground level). As a result the 12 volt relay starts to operate. The resistor connected at the base of transistor controls the sensitivity of the cutoff switch. Low value of this resistance will operate the switch after Zener starts conducting while higher value will operate the switch when voltage goes beyond 13V by good range. When relay operates, battery is isolated from the automatic battery charger.

Design note – charger voltage: The circuit described above charges a single 12 V battery module. Because the AGV uses a 24 V battery pack formed by connecting two 12 V modules in series, either two identical charger circuits must be used (one per module, with the pack disconnected for charging) or the charger must be redesigned for a 24 V output. This is identified as a limitation of the current design and is left as future work.

5.3 Selection of Controller

The controller is the brain of the automated system, which compares the set point that is set by the computer to a feedback signal from measuring device. And ensure that a process variable is maintained at specific limit. If some disturbances cause the desired robot variables to deviate from the set point, the controller will call for a corrective action. In the system there is a composition of command that is set by the program, the actuators are told what to do or when to run.

Most commonly this controller devices are either a microcontroller or programming logic controllers (PLCs) the selection of this devices for our specific case is discussed in this section.

Microcontroller. A micro-controller is a small computer on a single integrated circuit containing a processor core, memory, and programmable input/output peripherals. Program memory is in the form of RAM (Random access memory) [18]. Micro-controllers are generally designed for embedded applications.

Any microcontroller system consists of two primary components: hardware and software. The hardware is the actual physical components of the system. The software is a list of instructions which reside inside the hardware, and then write a software program to control our system.

Some of the advantages of microcontrollers are: They are small in size therefore they are easily portable, they are cheap in price, programming of microcontrollers is simple to learn easy for troubleshooting and maintenance, and they consume a very amount

power while they operate. But there are also some disadvantages of using associated to using microcontrollers among them: they have limited number of I/O ports when trying to implement in complex industrial applications, their processing power is usually limited for large scale implementation, they also can't operate in extreme environments and can't be directly interfaced with high power cables.

PROGRAMMING LOGIC CONTROLLER (PLC)

A programmable logic controller (PLC) or programmable controller is a digital computer used for automation of electromechanical processes. PLCs are used across many industries and machine types. Unlike microcontrollers, the PLC is designed for multiple inputs and output arrangements, extended temperature ranges, immunity to electrical noise, and resistance to vibration and impact. Programs to control machine operation are typically stored in battery-backed-up or non-volatile memory [19].

Some of the advantages of PLCs are: the wiring of PLCs is simple and less, they have increased operational reliability, the controller has fast operation, and have easily understood programming language. But there are also some disadvantages of PLCs among them: it's always difficult to find errors therefore maintenance and troubleshooting of this systems requires skillful operator, and also it's expensive for small and less complex systems.

Therefor based on the above stated merits and demerits of microcontrollers and PLCs the choice of a controller for our forklift AGV will be microcontroller. Since our application is simple and doesn't require a multiple number of I/O ports microcontrollers are the best fit controllers for our application.

Once the design has decided to use microcontroller to be our controller device, the next task will be selecting the microcontroller type from the large family of microcontroller.

Selection of Microcontroller

Two different types of microcontrollers were considered and based on their respective advantages a decision was made.

PIC 16F877A

The popular microcontroller PIC16F877A together with the development board from Olimex was considered as the first option.

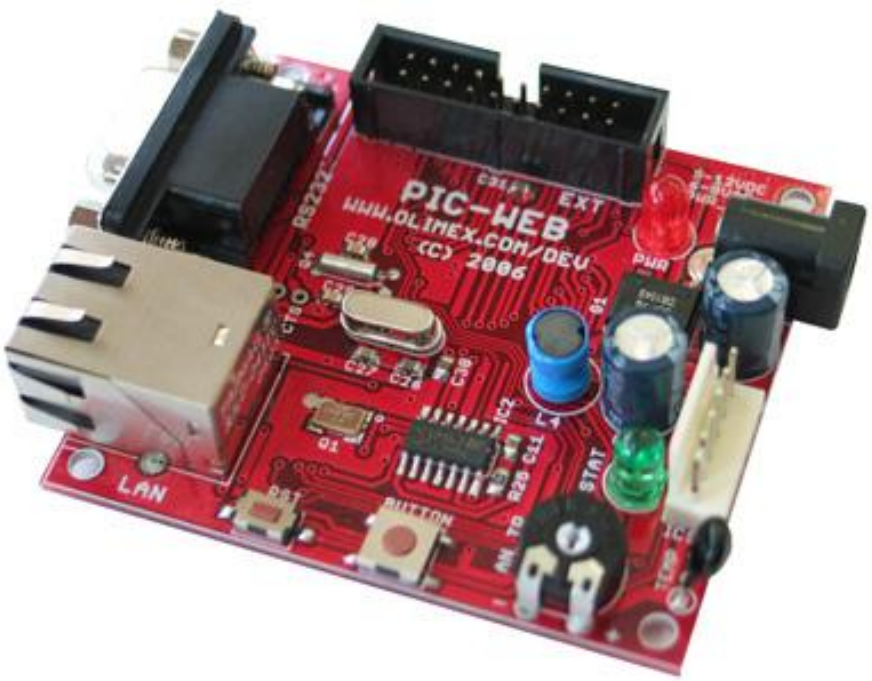

Figure 5.3. *Olimex development board for PIC16F877A microcontroller.*[1]

The properties of the PIC16F877A chip are as follows

The PIC16F877A provides 14 KB of Flash program memory, 256 bytes of EEPROM, 386 bytes of RAM, 8 analog inputs, and 35 digital I/O pins of which 2 support PWM output.

Some of the advantages of PIC16F877A are: it's a widely used microcontroller therefore it's easily accessible, when compared to other microcontrollers it contains a huge number of ports available. But the disadvantages of this PIC microcontroller is somewhat more than the advantages of the microcontroller. Among them: although they have many I/O ports, the number of PWM outputs is limited, very limited online and offline reference available, it can only be programmed through serial RS 232 port and most modern computers are equipped with only USB, and also the cost of PIC and its development board is relatively high, and it's difficult to program.

ATmega 328

The second microcontroller that was considered was the ATmega 328 that comes with the Arduino Uno Board. Arduino Uno is a modern development board that is becoming increasingly popular among engineers and hobbyists.

[1]Image source: https://www.olimex.com/Products/PIC/Development/

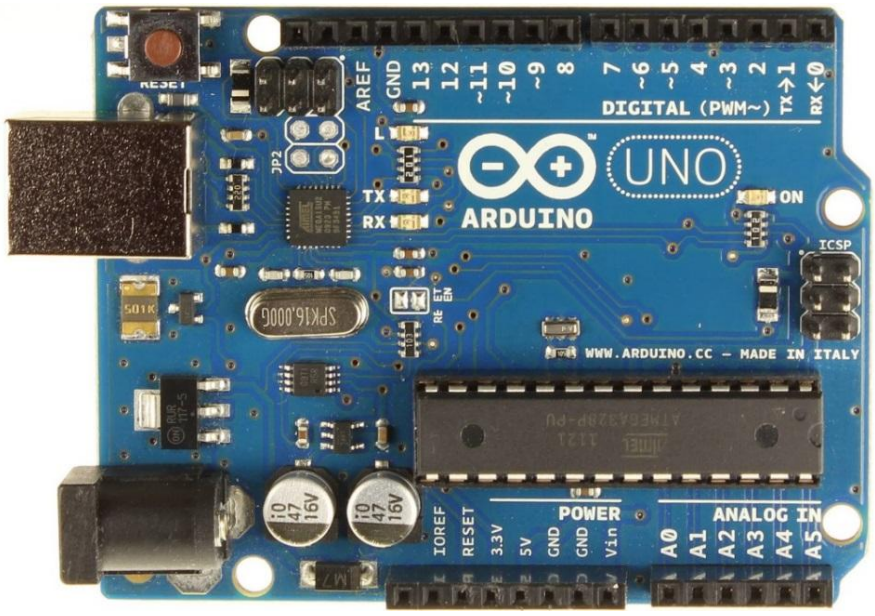

Figure 5.4. *Arduino Uno board with ATmega 328 chip.*[2]

The properties of the ATmega 328 chip are as follows:

32KB Flash program memory, 1KB EEPROM Data, 2KB RAM, 6 Analog Inputs, and 14 Digital Inputs or Outputs.

The major advantages of Arduino Uno are: there is huge library available online for implementation with various components, it can be easily programmed via USB, relatively cheap, contains huge number of PWM ports, can be easily interfaced with different application software such as MATLAB and LABVIEW which are very important to generate the path to be followed by the AGV. The major disadvantage of Arduino Uno when compared to other microcontrollers is it contains a limited number of digital input and output ports. Therefore The Arduino Uno was the microcontroller carefully chosen.

Communication network. ZigBee is a type of wireless protocol designed to transmit data through RF signals especially in harsh manufacturing environments. The XBee is a module based on the ZigBee protocol using a frequency of 2.4GHz to transmit data. XBee modules could be used, one would be connected to the PC and the other one to the forklift.

Its advantages include support for multiple network topologies, low battery consumption, low latency, and 128-bit encryption; its main limitation is a medium communication range of approximately 100 m.

[2]Image source: http://forefront.io/a/beginners-guide-to-arduino/

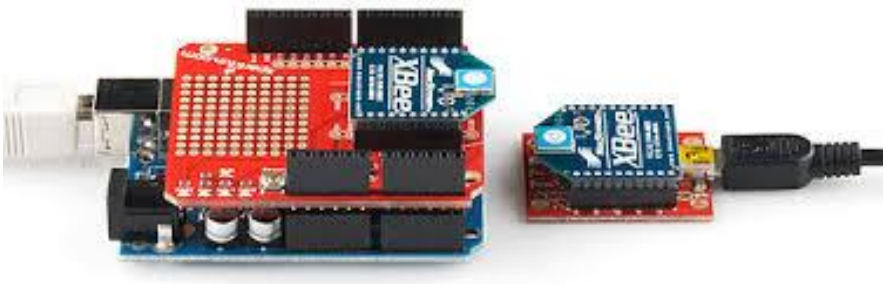

Figure 5.5. *XBee communication module.*[3]

5.4 Drive System

A drive amplifies small command signals generated by the controller to the high-power voltage and current levels necessary to operate a motor; it is therefore also called an amplifier. In motion control systems, each axis operates under closed-loop control. Typically there are three loops per axis: current, velocity, and position. The motor's velocity and position are fed back to the controller, while the motor's current is fed back to the drive, which closes the current loop [20].

The speed of a DC motor is approximately proportional to the supply voltage, so reducing the supply voltage by half will reduce the speed by approximately one-half. The speed of the motor can therefore be controlled by varying the average supply voltage. Pulse width modulation (PWM) is a popular technique in order to control the speed of dc motors by varying the voltage and current that is supplied to the motor through the motor terminals.

A pulse-width modulated (PWM) signal is a constant period square wave with a varying duty cycle (on-time compared to off-time). In other words, the frequency of a PWM signal is constant but the time the signal remains high varies as shown in Figure 2.13. PWM signal is basically a high frequency square wave. The duty cycle of this square wave is varied in order to vary the power supplied to the load. Duty cycle is usually stated in percentage and it can be expressed using the equation:

$$Duty\ cycle = \frac{T_{\mathrm{ON}}}{(T_{\mathrm{ON}} + T_{\mathrm{OFF}})} \times 100 \tag{5.2}$$

Where T_{extON} is the time for which the square wave is high and T_{extOFF} is the time for which the square wave is low. When duty cycle is increased the power given to the load increases and when duty cycle is reduced, power across the load decreases.

[3]Image source: https://learn.sparkfun.com/tutorials/xbee-shield-hookup-guide

Shown below are examples of a 10%, 50%, and 90% duty cycle.

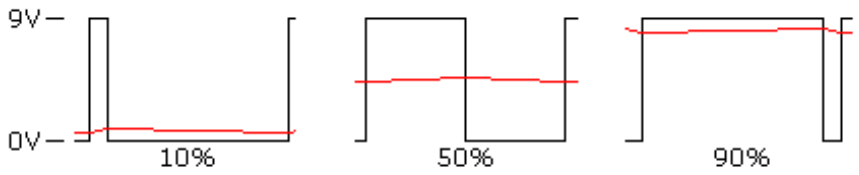

Figure 5.6. *PWM waveforms showing 10%, 50%, and 90% duty cycles.*[4]

$$V_{motor,average} = V_{\text{supply}} \times Duty\ cycle \tag{5.3}$$

PWM is often used in combination with an H-Bridge. This configuration is named H-bridge because it looks like the letter H, and allows the effective voltage across the load to be doubled, since the power supply can be switched across both sides of the load. In the case of inductive loads, such as motors, diodes are used to suppress inductive spikes, which may damage the transistors. The inductance in a motor also tends to reject the high frequency component of the waveform [21].

The L293D dual H-Bridge is a motor driver that is used in conjunction with the PWM signal generated by the Arduino Uno. The major advantages are: it can supply motors with voltages in the range of 4.5 to 36 V, it has two enable pins compatible with PWM, and it interfaces easily with the Arduino Uno.

Design note – current rating: The L293D is rated for a maximum of 1 A continuous current per channel. The drive motors selected in Chapter 4 require peak torques of approximately 85 Nm and the lift motor approximately 9.6 Nm; the corresponding peak motor currents are on the order of tens of amperes, far exceeding the L293D's 1 A rating. In a physical implementation the L293D must be replaced by a higher-current motor driver (e.g., a BTN7971-based full H-bridge module rated for 43 A, or a MOSFET H-bridge designed for the required current). The L293D is retained here as a proof-of-concept interface component for control-signal routing only.

[4]Image source: https://www.allaboutcircuits.com/textbook/semiconductors/chpt-11/pulse-width-modulation/ (accessed May 2017).

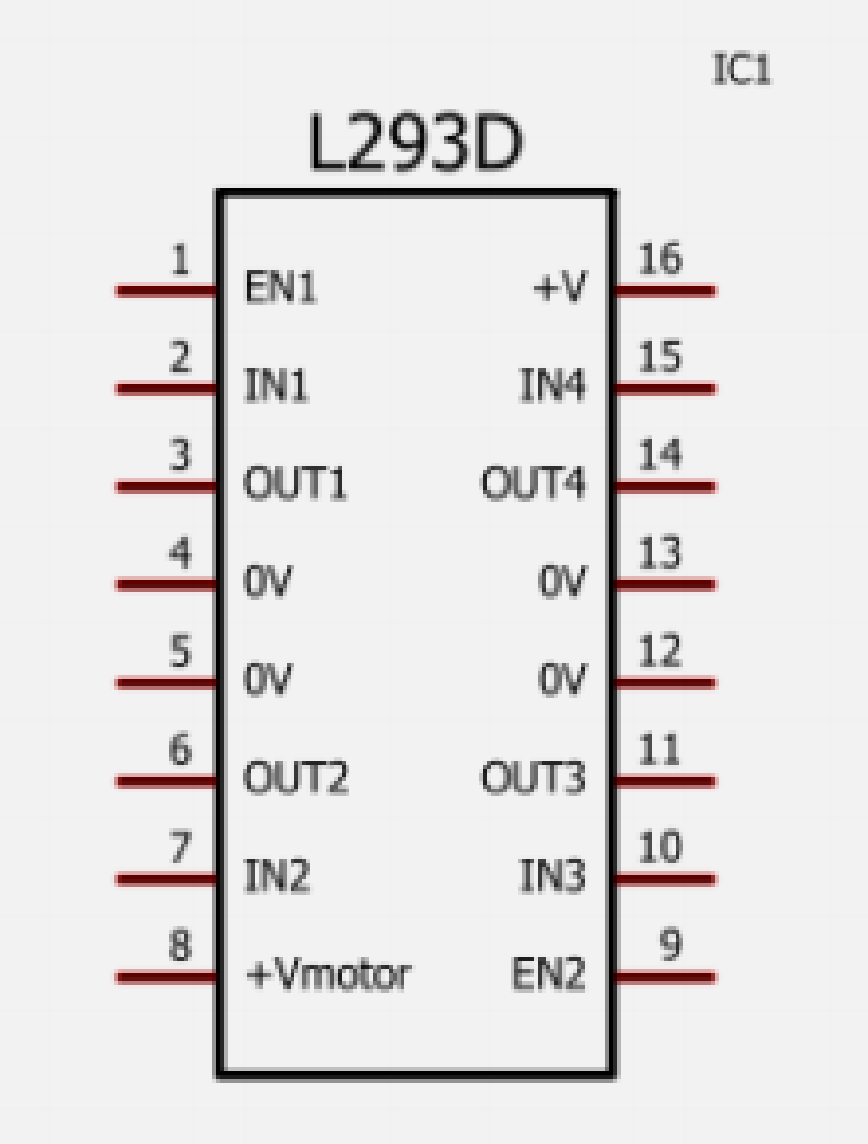

Figure 5.7. *L293D Bridge IC*

5.5 Selection of Actuator

Electrically actuated system are very widely used in control system because they are easy to interface with the control system which are also electrical and because electricity is easily available unlike fluid power which require pumps and compressors.

Motors are the most common way to control the movements of robots and are known as actuators. They can be connected to gears and wheels and are a perfect way of adding mobility. There are a number of different types of motors that can be used, dc, stepper and servo.

DC motor. DC motors are commonly used and widely available type of actuators. DC motors works by applying a DC power through the terminals of the motor. The

direction of rotation can be altered by reversing the polarity of the motor supply voltage. These motors have several advantages that makes them popular for motion control applications. Among these advantages their good controllability, linear torque-current curve and their low cost are the major ones.

Stepper motor. Stepper motors work in a similar way to dc motors, however where a dc motor has just one electromagnet, the stepper has many. The stepper is controlled by the sequential turning on and off of these coils. Each time a new coil is energized the motor rotates another couple of degrees. The number of degrees that a motor turns with each pulse is called the step angle. Repeating the sequence causes it to move a few more degrees, this continues until a full rotation is achieved [22].

Although stepper motors have high holding torque capability and precise controllability, they haven't a brushed rotor using this motors for applications with high rpm makes them highly susceptible for wear. Due to this stepper motors are usually applied for printer control, photo or film processing machines and also scanners.

Servo motor. The term "servomotor" does not refer to one single kind of motor. Instead it refers any type of motor that receives a command signal from a controller. In this same respect, any closed loop system can be referred to as a servo system. Servo motor offers the smoothest and greatest control. However the rotation of a servo is limited; most rotate from 0° to 180° though some can complete a full rotation. They cannot rotate continually due to their structure so are unsuitable for driving wheels.

Chapter 6

Design and Analysis of the Control System

6.1 Wheel and Drive Type Selection

As is stated in chapter two there are a lot of wheel and drive types which are currently used in mobile robots. Before doing any other task first the design has to select the optimum wheel and drive types which are suitable for our application based on the following criteria.

Table 6.1. *Comparison of different drive systems for AGV*

	Differential	Ackerman	Synchro	Omnidirectional
Maneuverability	Good	Poor	Good	Best
Stability	Best	Best	Best	Best
Controllability	Good	Good	Poor	Poor
Cost of implementation	Best	Poor	Good	Poor

Therefore based on the above comparison the differential steering is the perfect choice for the AGV. And due to their easily controllability, applicability in different floor conditions and cheap cost the design has decided to use conventional type of wheels in our forklift AGV.

6.2 Kinematic and Dynamic Modelling of the Robot

The design and control of any robotic system requires a proper understanding and modelling the system. Modeling of a mobile robot consists the kinematic and dynamic modeling and the modeling of the actuators. Kinematic modeling deals with the geometric relationships that govern the motion of the system without considering the affecting forces. Whereas the dynamic modeling is the study of the motion considering the forces and energies acting in the system. The preceding section of this chapter deals with the kinematic and dynamic modeling of the system.

Note that the modelling of both kinematic and dynamic system of the robot which is presented here is based on the research works of [23], [31] and [32].

The first step for the mechanical modeling is to define appropriate coordinate systems for the robot which is discussed in the next section.

COORDINATE SYSTEMS

The main purpose of the coordinate systems is to represent the position of the robot. The following two coordinate systems are used for mobile robot modeling:

Inertial Frame: $\{X_I, Y_I\}$ This is the fixed coordinate system in the plane of the robot.

The above two coordinate systems are shown in Figure below:

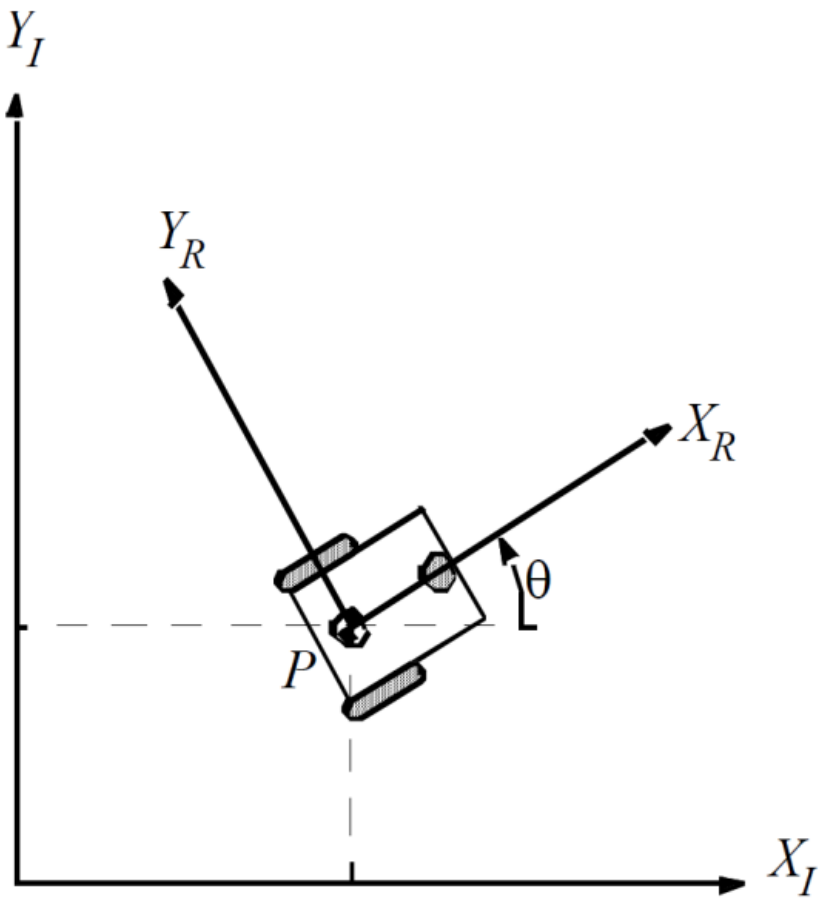

Figure 6.1. *Inertial and Robot coordinate systems of a mobile robot*

The robot's position in the inertial and robot frame can be defined as follows:

$$q_I = \begin{bmatrix} x_I \\ y_I \\ \theta_I \end{bmatrix} \tag{6.1}$$

The transformation between these two frames is through the standard rotational matrix:

$$\dot{q}_R = R(\theta)\dot{q}_I \tag{6.2}$$

Using the above equations, we can know the relation between the robot velocities in the inertial frame the local frame which is very essential in the robot kinematics.

KINEMATIC MODELING OF THE MOBILE ROBOT

The purpose of the kinematic modeling of robots is to find the speed of the robot in the inertial frame in terms of the wheels speeds and the geometric parameters of the robot.

The robot kinematics generally contains two major analyses. The forward and inverse kinematics:

Forward kinematic modelling

Considering a differential drive mobile robot which has two wheels with the radius of R_a placed with a distance L from the robot center as shown in Figure below:

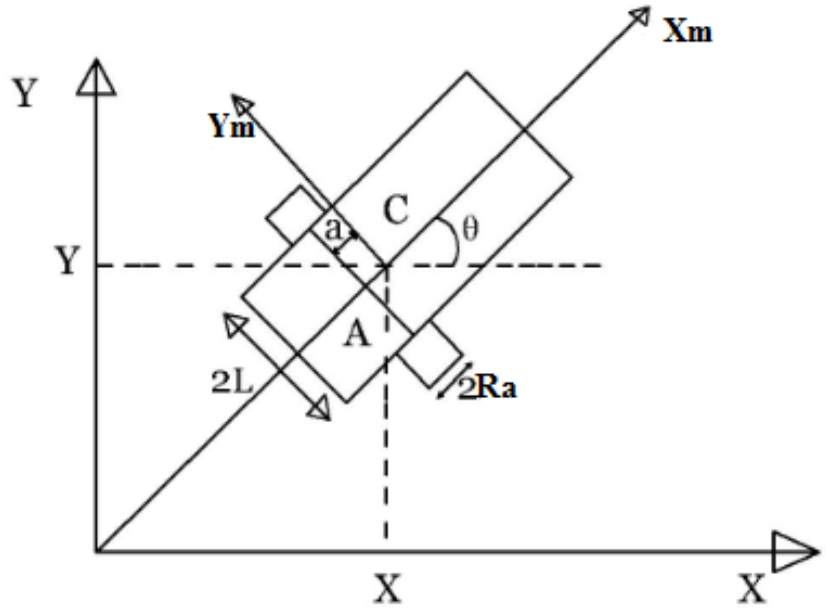

Figure 6.2. *The differential drive mobile robot model*

Where:-

A: The intersection of the axis of symmetry with the driving wheels axis

C: Robot's center of mass

a: The distance between the center of mass and driving wheels axis in x-direction

L: The distance between each driving wheel and the robot axis of symmetry in y-direction

R_a: The radius of each driving wheel

$\dot{\varphi}_R$: The rotational velocity of the right wheel

$\dot{\varphi}_L$: The rotational velocity of the left wheel

V: The translational velocity of the robot in the local frame

ω: The rotational velocity of the robot in the local and global frames

The forward kinematic problem can be generalized as the problem of finding the following function:

$$\dot{q} = \begin{bmatrix} \dot{x} \\ \dot{y} \\ \dot{\theta} \end{bmatrix} = f(\dot{\varphi}_R, \dot{\varphi}_L,\ L,\ R_a, \theta) \tag{6.3}$$

The speed of each wheel in the robot frame is $R_a\dot{\varphi}$, therefore the translational speed in the robot frame is given as:

$$R_{\mathrm{a}}\ \frac{\dot{\varphi}_R + \dot{\varphi_L}}{2} \tag{6.4}$$

Given that $\dot{q}_I = R(\theta)^{-1}\dot{q}_R$, the full model which is the robot velocity in the inertial frame is:

$$\dot{q}_I = R(\theta)^{-1}\frac{R_a}{2}\begin{bmatrix} \dot{\varphi}_R + \dot{\varphi}_L \\ 0 \\ \frac{\dot{\varphi}_R - \dot{\varphi}_L}{L} \end{bmatrix} \tag{6.5}$$

The inverse of the rotation matrix is:

$$R(\theta)^{-1} = \begin{bmatrix} \cos\theta & -\sin\theta & 0 \\ \sin\theta & \cos\theta & 0 \\ 0 & 0 & 1 \end{bmatrix} \tag{6.6}$$

Therefore the robot velocity in the global or inertial frame is:

$$\begin{aligned}\dot{q}_I &= \begin{bmatrix}\cos\theta & -\sin\theta & 0\\ \sin\theta & \cos\theta & 0\\ 0 & 0 & 1\end{bmatrix}\frac{R_a}{2}\begin{bmatrix}\dot{\varphi}_R+\dot{\varphi}_L\\ 0\\ \dfrac{\dot{\varphi}_R-\dot{\varphi}_L}{L}\end{bmatrix}\\ &= \begin{bmatrix}R_a\dfrac{\dot{\varphi}_R+\dot{\varphi}_L}{2}\cos\theta\\ R_a\dfrac{\dot{\varphi}_R+\dot{\varphi}_L}{2}\sin\theta\\ \dfrac{R_a}{2L}(\dot{\varphi}_R-\dot{\varphi}_L)\end{bmatrix}\end{aligned} \tag{6.7}$$

The above equation is the general forward kinematic equation for a differential drive mobile robot.

Kinematic constraints

The following assumptions about the wheel motion will cause the robot kinematic constraints:

Movement on a horizontal plane, Point contact between the wheels and ground, Wheels are not deformable, Pure rolling which means that the design has the instantaneous center of zero velocity at the contact point of the wheels and ground., No slipping and skidding, No friction for rotation around contact points, and Steering axes perpendicular to the surface.

Considering the above assumptions about the wheel motion, the robot will have a special kind of constraint called Nonholonomic constraint. A nonholonomic constraint is a constraint on the feasible velocities of a body. For a differential drive mobile robot, it can simply mean that the robot can only move in Forward and backward directions but not Sideward.

The equations of the nonholonomic constraints for the differential drive mobile robot are as follows:

$$\dot{y}_c\cos\theta - \dot{x}_c\sin\theta - \dot{\theta}a = 0 \tag{6.8}$$

$\dot{y}_c$ And $\dot{x}_c$ are the robot velocity components in the inertial frame. This constraint indicates that the velocity of the robot center point will be in the direction of the axis of symmetry and the motion in the orthogonal plane will be zero.

$$\dot{x}_c\cos\theta + \dot{y}_c\sin\theta + L\dot{\theta} = R_a\dot{\varphi}_R \tag{6.9}$$

This constraint indicates that the driving wheels do not slip. The three constraints can be written in the following form:

$$A(q)\dot{q} = 0 \tag{6.10}$$

In which

$$A(q) = \begin{bmatrix} -\sin\theta & \cos\theta & a \\ 0 & \cos\theta & \sin\theta \end{bmatrix} \tag{6.11}$$

This expression of the nonholonomic constraint is useful while we want to take the constraints into account in the dynamic modeling.

DYNAMIC MODELLING OF THE ROBOT

The dynamic modelling, of a robot is important in the analysis, design and control of a robot. Dynamic modeling is the study of the system's motion in which forces are modeled and including energies and the speeds related with the motions.

A differential drive robot having a $n-$ dimensional configuration space L with generalized coordinates $(q_1, q_2, \ldots, q_n)$ and subject to m constraints can be defined by the following general dynamic equation:

$$M(q)\ddot{q} + V(q,\dot{q}) + F(\dot{q}) + G(q) + \tau_d = B(q)\tau - A^T(q)\lambda \tag{6.12}$$

Where:

$M(q)$ is the inertia matrix

$V(q,\dot{q})$ is the centripetal and coriolis matrix

$F(\dot{q})$ is the surface friction matrix

$G(q)$ is the gravitational vector

τ_d Denoted bounded unknown disturbances including unmodeled dynamics

$B(q)$ is the input transformation matrix

τ is the input vector

$A^T(q)$ is the matrix associated with the constraints

λ is the vector of the constraint forces

In the following sections, the energy-based Lagrangian approach and which is relatively more convenient to formulate and implement used for expressing the dynamics of this robot.

LAGRANGIAN DYNAMICS APPROACH

Analytical dynamics is an approach in dynamics which treats the system as a whole dealing with scalar quantities such as the kinetic and potential energies of the system. Lagrange (1736-1813) proposed an approach which provides a powerful and versatile method for the formulation of the equations of motion for any dynamical system. In order to drive the Lagrange equation for holonomic systems the generalized coordinates must be independent.

For a nonholonomic system, there must be more number of generalized coordinates than the number of degrees of freedom due to constraints on the motion of the system.

If there are m nonholonomic constraint equations of the following form in the system:

$$a_{\mathrm{ij}} dq_i + a_{\mathrm{jt}} dt = 0, \qquad j = 1, 2, \ldots m \tag{6.13}$$

Where a_{ij} are functions of the generalized coordinates, then the general form of the Lagrange equation is as follows:

$$\frac{d}{dt}\left(\frac{\partial L}{\partial \dot{q}_i}\right) - \frac{\partial L}{\partial q_i} = \lambda_j a_{\mathrm{ji}} + Q_i, \qquad i = 1, 2, \ldots n \tag{6.14}$$

Where:

$q_1, q_2, \ldots\ q_n$ are the generalized coordinates

$L = T - V$ is the Lagrangian which is the difference between the systems kinetic and potential energy.

λ_j is the Lagrangian multiplier which relates the constraints to the constraint forces

Q_i Noncoservative forces in the system like frictional force

In addition to these n equations, the design has m equations of the constraints to solve for the $(m + n)$ unknowns, i.e. q's and λ's.

In order to find the dynamic equation, first the design has to find the systems kinetic and potential energy. In case of our system, the potential energy is zero since the motion is restricted to the ground. The expression for the kinetic energy of the robot can be derived using the velocities shown in Figure below:

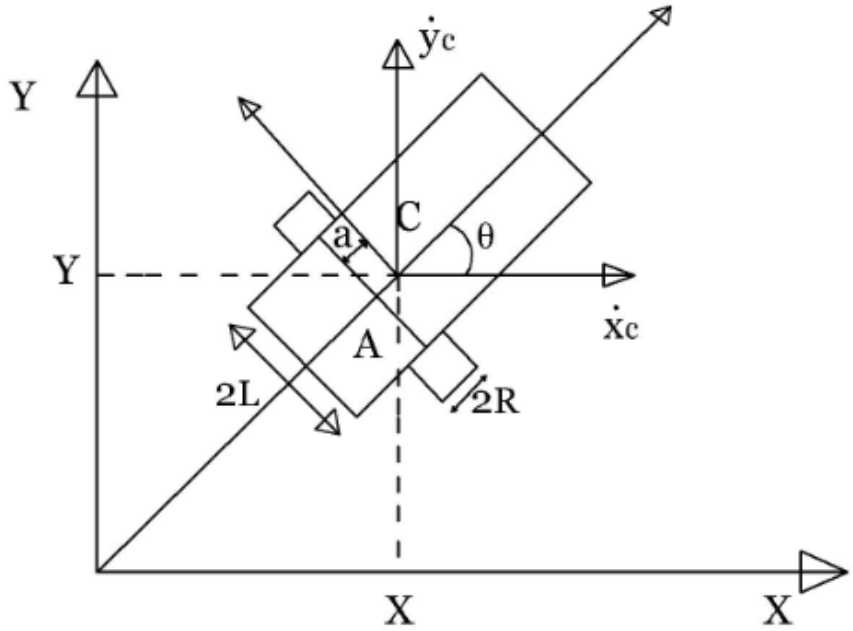

Figure 6.3. *The velocities of the robot center*

The velocity of the robot at point A and C is given as:

$$x_c = x_A + a\cos\theta$$

From the above expressions

$$\dot{y}_c = \dot{y}_A + a\dot{\theta}\cos\theta$$

The velocity the robot at the center of rotation A is:

$$v_A = \dot{x}_c \overrightarrow{i} + \dot{y}_c \overrightarrow{j} + a\dot{\theta}\sin\theta \overrightarrow{i} - a\dot{\theta}\cos\theta \overrightarrow{j} \tag{6.15}$$

The kinetic energy is:

$$T = \frac{1}{2} m {v_A}^2 + \frac{1}{2} I_A \dot{\theta}^2 \tag{6.16}$$

$$T = \frac{1}{2} m \left[\dot{x}_c^2 + 2\dot{x}_c a\dot{\theta}\sin\theta + a^2\dot{\theta}^2\sin^2\theta + \dot{y}_c^2 - 2\dot{y}_c a\dot{\theta}\cos\theta + a^2\dot{\theta}^2\cos^2\theta\right] + \frac{1}{2} I_A \dot{\theta}^2 \tag{6.17}$$

$$T = \frac{1}{2} m\dot{x}_c^2 + \frac{1}{2} m\dot{y}_c^2 + m\dot{x}_c a\dot{\theta}\sin\theta - m\dot{y}_c a\dot{\theta}\cos\theta + \frac{1}{2} m a^2\dot{\theta}^2 + \frac{1}{2} I_A \dot{\theta}^2 \tag{6.18}$$

From the parallel axis theorem we know that:

$$I_C + ma^2 = I_A \tag{6.19}$$

Therefore the kinetic energy of the system will be:

$$T = \frac{1}{2}m\dot{x}_c^2 + \frac{1}{2}m\dot{y}_c^2 + \frac{1}{2}I_C\dot{\theta}^2 + ma^2\dot{\theta}^2 + m\dot{x}_c a\dot{\theta}\sin\theta - m\dot{y}_c a\dot{\theta}\cos\theta \tag{6.20}$$

Combining the above expressions for kinetic and potential energy, the Lagrangian equation will become:

$$L = \frac{1}{2}m\dot{x}_c^2 + \frac{1}{2}m\dot{y}_c^2 + \frac{1}{2}I_C\dot{\theta}^2 + ma^2\dot{\theta}^2 + m\dot{x}_c a\dot{\theta}\sin\theta - m\dot{y}_c a\dot{\theta}\cos\theta \tag{6.21}$$

The generalized coordinates to use in the Lagrange formulation are as follows:

$$q = [x_c, y_c, \theta] \tag{6.22}$$

$$\dot{q} = \left[\dot{x}_c, \dot{y}_c, \dot{\theta}\right] \tag{6.23}$$

The step by step approach to find the dynamic equations using the above generalized coordinates and Lagrangian is as follows:

$$\frac{\partial L}{\partial \dot{x}_c} = m\dot{x}_c + ma\dot{\theta}\sin\theta \tag{6.24}$$

$$\frac{\partial L}{\partial \dot{y}_c} = m\dot{y}_c - ma\dot{\theta}\cos\theta \tag{6.25}$$

$$\frac{\partial L}{\partial \dot{\theta}} = I_C\dot{\theta} + 2ma^2\dot{\theta} + m\dot{x}_c a\sin\theta - m\dot{y}_c a\cos\theta \tag{6.26}$$

Differentiating the above equation with respect to time gives:

$$\frac{d}{dt}\left(\frac{\partial L}{\partial \dot{x}_c}\right) = m\ddot{x}_c + ma\ddot{\theta}\sin\theta + ma\dot{\theta}^2\cos\theta \tag{6.27}$$

$$\frac{d}{dt}\left(\frac{\partial L}{\partial \dot{y}_c}\right) = m\ddot{y}_c - ma\ddot{\theta}\cos\theta + ma\dot{\theta}^2\sin\theta \tag{6.28}$$

$$\frac{d}{dt}\left(\frac{\partial L}{\partial \dot{\theta}}\right) = I_C\ddot{\theta} + 2ma^2\ddot{\theta} + ma\ddot{x}_c\sin\theta + ma\dot{x}_c\dot{\theta}\cos\theta - ma\ddot{y}_c\cos\theta + m\dot{y}_c a\dot{\theta}\sin\theta \tag{6.29}$$

Other differentiations in the Lagrange equation are:

$$\frac{\partial L}{\partial x_c} = 0 \tag{6.30}$$

$$\frac{\partial L}{\partial y_c} = 0 \tag{6.31}$$

$$\frac{\partial L}{\partial \theta} = m\dot{x}_c a\dot{\theta}\cos\theta + m\dot{y}_c a\dot{\theta}\sin\theta \tag{6.32}$$

Substituting the above term in the Lagrange equation gives:

$$m\ddot{x}_c + ma\ddot{\theta}\sin\theta + ma\dot{\theta}^2\cos\theta = F_x + C_1 \tag{6.33}$$

$$m\ddot{y}_c - ma\ddot{\theta}\cos\theta + ma\dot{\theta}^2\sin\theta = F_y + C_2 \tag{6.34}$$

$$\begin{aligned}(I_C + 2ma^2)\ddot{\theta} + ma\ddot{x}_c\sin\theta + ma\dot{x}_c\dot{\theta}\cos\theta \\ - ma\ddot{y}_c\cos\theta + m\dot{y}_c a\dot{\theta}\sin\theta - m\dot{x}_c a\dot{\theta}\cos\theta - m\dot{y}_c a\dot{\theta}\sin\theta = \tau + C_3\end{aligned} \tag{6.35}$$

Simplifying the above equations the design has:

$$m\ddot{x}_c + ma\ddot{\theta}\sin\theta + ma\dot{\theta}^2\cos\theta = F_x + C_1 \tag{6.36}$$

$$m\ddot{y}_c - ma\ddot{\theta}\cos\theta + ma\dot{\theta}^2\sin\theta = F_y + C_2 \tag{6.37}$$

$$(I_C + 2ma^2)\ddot{\theta} + ma\ddot{x}_c\sin\theta - ma\ddot{y}_c\cos\theta = \tau + C_3 \tag{6.38}$$

where, F_x is the actuator force in the x-direction; F_y is the actuator force in the y-direction; τ is the actuator rotational torque on the robot; C_X, C_Y, C_θ are the constraint forces in the x ,y and θ directions. Representing the above equations in the matrix form the design has:

$$\begin{bmatrix} m & 0 & ma\sin\theta \\ 0 & m & -ma\cos\theta \\ ma\sin\theta & -ma\cos\theta & I_C + 2ma^2 \end{bmatrix} \ddot{q} + \begin{bmatrix} ma\dot{\theta}^2\cos\theta \\ ma\dot{\theta}^2\sin\theta \\ 0 \end{bmatrix} = \begin{bmatrix} F_x \\ F_y \\ \tau \end{bmatrix} + \begin{bmatrix} C_X \\ C_Y \\ C_\theta \end{bmatrix} \tag{6.39}$$

We can relate the forces in the x, y and θ directions to the actuator torques on each wheel according to the free body diagram of the robot shown in Figure below:

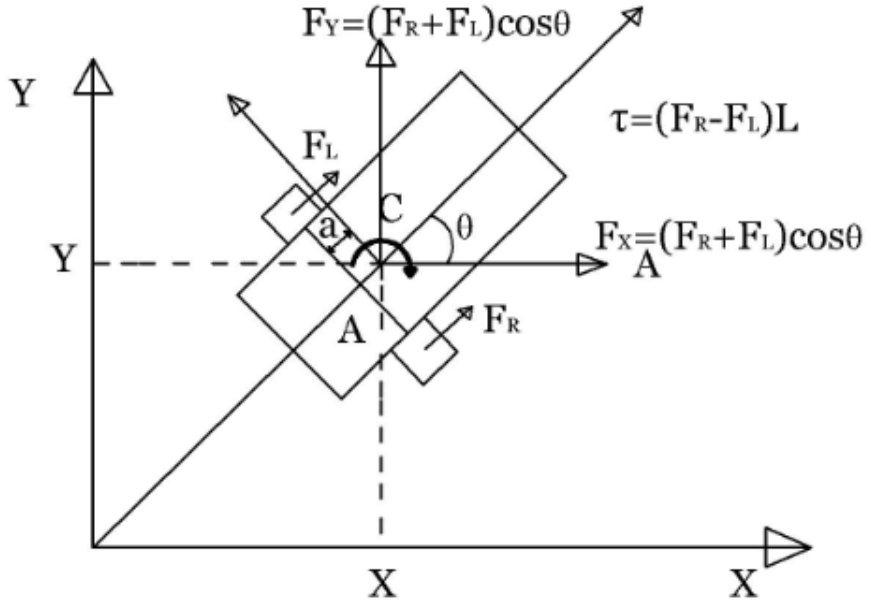

Figure 6.4. *The robots free body diagram*

$$F_R = \frac{\tau_R}{R_a} \tag{6.40}$$

$$F_L = \frac{\tau_L}{R_a} \tag{6.41}$$

$$F_X = (\frac{\tau_R}{R_a} + \frac{\tau_L}{R_a})\cos\theta = \frac{\cos\theta}{R_a}(\tau_R + \tau_L) \tag{6.42}$$

$$F_y = (\frac{\tau_R}{R_a} + \frac{\tau_L}{R_a})\sin\theta = \frac{\sin\theta}{R_a}(\tau_R + \tau_L) \tag{6.43}$$

According to the above equations, we can write the input force matrix in the system's dynamic equation as follows:

$$\begin{bmatrix} F_x \\ F_y \\ \tau \end{bmatrix} = \begin{bmatrix} \frac{\cos\theta}{R_a}(\tau_R + \tau_L) \\ \frac{\sin\theta}{R_a}(\tau_R + \tau_L) \\ \frac{L}{R_a}(\tau_R - \tau_L) \end{bmatrix} = \frac{1}{R_a}\begin{bmatrix} \cos\theta & \cos\theta \\ \sin\theta & \sin\theta \\ L & -L \end{bmatrix}\begin{bmatrix} \tau_R \\ \tau_L \end{bmatrix} \tag{6.44}$$

As it is mentioned in the previous section the nonholonomic constraints of this system are:

$$\dot{y}_c\cos\theta - \dot{x}_c\sin\theta - \dot{\theta}a = 0 \tag{6.45}$$

$$\dot{x}_c\cos\theta + \dot{y}_c\sin\theta + L\dot{\theta} = R_a\dot{\varphi}_R \tag{6.46}$$

$$\dot{x}_c\cos\theta + \dot{y}_c\sin\theta - L\dot{\theta} = R_a\dot{\varphi}_L \tag{6.47}$$

According to these constraint equations, the constraint forces will become:

$$C_X = m(\dot{x}_c \cos\theta + \dot{y}_c \sin\theta)\dot{\theta}\sin\theta \tag{6.48}$$

$$C_Y = -m(\dot{x}_c \cos\theta + \dot{y}_c \sin\theta)\dot{\theta}\cos\theta \tag{6.49}$$

$$C_\theta = ma(\dot{x}_c \cos\theta + \dot{y}_c \sin\theta)\dot{\theta} \tag{6.50}$$

The matrix representation of the above constraint forces is as follows:

$$\begin{bmatrix} C_X \\ C_Y \\ C_\theta \end{bmatrix} = \begin{bmatrix} m(\dot{x}_c \cos\theta + \dot{y}_c \sin\theta)\dot{\theta}\sin\theta \\ -m(\dot{x}_c \cos\theta + \dot{y}_c \sin\theta)\dot{\theta}\cos\theta \\ ma(\dot{x}_c \cos\theta + \dot{y}_c \sin\theta)\dot{\theta} \end{bmatrix} = A^T(q)\lambda \tag{6.51}$$

where $A^T(q)$ is as defined in (6.53), and $\lambda = -m(\dot{x}_c \cos\theta + \dot{y}_c \sin\theta)\dot{\theta}$. According to the above derivations, the complete form of the differential drive mobile robot dynamic equation is as follows:

$$\begin{bmatrix} m & 0 & ma\sin\theta \\ 0 & m & -ma\cos\theta \\ ma\sin\theta & -ma\cos\theta & I_C + 2ma^2 \end{bmatrix} \ddot{q} + \begin{bmatrix} ma\dot{\theta}^2\cos\theta \\ ma\dot{\theta}^2\sin\theta \\ 0 \end{bmatrix}$$
$$= \frac{1}{R_a}\begin{bmatrix} \cos\theta & \cos\theta \\ \sin\theta & \sin\theta \\ L & -L \end{bmatrix}\begin{bmatrix} \tau_R \\ \tau_L \end{bmatrix} + \begin{bmatrix} m(\dot{x}_c \cos\theta + \dot{y}_c \sin\theta)\dot{\theta}\sin\theta \\ -m(\dot{x}_c \cos\theta + \dot{y}_c \sin\theta)\dot{\theta}\cos\theta \\ ma(\dot{x}_c \cos\theta + \dot{y}_c \sin\theta)\dot{\theta} \end{bmatrix} \tag{6.52}$$

Comparing the above equation with the general dynamic form (6.12), the parameters for the differential drive robot are:

$$\begin{aligned} M(q) &= \begin{bmatrix} m & 0 & ma\sin\theta \\ 0 & m & -ma\cos\theta \\ ma\sin\theta & -ma\cos\theta & I_C + 2ma^2 \end{bmatrix} \\ \tau &= \begin{bmatrix} \tau_R \\ \tau_L \end{bmatrix} \\ A^T(q) &= \begin{bmatrix} -\sin\theta & \cos\theta & -a \end{bmatrix} \\ \lambda &= -m(\dot{x}_c \cos\theta + \dot{y}_c \sin\theta)\dot{\theta} \\ B(q) &= \frac{1}{R_a}\begin{bmatrix} \cos\theta & \cos\theta \\ \sin\theta & \sin\theta \\ L & -L \end{bmatrix} \end{aligned} \tag{6.53}$$

Since the robot operates on a flat horizontal surface at low speed, friction, gravitational

effects, and external disturbances are neglected, so $F(\dot{q}) = G(q) = \tau_d = 0$.

The above system can be transformed into a more convenient expression for control and simulation purposes. In this transformation, we are trying to find a way to eliminate the constraint term from the equation. The following two matrices are defined to do this transformation:

$$v_a(t) = \begin{bmatrix} v \\ \omega \end{bmatrix} = \begin{bmatrix} \dot{X}_R \\ \dot{\theta} \end{bmatrix} = \begin{bmatrix} v_1 \\ v_2 \end{bmatrix} \tag{6.54}$$

From the forward kinematic equation, we can realize that the $S(q)$ matrix is the modified forward kinematic matrix which has two velocity terms related to the distance between the robot centroid and wheel axis. Therefore, we can write the following equation for the system

$$\dot{q} = \begin{bmatrix} \dot{x}_c \\ \dot{y}_c \\ \dot{\theta} \end{bmatrix} = S(q)v_a(t) = \begin{bmatrix} \cos\theta & -a\sin\theta \\ \sin\theta & a\cos\theta \\ 0 & 1 \end{bmatrix} \begin{bmatrix} v \\ \omega \end{bmatrix} \tag{6.55}$$

It can easily be proved that the *S (q)* matrix has the following relation with $A(q)$ matrix:

$$S^T(q)A^T(q) = 0 \tag{6.56}$$

Differentiating the above equation gives

$$\ddot{q} = \dot{S}(q)v_a(t) + S(q)\dot{v}_a(t) \tag{6.57}$$

Substituting the above equation in the dynamic equation of the robot will result the following equation

$$M(q)\left[\dot{S}(q)v_a(t) + S(q)\dot{v}_a(t)\right] + V_m(q,\dot{q})S(q)v_a(t) + F(\dot{q}) + G(q) + \tau_d = B(q)\tau - A^T(q)\lambda \tag{6.58}$$

$$M(q)\dot{S}(q)v_a(t) + M(q)S(q)\dot{v}_a(t) + V_m(q,\dot{q})S(q)v_a(t) + F(\dot{q}) + G(q) + \tau_d = B(q)\tau - A^T(q)\lambda \tag{6.59}$$

Where:

$$V_m(q,\dot{q}) = \begin{bmatrix} 0 & 0 & ma\dot{\theta}\cos\theta \\ 0 & 0 & ma\dot{\theta}\sin\theta \\ 0 & 0 & 0 \end{bmatrix} \tag{6.60}$$

The next step to eliminate the constraint matrix $A^T(q)\lambda$ is to multiply equation (6.59) by $S^T(q)$ as follows

$$\begin{aligned}\Big[S^T(q)M(q)S(q)\Big]\dot{v}_a(t) + \Big[S^T(q)M(q)\dot{S}(q) + S^T(q)V_m^T(q,\dot{q})S\Big]v_a(t) \\ + S^T(q)F(\dot{q}) + S^T(q)G(q) + S^T(q)\tau_d = S^T(q)B(q)\tau - S^T(q)A^T(q)\lambda\end{aligned} \tag{6.61}$$

As it can be seen from the above equation, the design has $S^T(q)A^T(q)$ which is zero according to equation. Therefore the constraint term is eliminated and the new dynamic equation is

$$\begin{aligned}\Big[S^T(q)M(q)S(q)\Big]\dot{v}_a(t) + \Big[S^T(q)M(q)\dot{S}(q) + S^T(q)V_m^T(q,\dot{q})S\Big]v_a(t) \\ + S^T(q)F(\dot{q}) + S^T(q)G(q) + S^T(q)\tau_d = S^T(q)B(q)\tau\end{aligned} \tag{6.62}$$

By the following definitions (Dhaouadi & Hatab, 2013 [23]), we can rewrite the above equation in reduced form as:

$$\tilde{M}(q)\dot{v}_a(t) + \tilde{C}_m(q,\dot{q})\,v_a(t) + \tilde{F}(\dot{q}) + \tilde{G}(q) + \tilde{\tau}_d = \tilde{B}(q)\,\tau \tag{6.63}$$

This reduced equation eliminates the constraint term and is used for control design and simulation. The tilde quantities are defined as:

$$\tilde{M}(q) = S^T(q)M(q)S(q) \tag{6.64}$$

$$\tilde{C}_m(q,\dot{q}) = S^T(q)M(q)\dot{S}(q) + S^T(q){V_m}^T(q,\dot{q})S \tag{6.65}$$

$$V_m(q,\dot{q}) = \begin{bmatrix} 0 & 0 & ma\dot{\theta}\cos\theta \\ 0 & 0 & ma\dot{\theta}\sin\theta \\ 0 & 0 & 0 \end{bmatrix} \tag{6.66}$$

Since the robot operates on a flat horizontal surface at low speed, friction, gravitational effects, and external disturbances are neglected, so $\tilde{F} = \tilde{G} = \tilde{\tau}_d = 0$.

$$\tilde{B}(q) = S^T(q)B(q) \tag{6.67}$$

The reduced inertia matrix $\tilde{M}(q)$ evaluates to:

$$\tilde{M}(q) = S^T(q)M(q)S(q) = \begin{bmatrix} m & 0 \\ 0 & I_C + ma^2 \end{bmatrix} \tag{6.68}$$

The reduced Coriolis matrix $\tilde{C}_m(q, \dot{q})$ evaluates to:

$$\tilde{C}_m(q, \dot{q}) = \begin{bmatrix} 0 & -ma\dot{\theta} \\ ma\dot{\theta} & 0 \end{bmatrix} \tag{6.69}$$

6.3 Modeling of the Actuator

The actuator is a device that generates the torque that is required to create the desired motion. In case of our project there are three actuators each of them are selected to be DC motors. Two of them are coupled with chain sprocket mechanism in order to actuate the drive mechanism. The other one is connected to the power screw that actuates the lifting mechanism. In this section we will develop the mathematical model of these actuators.

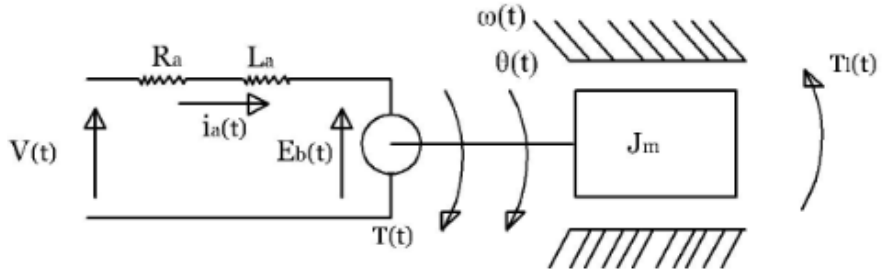

Figure 6.5. *Modeling diagram of DC motor*

We can write electrical and mechanical equation of dc motor as follows:

According to Kirchhoff's voltage law (KVL) the electrical equation of the dc motor is:

$$V(t) = R_a I_a(t) + L_a \frac{di_a(t)}{dt} + E_b(t) \tag{6.70}$$

Where: K_b back-EMF constant

In addition to these the motor generate a torque $\tau(t)$ which is proportional to the armature current $I_a(t)$.

$$\tau(t) = K_T I_a(t) \tag{6.71}$$

Converting the above equations into Laplace domain and substituting the above expressions for torque and back-EMF:

$$V(s) = (R + Ls)I_a(s) + K_b\omega(s) \tag{6.72}$$

Based on Euler's second law:

$$\tau(s) = (Js + B)\omega(s) \tag{6.73}$$

Substituting the equation for the torque into KVL equation:

$$V(s) = (R + Ls)I_a(s) + K_b(\frac{\tau(s)}{Js + B}) \tag{6.74}$$

From equations for the torque we can describe the I_a as:

$$I_a = \frac{Js + B}{K_t}\omega(s) \tag{6.75}$$

$$V(s) = \frac{(R + Ls)(Js + B)\omega(s)}{K_t} + K_b\omega(s) \tag{6.76}$$

$$\frac{\omega(s)}{V(s)} = \frac{K_t}{(R + Ls)(Js + B) + K_t K_b} \tag{6.77}$$

The following tables show representative parameters for the two DC motor types used in this project. Values are taken as representative from publicly available planetary motor manufacturer catalogs and are clearly labelled as such; they serve as a basis for the transfer function analysis that follows.

Table 6.2. *Representative parameters of the drive DC motor (PM71-110 PG56)*

Parameter	Symbol	Representative value
Armature resistance	R_a	$1.2\,\Omega$
Armature inductance	L_a	$8\,\mathrm{mH}$
Back-EMF constant	K_b	$0.95\,\mathrm{V\,s/rad}$
Torque constant	K_t	$0.95\,\mathrm{Nm/A}$
Rotor inertia	J_m	$5.2 \times 10^{-3}\,\mathrm{kg\,m^2}$
Viscous friction coefficient	B	$0.025\,\mathrm{Nm\,s/rad}$
Rated speed	ω_r	$318\,\mathrm{rpm}$

Representative values from manufacturer catalog (planetary motors).

Table 6.3. *Representative parameters of the lift DC motor (PM60-105 PG28)*

Parameter	Symbol	Representative value
Armature resistance	R_a	$3.5\,\Omega$
Armature inductance	L_a	$15\,\mathrm{mH}$
Back-EMF constant	K_b	$0.38\,\mathrm{V\,s/rad}$
Torque constant	K_t	$0.38\,\mathrm{Nm/A}$
Rotor inertia	J_m	$1.3417 \times 10^{-4}\,\mathrm{kg\,m^2}$
Viscous friction coefficient	B	$0.008\,\mathrm{Nm\,s/rad}$
Rated speed	ω_r	$3249\,\mathrm{rpm}$

Representative values from manufacturer catalog (planetary motors).

6.4 Trajectory Generation

The trajectory generator generates different desired trajectories for the robot. A trajectory is a function of time *q(t)* such that $q(t_0) = q_s$ and $q(t_f) = q_f$. In this case $t_f - t_0$ represents the amount of time taken to execute the trajectory. Since the trajectory is parameterized by time, we can compute velocities and accelerations by differentiation. It is common practice to choose trajectories from a finitely differentiable family for example polynomials of degree n, where n depends on the number of constraints to be satisfied. Consider the mobile robot case in which we wish to generate a polynomial joint trajectory between two configurations and that we wish to specify the start and end velocities for the trajectories. This gives four constraints that the trajectory must satisfy. Therefore at minimum we require a polynomial with four independent coefficients that can be chosen to satisfy these constraints. Thus we consider a cubic trajectory of the form:

$$q(t) = a_0 + a_1 t + a_2 t^2 + a_3 t^3 \tag{6.78}$$

Then the desired velocity will be given as:

$$\dot{q}(t) = a_1 + 2a_2 t + 3a_3 t^2 \tag{6.79}$$

Combining the above equations with four constraints yields four equations with fours unknowns as follows:

The trajectory boundary conditions in matrix form are

$$A\,\mathbf{a} = \mathbf{b} \tag{6.80}$$

where

$$A = \begin{bmatrix} 1 & t_0 & t_0^2 & t_0^3 \\ 0 & 1 & 2t_0 & 3t_0^2 \\ 1 & t_f & t_f^2 & t_f^3 \\ 0 & 1 & 2t_f & 3t_f^2 \end{bmatrix}, \quad \mathbf{a} = \begin{bmatrix} a_0 \\ a_1 \\ a_2 \\ a_3 \end{bmatrix}, \quad \mathbf{b} = \begin{bmatrix} q_0 \\ v_0 \\ q_f \\ v_f \end{bmatrix} \tag{6.81}$$

The above equation always has a unique solution for nonzero time interval provided for the trajectory execution. For the control simulation purpose, we define q_0 and q_f as the start and end position of the robot and we assume $v_0 = v_f = 0$ for this case. The shape of the path which can be any path such as a straight line or a sinusoidal is defined as a function between x and y component of the robot path.

6.5 Control System Design for the Drive System

The proposed controller for the drive system is called kinematic based backstepping controller. The kinematic based backstepping controller for a nonholonomic mobile robot is a controller which is a popular controller in the field of mobile robotics. It's a stable tracking control rule for a nonholonomic mobile robot which neglects the vehicle dynamics and is based on the steering system.

In this control system two positions and orientations for the robot are going to be used: the reference position $q_r = \begin{bmatrix} x_r \\ y_r \\ \theta_r \end{bmatrix}^T$ and a current position $q_c = \begin{bmatrix} x_c \\ y_c \\ \theta_c \end{bmatrix}^T$. The reference position is the goal position and the current position is the real position at the moment.

The block diagram of this control structure is shown in Figure below:

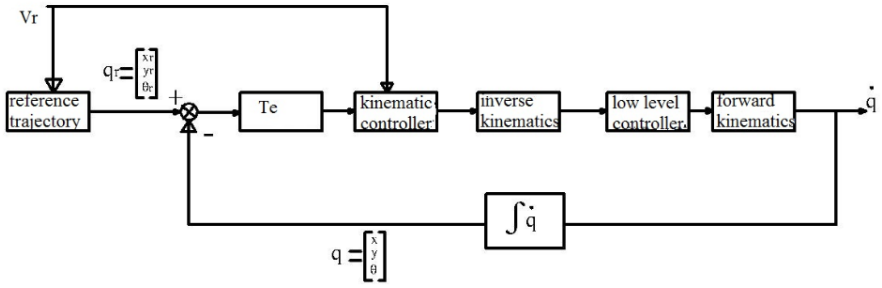

Figure 6.6. *Block diagram of kinematic back stepper controller*

We define an error posture or the tracking error e_p in the basis of the frame linked to the mobile platform or the local frame as follows:

$$e_p = \begin{bmatrix} e_x \\ e_y \\ e_\theta \end{bmatrix} = T_e(q_r - q) \tag{6.82}$$

$$\begin{bmatrix} e_x \\ e_y \\ e_\theta \end{bmatrix} = \begin{bmatrix} \cos\theta & \sin\theta & 0 \\ -\sin\theta & \cos\theta & 0 \\ 0 & 0 & 1 \end{bmatrix} \begin{bmatrix} x_r - x \\ y_r - y \\ \theta_r - \theta \end{bmatrix} \tag{6.83}$$

The control problem in this case will be to calculate a control rule for the vehicle, which calculated the target velocities $v_c = f(e_p, v_r, K)$ that makes the system asymptotically stable. The proposed [23] kinematic based control rule is as follows:

$$v_c = \begin{bmatrix} v_r \cos e_\theta + K_x e_x \\ \omega_r + K_y v_r e_y + K_\theta v_r \sin e_\theta \end{bmatrix} \tag{6.84}$$

where $K = (K_x, K_y, K_\theta)$ are positive gain constants.

The stability of the above control rule will be proved using the Lyapunov stability method in the next section.

6.6 Lyapunov Stability of the Controller

The Lyapunov stability analysis of the controller is done based on [23]

Lemma1:

From the above equation for error posture e_p

$$\dot{e}_p = f(t, e_p) = \begin{bmatrix} \omega(e_p, q_r)e_y - v(e_p, q_r) + v_r \cos e_\theta \\ -\omega(e_p, q_r)e_x + v_r \sin e_\theta \\ \omega_r - \omega(e_p, q_r) \end{bmatrix} \tag{6.85}$$

The above expression can be proved Based on the tracking error and the kinematic equations of the robot:

$$e_p = \begin{bmatrix} \cos\theta & \sin\theta & 0 \\ -\sin\theta & \cos\theta & 0 \\ 0 & 0 & 1 \end{bmatrix} \begin{bmatrix} x_r - x \\ y_r - y \\ \theta_r - \theta \end{bmatrix} = \begin{bmatrix} e_x \\ e_y \\ e_\theta \end{bmatrix} \tag{6.86}$$

$$\dot{e}_x = (\dot{x}_r - \dot{x})\cos\theta + (\dot{y}_r - \dot{y})\sin\theta - (x_r - x)\dot{\theta}\sin\theta + (y_r - y)\dot{\theta}\cos\theta \tag{6.87}$$

$$\dot{e}_x = e_y\omega - v + \dot{x}_r \cos(\theta_r - \theta) + \dot{y}_r \sin(\theta_r - \theta) \tag{6.88}$$

$$\dot{e}_x = e_y\omega - v + v_r \cos e_\theta \tag{6.89}$$

$$\dot{e}_y = -(\dot{x}_r - \dot{x})\sin\theta + (\dot{y}_r - \dot{y})\cos\theta - (x_r - x)\dot{\theta}\cos\theta - (y_r - y)\dot{\theta}\sin\theta \tag{6.90}$$

$$\dot{e}_x = -e_x\omega - \dot{x}_r \sin(\theta_r - \theta) + \dot{y}_r \cos(\theta_r - \theta) \tag{6.91}$$

$$\dot{e}_y = -e_x\omega + v_r \sin e_\theta \tag{6.92}$$

$$\dot{e}_\theta = \dot{\theta}_r - \dot{\theta} = \omega_r - \omega \tag{6.93}$$

When we substitute v and ω by $v(e_p, q_r)$ and $\omega(e_p, q_r)$ we can obtain lemma1.

Proposition 1:

If we use the control rule in the equation for v_c, it can be said that when the reference velocity $e_p = 0$, $v_r > 0$ is a stable equilibrium point.

Let us propose a scalar function V as a Lyapunov function candidate for the above system:

$$V = \frac{1}{2}({e_x}^2 + {e_y}^2) + \frac{(1 - \cos\,(e_y)\,)}{K_y} \tag{6.94}$$

Clearly $V \geq 0$ and $V = 0\ if\ e_p = 0$, therefore the above V function is a positive definite function. Furthermore, by using Lemma 1 the design has:

$$\dot{V} = \dot{e}_x e_x + \dot{e}_y e_y + \frac{\dot{e}_\theta \sin(e_\theta)}{K_y} \tag{6.95}$$

Substituting the controller expressions $v = v_r \cos e_\theta + K_x e_x$ and $\omega = \omega_r + v_r(K_y e_y +$

$K_\theta \sin e_\theta$):

$$\begin{aligned}\dot{V} = &\Big[(\omega_r + v_r(K_y e_y + K_\theta \sin e_\theta))e_y - K_x e_x\Big]e_x \\ &+ \Big[-(\omega_r + v_r(K_y e_y + K_\theta \sin e_\theta))e_x + v_r \sin e_\theta\Big]e_y \\ &+ \frac{[-v_r(K_y e_y + K_\theta \sin e_\theta)]\sin(e_\theta)}{K_y}\end{aligned} \tag{6.96}$$

Collecting and cancelling the cross-terms $\pm\,\omega_r e_x e_y$ and $\pm\, v_r K_y e_y^2$:

$$\dot{V} = -K_x {e_x}^2 - \frac{v_r K_\theta \sin^2 e_\theta}{K_y} \leq 0 \tag{6.97}$$

Consequently the Lyapunov function V's derivative is a negative definite function. That means uniformly asymptotically stability around $e_p = 0$ under the conditions that are $v_r,\ \omega_r,\ K_x,\ K_y$ bounded and, that v_r and ω_r are continuous. Please note that the Lyapunov stability analysis which is presented here is based on the research work [32].

6.7 Control System Design for the Lifting Mechanism

The lifting mechanism as it's illustrated in chapter three is the mechanism that makes the fork to perform its task normally lifting and carrying the load to the desired position. In order to make the fork to do such task, the motion of the lifting mechanism have to be controlled appropriately. This section deals with the design of control system for the lifting mechanism.

The overall closed loop control of the system seems:

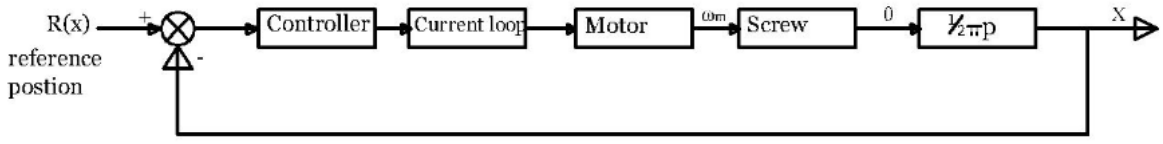

Figure 6.7. *Block diagram of the control loop of the lifting mechanism*

Since our motor is a DC one the current loop, that converts the control signal to the current supplied to the motor and be modelled as a constant gain. And the transfer function of the motor which is computed in the previous section is:

$$\frac{\omega(s)}{V(s)} = \frac{K_t}{(R + Ls)(J_m s + B) + K_t K_b} \tag{6.98}$$

And we know that the torque of the motor $\tau(s)$ has a relation with the angular speed of the motor $\omega(s)$ as:

$$\frac{\omega(s)}{\tau(s)} = \frac{1}{(J_m s + B)} \tag{6.99}$$

The transfer function of the motor taking the Voltage as an input and torque as an output will be:

$$\frac{\tau(s)}{V(s)} = \frac{K_t(J_m s + B)}{(R + Ls)(J_m s + B) + K_t K_b} \tag{6.100}$$

And the transfer function of the lead screw which is computed in the previous section is:

$$\frac{\theta(s)}{\tau(s)} = \frac{1}{(J_{\text{screw}} s^2 + C_{\text{screw}} s + K_{\text{screw}})} \tag{6.101}$$

The combined transfer function of the motor and the screw will be:

$$\frac{\theta(s)}{\omega_m(s)} = \frac{K_t(J_m s + B)}{(J_{\text{screw}} s^2 + C_{\text{screw}} s + K_{\text{screw}})\Big[(R + Ls)(J_m s + B) + K_t K_b\Big]} \tag{6.102}$$

In order to find the spring (K_{screw}) and viscous friction (C_{screw}) constants of the screw the design has to undergo some additional computations. We can calculate the spring constant (K_{screw}) of the screw from the manufacturer's manual by using the formula [39] :

$$K_{\text{screw}} = \frac{165 D^2}{l} \tag{6.103}$$

where D is the mean diameter of the screw and l length of the screw.

$$K_{\text{screw}} = \frac{165 D^2}{l} = \frac{165 \times (30 \times 10^{-3})^2}{2} = 0.07425 \tag{6.104}$$

Chapter 7

Simulation and Results

7.1 Simulation of the Mechanical Design

Stress – Strain analysis of Automatic guided vehicle

Stress and strain are the two building blocks of structural analysis. They are used to understand where a components is in relationship to material failure, both response to applied loads on a structure, and measurements of both determine material failure criteria and behavior. Stress is the pressure a material is seeing in response to load. Strain is the distance the spring stretches when pulled, divided by original length.

The stress-strain analysis of frame, lift and fork shown by using Solid works software. The maximum and minimum stress and strain values are shown in the form of color. Each color has its own stress and strain value. Red color indicate maximum stress and strain and Blue color indicate minimum stress and strain of the body.

Structural analysis of frame of the AGV

The structure of frame was built using Cast alloy steel (AISI 1006). A normal force of 200 N was applied to the structure in the FEA model.

FEA load limitation: The 200 N applied load is a conservative placeholder used for an initial feasibility check; it is substantially lower than the actual design loads derived in Chapter 4 (total driving force $F \approx 4{,}016$ N, corresponding frame reactions on the order of 1,600 N per side). The FEA results below should therefore be treated as qualitative indicators of stress distribution, not as quantitative verification of structural adequacy. A re-analysis with the correct loading conditions is recommended as part of any future detailed design review.

Stress- Strain analysis for frame of AGV

Stress analysis of the structure

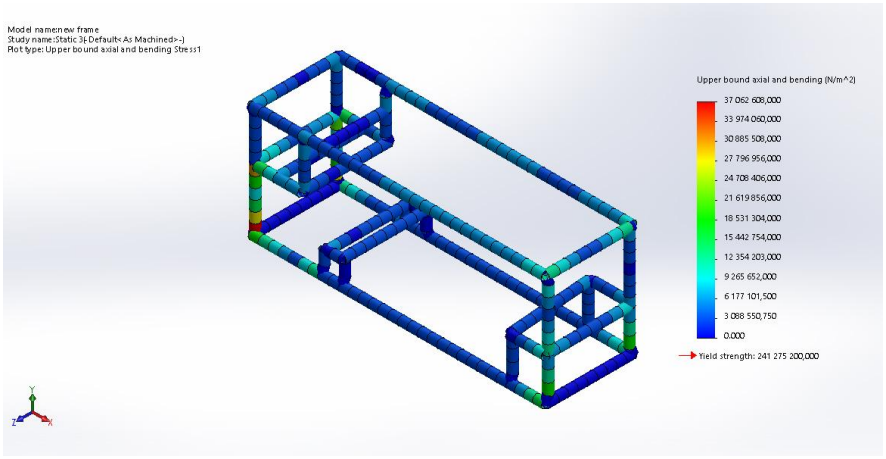

Figure 7.1. *Stress analysis of the AGV frame*

Observation

The area of low stress (dark blue) occur at the middle side of the model. The lowest von Mises stress is approximately zero N/m. Region at high stress are indicated in red. The maximum stress indicated is 37.063Mpa which occurs at joint of structure.

Stress- Strain analysis for lift

structure

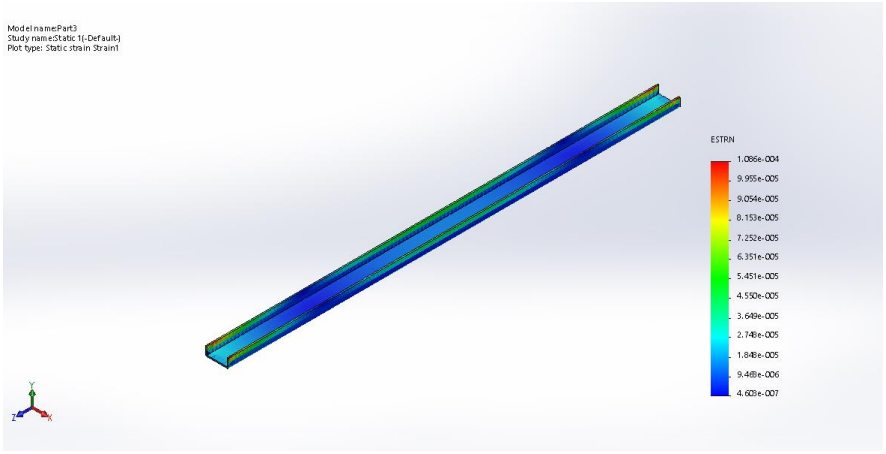

Figure 7.2. *Stress analysis of the lift structure*

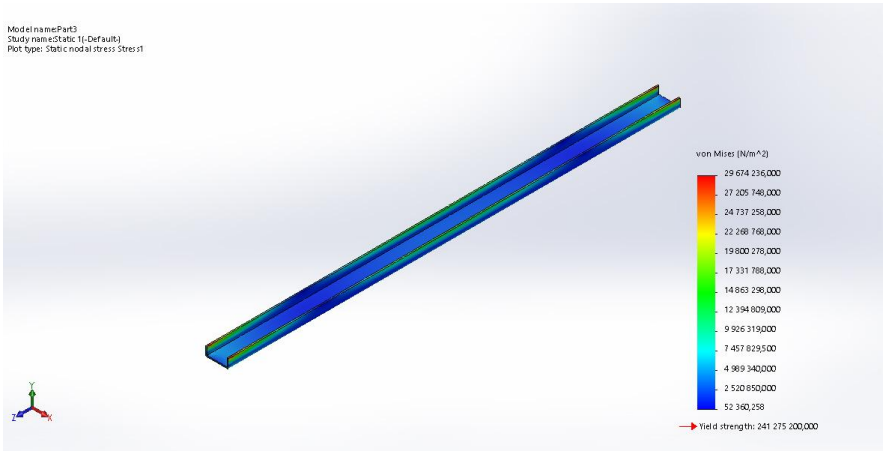

Figure 7.3. *Strain analysis of the lift structure*

Observation

The area of low stress (dark blue) occurs at the middle of the model. The lowest von Mises stress is approximately 52.36 MPa. Regions of high stress are indicated in red. The maximum von Mises stress is 296 MPa, occurring at a structural joint.

Yield-strength limitation: The yield strength of AISI 1006 steel is $S_y \approx 170$ MPa. The maximum FEA stress of 296 MPa exceeds this value, indicating that the lift structure would yield under the applied load in this FEA scenario. It should be noted that the FEA used a conservative 200 N applied load (see frame analysis note above), which for the lift structure corresponds to a fraction of the actual 1.2 kN lift load. With the correct loading the maximum stress would be even higher. It is therefore recommended that the lift structure material be upgraded to a higher-strength steel such as AISI 4140 ($S_y \approx 655$ MPa, $S_{ut} \approx 1020$ MPa) in a future detailed design iteration, and that an FEA re-analysis be performed with the correct loading.

Stress-Strain analysis of fork

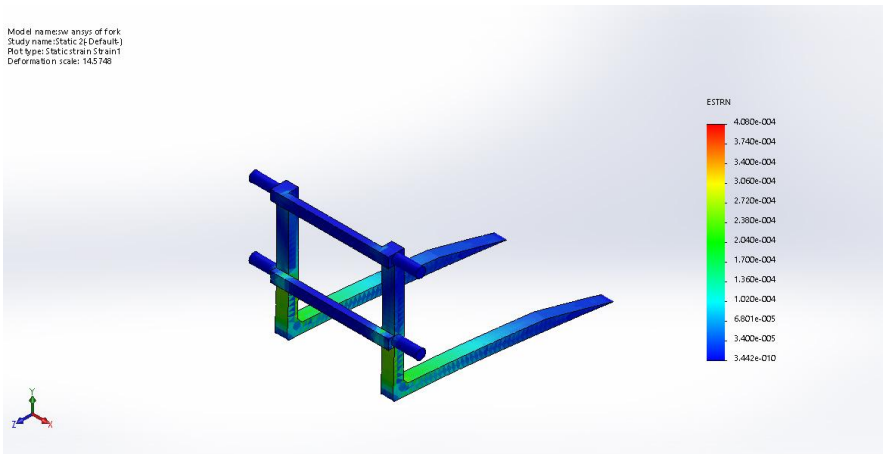

Figure 7.4. *Strain analysis of fork*

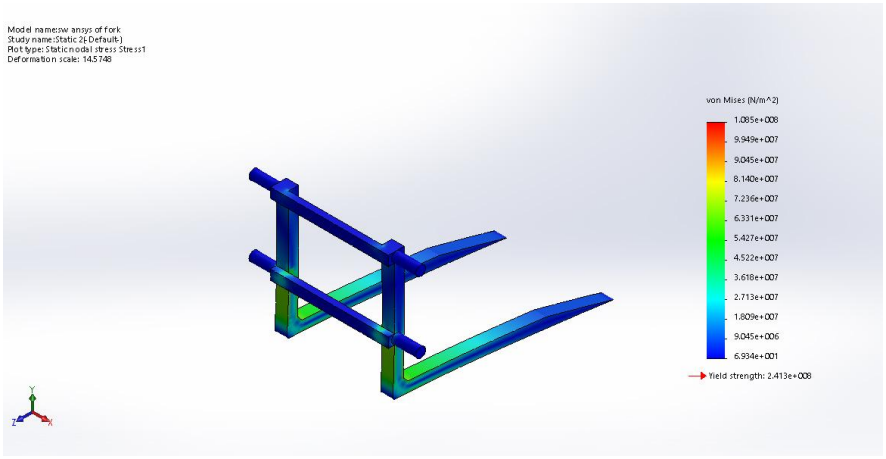

Figure 7.5. *Stress analysis of the fork*

Observation

The area of low stress (dark blue) occur at the middle side of the model. The lowest von Mises stress is approximately 69.34 N/m. Region at high stress are indicated in red. The maximum stress indicated is 10.85 Mpa which occurs at joint of structure.

7.2 Simulation of the Control System

Simulation of the drive control system

As it's discussed in chapter 6 the controller which is implemented on the drive mechanism is called kinematic back stepped controller. The implementation and simulation of the controller on Matlab/Simulink is presented here. The task of this controller is to make sure the motion of the robot to follow the trajectory which is generated by the trajectory generator. The control system of the drive mechanism is an integration of the kinematic controller and the low level PID controller for the actuators. The main purpose of the kinematic controller is to correct the motion of the robot to follow the trajectory which is generated by the trajectory generator. In order to do this the control system computes the error of the robot's motion then generates a reference input signal for the low level controller or the controller of the actuator. The controller of the actuator makes the actuator to generate the desired motion which will make the robot to move along the generated trajectory.

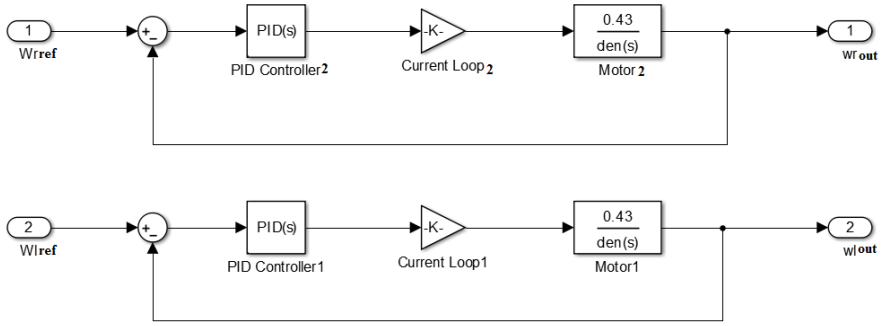

Figure 7.6. *Simulink simulation diagram of the low level controller*

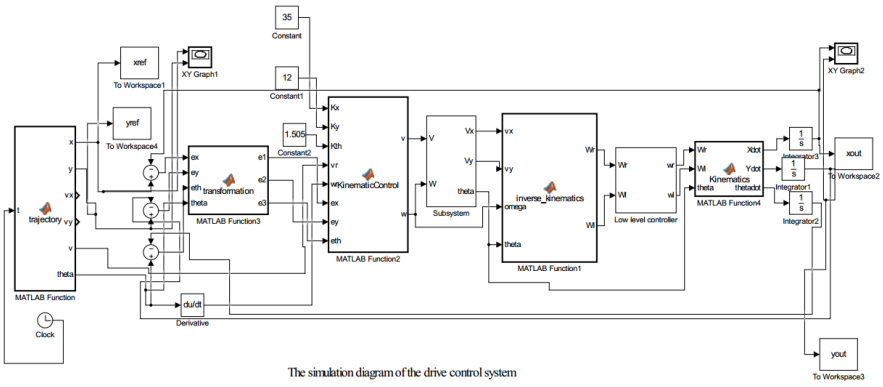

Figure 7.7. *Simulation diagram of the control system*

The motion of the AGV which is controlled by the designed controller with $K_x = 35,\ K_y = 12,\ K_\theta = 1.505$ will be:

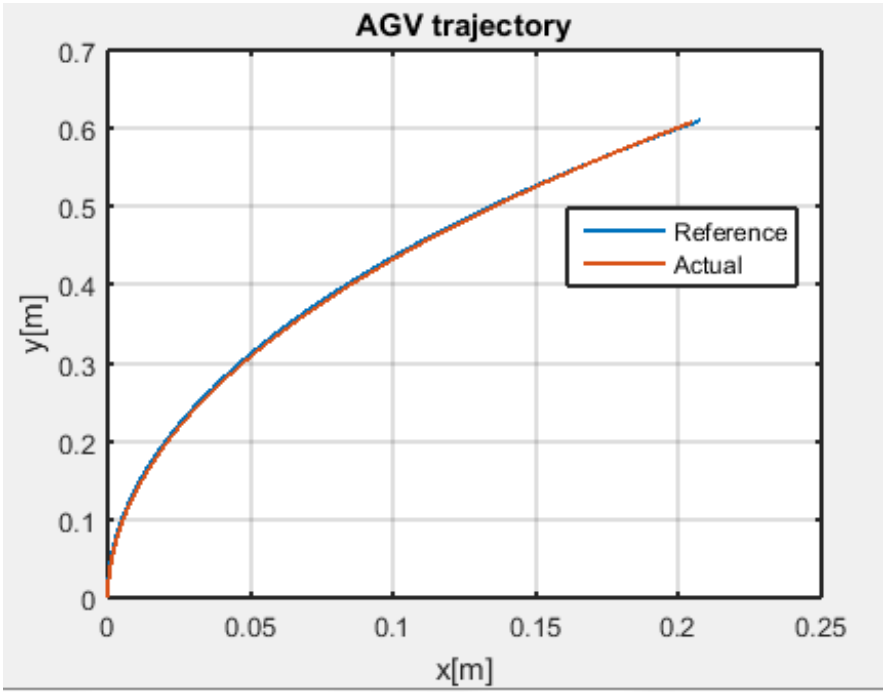

Figure 7.8. *Kinematic back stepping controller simulation*

As the result of the simulation shows the actual motion of the robot which is designated by the red color follows very well the reference trajectory which is designated by the blue color.

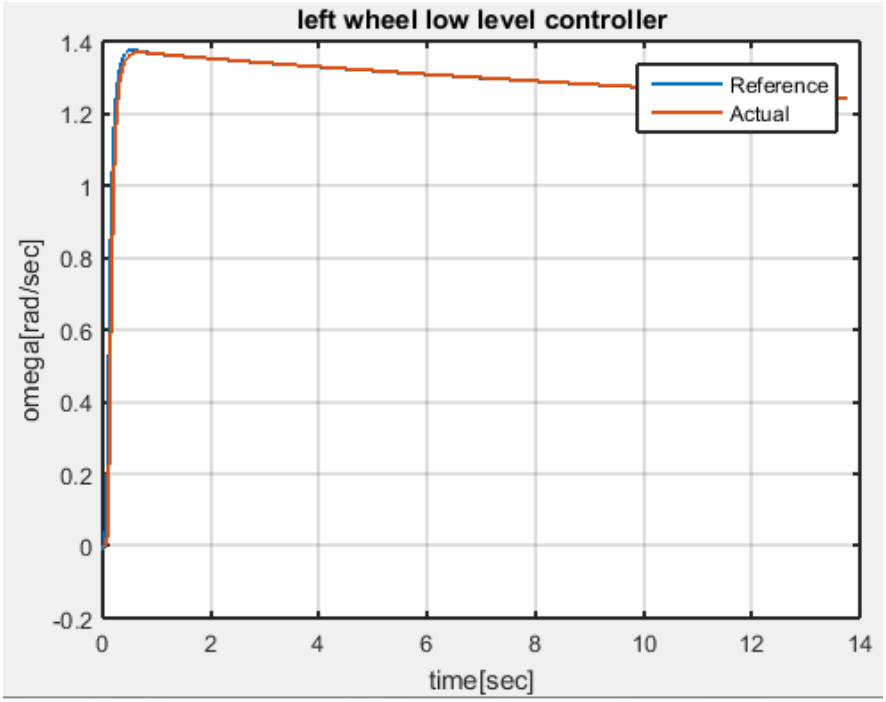

Figure 7.9. *The simulation result of low level controllers of the left and right motors*

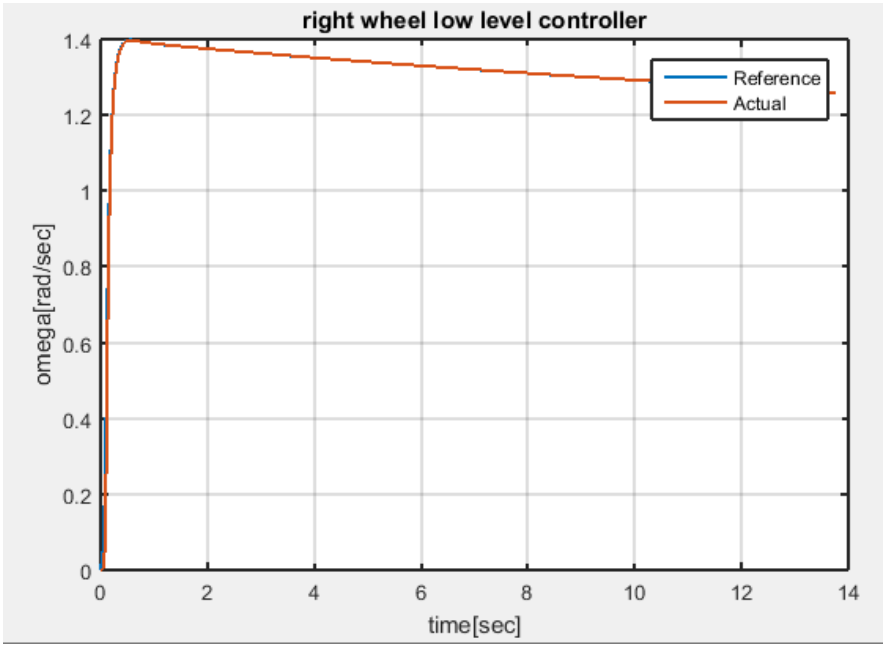

Figure 7.10. *Control system simulation output — angular speed response*

The output of the low level controllers with an input of angular speed from the controller is shown in the figure above. This controllers are design to be a PID

controller with Kd =0.00795, Kp=0.235, Ki=1.616 that makes the actuator to generate the desired motion based on the command that comes from the kinematic controller. The performance criteria of this controllers are rise time=0.021 s, settling time=0.12 s, percent overshoot=9.4%.

SIMULATION OF THE CONTROL SYSTEM OF LIFTING MECHANISM

The controller of the lifting mechanism is designed to be a PID controller that controls the motion of the fork along the screw. The implementation and simulation of the controller on Matlab/Simulink is shown below.

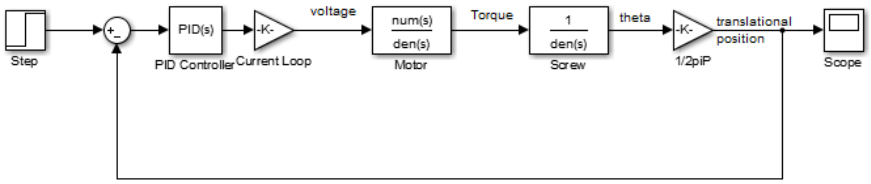

Figure 7.11. *Simulink simulation diagram of the lift control system*

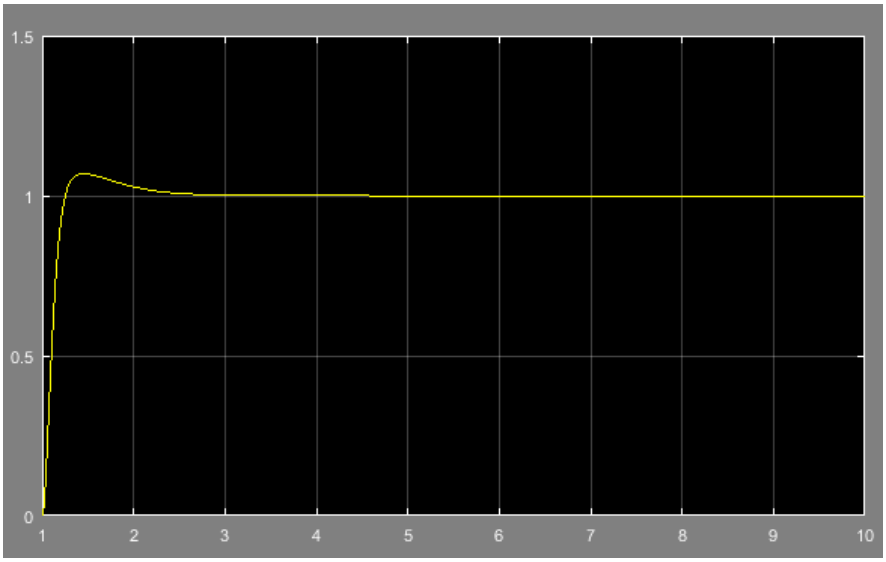

Figure 7.12. *Simulation result of the lift control system*

The performance criteria of the controller with Kp =16.91, Ki=26.9, Kd=1.256 are rise time=0.773 s, settling time=2.97 s, percent overshoot=7%.

Chapter 8

Economic Analysis

In order to check the economic viability or to calculate the saving attained by implementing an AGV material handling system in EPHARM pharmaceutical industry, the design has to consider the following factors. Taxes, Depreciation - assets with finite times loose value over time, Inflation - a rise in prices with respect to purchasing power over time, Ongoing or operational cost, Initial cost, Time value of money, and Interest rate.

Number of vehicle required

Number of vehicles can be calculated from the following parameters that are taken from our work space design. Loading time at the load station= 0.75min. Unloading time =0.5min. The following performance parameters are given: Vehicle velocity=80m/min. Availability=0.95. Traffic factor=0.90.

a) Travel distance loaded and empty, taken from our design work space

$$L_{d=}\ \ 8m + 20m = 28\ meter \tag{8.1}$$

$$L_{\mathrm{e}}\ = 15\ metres \tag{8.2}$$

b) Ideal vehicle delivery cycle time

$$T_C = \ T_{\mathrm{L}}\ +\ \frac{L_{\mathrm{D}}}{V_C} + T_{\mathrm{V}}\ +\ \frac{L_e}{V_C} \tag{8.3}$$

$$T_C = 0.75 + \frac{28}{80} + 0.5 + \frac{15}{80} = 1.7875\ min \tag{8.4}$$

c) Determine number of vehicles to make 30del/hr. Work load time

$$WL = R_f \times T_C = \frac{30del}{\mathrm{hr}} \times 1.7875min\ = 53.625\ min/hr \tag{8.5}$$

Available time

$$AT = 60 \times A \times T_f = 60 \times 0.95 \times 0.9 = 51.3\ min \tag{8.6}$$

Number of vehicles can be calculated as

$$\frac{W_L}{A_T} = \frac{53.625}{51.3} = 1.042\ \approx 1 \tag{8.7}$$

Since the number of vehicles should be an integer.

8.1 Future Value

Future value is the value of an asset at a specific date. It measures the nominal future sum of money that a given sum of money is "worth" at a specified time in the future assuming a certain interest rate.

$$FV = OI * (1 + i)^n \tag{8.8}$$

Where: FV = future value; OI = original investment; i = interest rate; n = number of years. The FV calculation will allow us to predict, with the assumption of stable growth rate, the amount of saving that can be generated by using different material handling systems. The interest rate of Ethiopia at current times is 5% [1]

A. TOTAL INITIAL COST

The total initial cost of the project including the manufacturing cost is estimated at Birr 135,000 of which 95 per cent will be required in domestic currency. The major breakdown of the total initial cost is shown in Table below. The manufacturing cost comprises three components: total cost of materials directly used, total cost of labour directly related to manufacturing, and total cost of the manufacturing process. Total cost of materials directly used

Table 8.1. *Operational cost of the project*

Name of Equipment	Price (Birr)
ARDINO UNO	1000
Electric cable	1000
Battery	3250
Resistors, Capacitors, Transistors and Diodes	750

[1] https://tradingeconomics.com/ethiopia/interest-rate

Table 8.1. *Operational cost of the project*

Name of Equipment	Price (Birr)
Transmitter and Receiver	800
Motor (geared DC motor)x3	15,853.02
Computer (personal computer)	10000
Idler wheel (caster type)	656.56
Coupling(X3)	5000
Bearing(X8)	4500
Power screw	5000
XB Communication module	550
Wheel (fixed type conventional wheel)x2	5500
Gear (2-small and 2-large) X4	3000
Sheet metal (2mX2m galvanized metal)	1000
Screw , Bolt, Nut, Washer	650
RHS rectangular tube	700
Lubrication (greases)	1500
RHS cylindrical tube	500

Therefore the Total budget required to finish this project is Birr 61,209.58ETB.

The total cost of labor directly related to manufacturing and the cost of manufacturing process can be assumed to be 10,000ETB

Table 8.2. *Detailed cost breakdown of AGV components*

No	Cost items	Cost(birr)
1	manufacturing cost	80,000
2	Installation cost	10,000
3	Miscellaneous cost*	12,000
4	Engineering cost**	30,000
5	Transportation cost	3,000
6	Total cost	135,000

*Miscellaneous cost is the cost other than above costs, incurred due to trainings, insurance

**Engineering costs include the price of design prepared by the engineering staff of the industry for installing the robot.

OPERATIONAL COST

Table 8.3. *Operational cost comparison: manual handling vs. AGV system*

No	Cost item	Cost
1	Maintenance cost	3,000
2	Spare parts cost	4,000
3	Energy cost	5,000
4	Indirect labour cost	10,000

Total annual cost for manual handling

The factory employs 11 workers across all shifts to transport packed items from the production line to the warehouse, each earning a monthly salary of 2,000 ETB. Additionally, 2 of the 5 hand trucks (each costing 10,000 ETB) are assumed to be replaced each year. The correct annual manual handling cost is therefore:

$$\begin{aligned} C_{\text{manual}} &= 11 \times 2{,}000\,\text{ETB/month} \times 12\,\text{months/year} \\ &\quad + 2 \times 10{,}000\,\text{ETB/year} \\ &= 264{,}000 + 20{,}000 = 284{,}000\,\text{ETB/year} \end{aligned} \tag{8.9}$$

The AGV annual operational cost from Table 8.3 is 22,000 ETB/year. The gross annual saving achieved by deploying the AGV is therefore $284{,}000 - 22{,}000 = 262{,}000$ ETB/year (before tax). Table 8.4 shows the year-by-year cash flow comparison over the 8-year analysis horizon ($i = 5\%$).

Table 8.4. *Eight-year cash flow comparison: manual handling vs. AGV system*

Year	Manual cost (ETB)	AGV cost (ETB)	Gross saving (ETB)	After-tax net CF (ETB)	Cumulative CF (ETB)
0	—	135,000	—	−135,000	−135,000
1	284,000	22,000	262,000	+166,625	+31,625
2	284,000	22,000	262,000	+166,625	+198,250
3	284,000	22,000	262,000	+166,625	+364,875
4	284,000	22,000	262,000	+166,625	+531,500
5	284,000	22,000	262,000	+166,625	+698,125
6	284,000	22,000	262,000	+166,625	+864,750
7	284,000	22,000	262,000	+166,625	+1,031,375
8	284,000	22,000	262,000	+166,625	+1,198,000

After-tax net CF $= 284{,}000 - 284{,}000 \times 0.35 + 11{,}500 \times 0.35 - 22{,}000 = 166{,}625$ ETB/year.

The cumulative cash flow turns positive during Year 1 (after approximately 10 months), confirming a payback period well under one year (see Section 8.2). For completeness, the future value of each system's total expenditure at year 8 (at $i = 5\%$) is:

$$FV_{\text{manual}} = 284{,}000 \times \frac{(1.05)^8 - 1}{0.05} = 284{,}000 \times 9.549 = 2{,}712{,}000\,\text{ETB} \tag{8.10}$$

$$FV_{\text{AGV}} = 135{,}000 \times (1.05)^8 + 22{,}000 \times \frac{(1.05)^8 - 1}{0.05} = 199{,}500 + 210{,}100 = 409{,}600\,\text{ETB} \tag{8.11}$$

Total 8-year saving (at future value) $= 2{,}712{,}000 - 409{,}600 = 2{,}302{,}400$ ETB.

	Using AGV				Using manual handling	
year	Initial cost	Operational cost	Total	Future cost of AGV	Operational cost	Future cost of manual handling
0	135000	22,000	157,000	157,000.00	45000	45000
1		22,000	22,000	23,100.00	45000	47250
2		22,000	22,000	24,255.00	45000	49612.5
3		22,000	22,000	25,467.75	45000	52093.125
4		22,000	22,000	26,741.14	45000	54697.78125
5		22,000	22,000	28,078.19	45000	57432.67031
6		22,000	22,000	29,482.10	45000	60304.30383
7		22,000	22,000	30,956.21	45000	63319.51902
Total				345,080.40		429709.8994

Figure 8.1. *Comparison of cash flow of the two material handling systems*

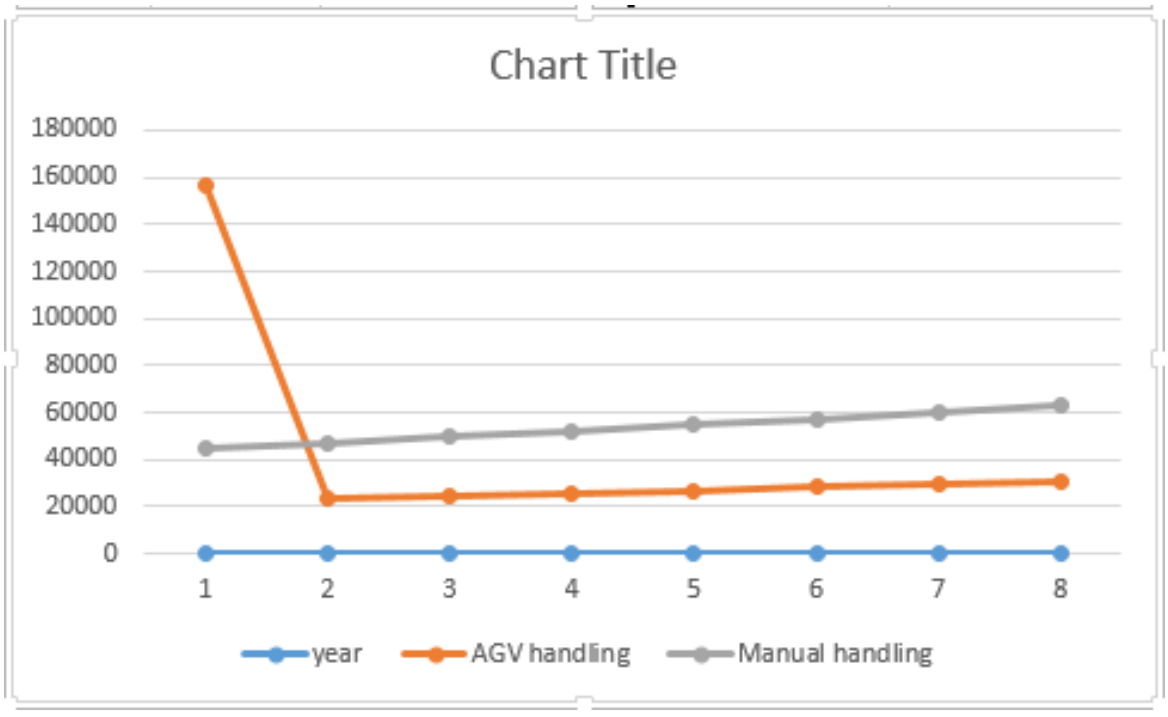

Figure 8.2. *Net present value over project lifetime*

8.2 Payback Period

The payback period, also called pay – off period is defined as the period required recovering the original investment outlay through the accumulated net cash flows earned by the project.

We can calculate the payback period of a machine using the following formula:

$$\text{Payback period} = \frac{\text{Total investment}}{S - S \cdot TR + DP \cdot TR - C_{\text{ops}}} \tag{8.12}$$

where:

- S = annual savings (gross manual handling cost avoided) = 284,000 ETB
- TR = corporate tax rate for pharmaceutical industry in Ethiopia = 35% [24]
- DP = annual depreciation (ETB)
- C_{ops} = annual AGV operational cost = 22,000 ETB

Annual depreciation (straight-line over product lifespan of 10 years [25], salvage value 20,000 ETB):

$$DP = \frac{\text{Purchase price} - \text{Salvage value}}{\text{Lifespan}} = \frac{135{,}000 - 20{,}000}{10} = 11{,}500\,\text{ETB/year} \tag{8.13}$$

Substituting all values:

$$\begin{aligned}\text{Net annual benefit} &= 284{,}000 - (284{,}000 \times 0.35) + (11{,}500 \times 0.35) - 22{,}000 \\ &= 284{,}000 - 99{,}400 + 4{,}025 - 22{,}000 = 166{,}625\,\text{ETB/year}\end{aligned} \tag{8.14}$$

$$\text{Payback period} = \frac{135{,}000}{166{,}625} = 0.81\,\text{years} \approx 9.7\,\text{months} \tag{8.15}$$

The corrected payback period is approximately **10 months**. This is substantially shorter than the previously stated 6.03 years, which arose from an underestimate of the annual manual handling cost (ETB 45,000 instead of the correct ETB 284,000). The 10-month payback confirms that the AGV investment is highly economically viable for EPHARM.

Chapter 9

Conclusion and Future Works

9.1 Conclusion

This paper presents the design and control of a forklift-type automated guided vehicle (AGV) intended to transport packed items from the end of the production line to the warehouse in the EPHARM pharmaceutical industry. The mechanical and electrical system designs are discussed in Chapters 4 and 5, respectively; the design of the robot's control system is presented in Chapter 6. Chapter 7 presents the simulation results for both the mechanical and control systems. Finally, Chapter 8 discusses the economic analysis of the proposed system within the specific firm.

The mechanical design of the robot includes selection of a lifting mechanism, stress analysis of key mechanical elements, and sizing of drive and lift motors. A DC motor-driven power screw is found to be an appropriate lifting mechanism for this application. The power screw was redesigned with a single-start thread ($n = 1$, lead $l = 4$ mm) to satisfy the self-locking condition ($l < \pi f d_m$), ensuring the load cannot back-drive the screw in the event of a power failure. Stress analysis of the screw and fork was performed and found to be within acceptable safety margins. An appropriate DC motor that provides the required torque was selected for both the drive and lift subsystems.

Nickel metal hydride (NiMH) battery, Arduino Uno microcontroller, DC motor actuators, XBee wireless communication module, and L293D H-bridge drivers constitute the electrical system of the robot. The battery charging circuit was also designed. These selections are discussed in Chapter 5.

A differential-drive kinematic model and Lagrangian dynamic model are developed for the robot drive system. A kinematic back-stepping controller is designed and its stability is verified using a Lyapunov function. A PID controller for the lifting mechanism is also designed. These topics are covered in Chapter 6.

The economic analysis in Chapter 8 demonstrates that replacing the current manual handling system with the proposed AGV yields a payback period of less than one year, offering substantial long-term savings for EPHARM.

9.2 Limitations

Several limitations of the present study should be acknowledged. First, the finite-element analyses (FEA) performed in Chapter 7 applied a conservative load of 200 N to the frame, which is significantly lower than the actual design loads of approximately 1,600 N; these results should be verified with correct loading conditions in future work. Second, the maximum von Mises stress in the lift structure (296 MPa) was found to exceed the yield strength of the AISI 1006 steel assumed in the FEA model ($S_y = 170$ MPa), indicating that a higher-strength material such as AISI 4140 ($S_y \approx 655$ MPa) should be specified for the lift structure in a detailed design phase. Third, the kinematic controller derived in Chapter 6 neglects vehicle dynamics (friction, inertia coupling, and external disturbances); this is acceptable at low speeds on flat, smooth flooring but would require a full dynamic controller for inclined surfaces or variable-load conditions. Fourth, the L293D H-bridge is rated for a maximum of 1 A continuous current, which is insufficient for the drive and lift motors selected; a higher-current motor driver must be substituted in the physical implementation. Fifth, chain-sprocket geometry and bearing selection were not completed within the scope of this project and remain as detailed design tasks.

9.3 Future Works

Some directions for future work include:

- **Path planning:** implementing an optimal path-planning algorithm that minimises travel distance, turning manoeuvres, and stopping events between the production line and the warehouse.
- **Detailed mechanical design:** completing the design of all remaining mechanical components, including bearings, chain-sprocket drive, bolt-and-nut connections, and welds, to the level required for manufacture.
- **Dynamic controller:** extending the kinematic back-stepping controller to account for vehicle dynamics, load variation, and floor disturbances using robust or adaptive control methods.
- **FMS integration:** interfacing the AGV with a flexible manufacturing system (FMS) so that the vehicle can respond automatically to changes in production scheduling.
- **Warehouse management integration:** linking the AGV to a warehouse management system (WMS) to enable real-time inventory tracking and task dispatching.

Bibliography

[1] D. Kitaw, *Materials Handling Equipment*. May 2001. The twenty principles of material handling, pp. 15–16.

[2] World Health Organization, "WHO good manufacturing practices for pharmaceutical products: Main principles," Technical Report Series 970, World Health Organization, 2011. Annex 3.

[3] D. Wigmore, "Pharmaceuticals manufacturing: What do we know about the occupational health and safety hazards?," March 2009.

[4] "European Commission – Pharmaceuticals." http://www.pharmacos.eudra.org. Accessed: 2017-01-06.

[5] S. Arjoo, "Design and implementation of an autonomous forklift," 2005.

[6] D. Kitaw, *Materials Handling Equipment*. May 2001. Forklift components, pp. 306–308.

[7] D. Kitaw, *Materials Handling Equipment*. May 2001. Automated guided vehicle, p. 314.

[8] D. Kitaw, *Materials Handling Equipment*. May 2001. Automated guided vehicle component parts, p. 315.

[9] D. Kitaw, *Materials Handling Equipment*. May 2001. Automated guided vehicle: non-wire, non-floor path guidance, p. 319.

[10] R. Siegwart and I. R. Nourbakhsh, *Introduction to Autonomous Mobile Robots*. MIT Press, 2004. Locomotion, p. 28.

[11] S. G. Tzafestas, *Introduction to Mobile Robot Control*. Elsevier, 2013. Ground robot locomotion, p. 10.

[12] S. G. Tzafestas, *Introduction to Mobile Robot Control*. Elsevier, 2013. Wheeled locomotion, p. 13.

[13] S. G. Tzafestas, *Introduction to Mobile Robot Control*. Elsevier, 2013. Wheel types, p. 13.

[14] R. Siegwart and I. R. Nourbakhsh, *Introduction to Autonomous Mobile Robots*. MIT Press, 2004. Wheel geometry and stability, p. 33.

[15] R. G. Budynas and J. K. Nisbett, *Shigley's Mechanical Engineering Design*. McGraw-Hill, 8th ed., 2008.

[16] H. Gurocak, *Industrial Motion Control: Motor Selection, Drives, Controller Tuning, Applications*. Wiley, 2011.

[17] D. Linden and T. B. Reddy, *Handbook of Batteries*. McGraw-Hill, 4th ed., 2010.

[18] M. Barr and A. Massa, *Programming Embedded Systems: With C and GNU Development Tools*. O'Reilly Media, 2nd ed., 2006.

[19] W. Bolton, *Programmable Logic Controllers*. Elsevier/Newnes, 5th ed., 2009.

[20] H. Gurocak, *Industrial Motion Control*. Wiley, 2013. p. 191.

[21] "Pulse-width modulation." https://www.allaboutcircuits.com/textbook/semiconductors/chpt-11/pulse-width-modulation/. Accessed: 2017-05-10.

[22] P. Acarnley, *Stepping Motors: A Guide to Modern Theory and Practice*. The Institution of Engineering and Technology, 4th ed., 2002.

[23] R. Dhaouadi and A. A. Hatab, "Dynamic modelling of differential-drive mobile robots using lagrange and newton–euler methodologies: A unified framework," *Advances in Robotics & Automation*, vol. 2, no. 2, 2013.

[24] Ethiopian Revenue and Customs Authority, "Income tax proclamation no. 286/2002 and regulation no. 78/2002." Federal Negarit Gazeta, Federal Democratic Republic of Ethiopia, 2002. Schedule C: corporate income tax; manufacturing sector rate.

[25] Material Handling Industry of America, *Automation Solutions: Automated Guided Vehicle Systems*. MHI, 2013. Typical AGV system service life 10 years or more.

Appendix A

MATLAB Functions for Drive Mechanism Simulation

Trajectory Function

```
function [x,y,vx,vy,v,theta] = trajectory(t)

x = 0; y = 0; vx = 0; vy = 0; v = 0; theta = 0;

T  = 50;                  % duration of the trajectory
xi = 0.00000000001;
xf = 2;
vxi = 0;
vxf = 0;

% initial and final time
t0 = 0;
tf = T;

% coefficients a0, a1, a2, a3 of the trajectory polynomial
coeff = inv([1 t0 t0^2 t0^3;
             0 1  2*t0 3*t0^2;
             1 tf tf^2 tf^3;
             0 1  2*tf 3*tf^2]) * [xi vxi xf vxf]';

a0 = coeff(1);
a1 = coeff(2);   % coefficient of t
a2 = coeff(3);   % coefficient of t^2
a3 = coeff(4);   % coefficient of t^3

% evaluate x(t)
x  = a0 + a1*t + a2*t^2 + a3*t^3;   % AGV trajectory along x
```

```
y  = (1 - (x-1)^2)^0.5;              % AGV trajectory along y
vx = a1 + 2*a2*t + 3*a3*t^2;         % AGV velocity along x
vy = -(x-1)*vx/y;                    % AGV velocity along y
v  = (vx^2 + vy^2)^0.5;              % AGV speed
theta = atan(y/x);

end
```

Transformation Function

```
function [e1,e2,e3] = transformation(ex,ey,eth,theta)

A  = [cos(theta)  sin(theta) 0;
     -sin(theta)  cos(theta) 0;
      0            0          1];
e1 = cos(theta).*ex + sin(theta).*ey;
e2 = -sin(theta).*ex + cos(theta).*ey;
e3 = eth;

end
```

Kinematic Controller

```
function [v,w] = KinematicControl(Kx,Ky,Kth,vr,wr,ex,ey,eth)

v = vr*cos(eth) + Kx*ex;
w = wr + Ky*vr*ey + Kth*vr*sin(eth);

end
```

Inverse Kinematics

```
function [Wr,Wl] = inverse_kinematics(vx,vy,omega,theta)

R  = 0.12;
L  = 0.17;
Wr = (vx*cos(theta)/R) + (vy*sin(theta)/R) + (L*omega);
Wl = (vx*cos(theta)/R) + (vy*sin(theta)/R) - (L*omega);
```

```
end
```

Forward Kinematics

```
function [Xdot,Ydot,thetadot] = Kinematics(Wr,Wl,theta)

Ra = 0.12;
a  = 0.05;
Xdot     = (Wr*sin(theta) + Wl*sin(theta)) * Ra / 2;
Ydot     = (Wr*cos(theta) + Wl*cos(theta)) * Ra / 2;
thetadot = (Wr - Wl) * Ra / (2*a);

end
```